Scatter

Marc Kachelrieß

German Cancer Research Center (DKFZ)
Heidelberg, Germany
www.dkfz.de/ct

Scatter Artifacts

- Measurement = Primary + Scatter
- Interaction processes
  - C = Compton scatter
  - R = Rayleigh scatter
  - P = photo effect

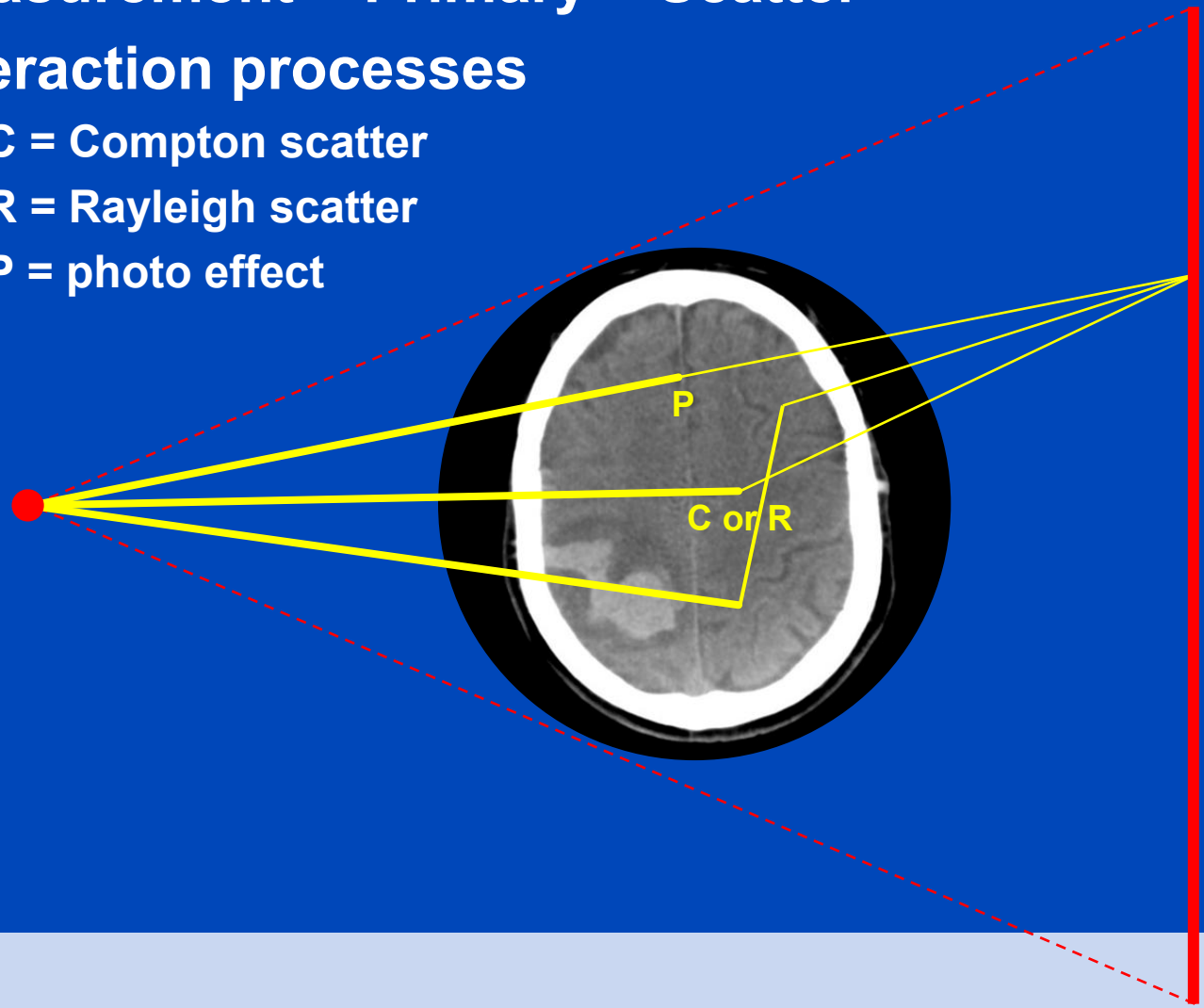

Primary

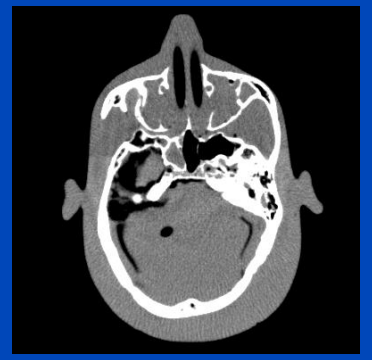

Primary + Scatter

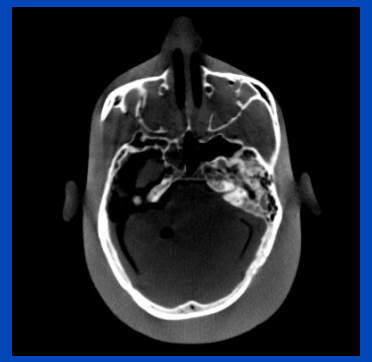

Scatter Artifact Reduction

- Several algorithmic methods found in the literature:
  - Monte Carlo-based (slow but good)
  - Convolution-based (fast, but not accurate)
  - Simple subtraction methods (even faster, but less accurate)
  - Deep scatter estimation (DSE, fast and accurate)
  - …
- Hardware-based methods
  - Anti scatter grid
  - Beam blockers
  - Primary modulators
  - …

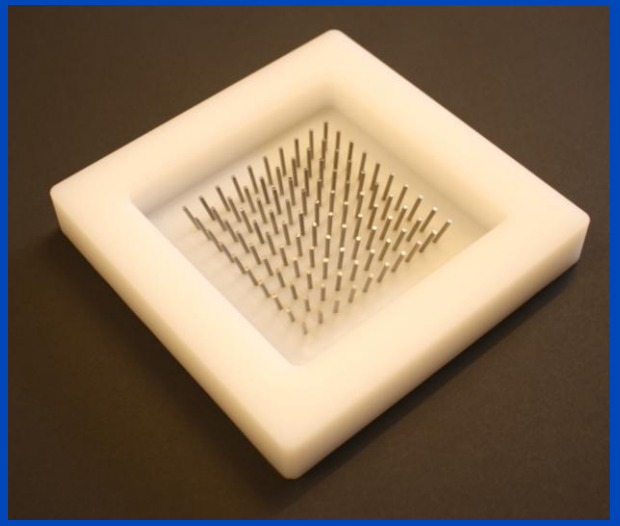

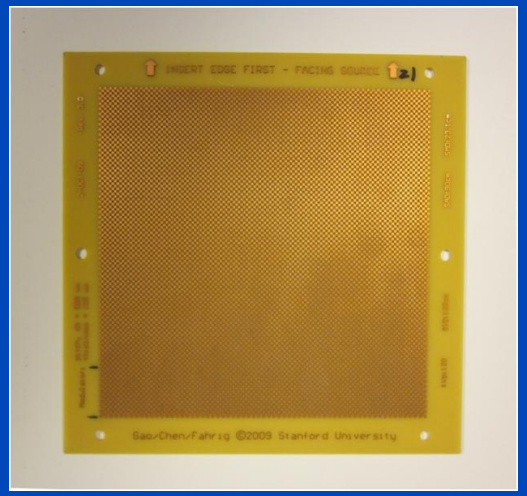

To Grid or not to Grid?

- A common misbelieve is that a good or perfect scatter reduction software can be used instead of using anti scatter grids.
- This is wrong, as will be shown in the next slices.
- Facts:
  - Anti scatter grids are beneficial iff the scatter-to-primary ratio (SPR) exceeds a certain threshold, i.e. for large cross-sections.
  - Scatter reduction software is always beneficial, with or without anti scatter grid.
  - Noise reduction software is always beneficial, with or without anti scatter grid.

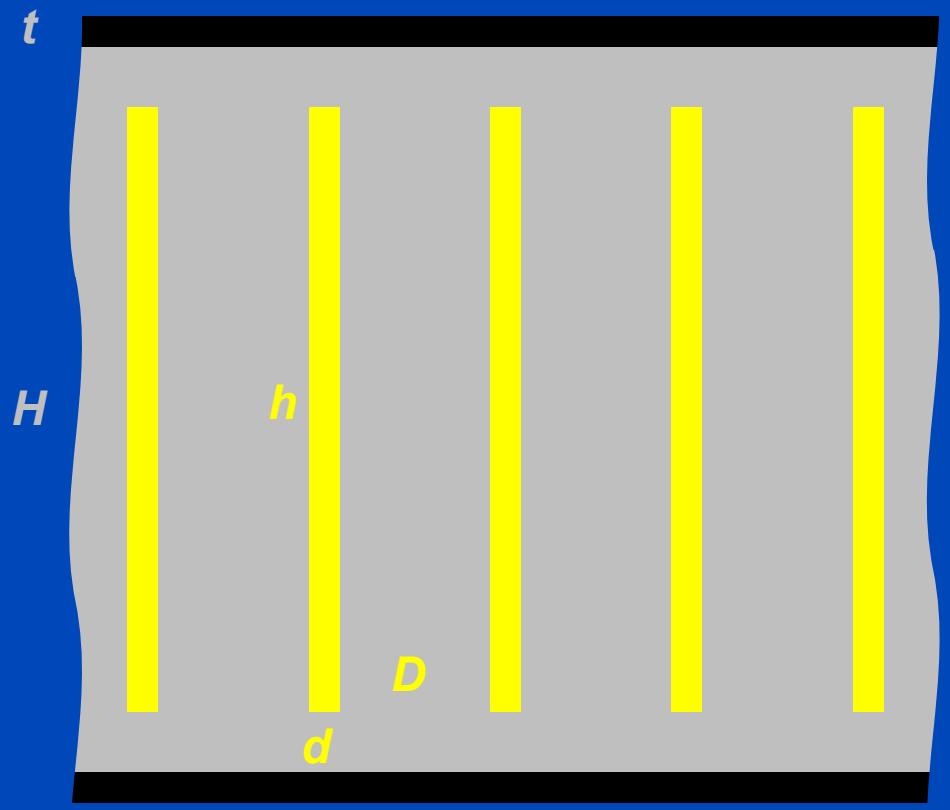

Cover thickness: *t*, e.g. 0.2 mm Al or 0.25 mm C
Height of strips: *h*
Thickness of strips: *d*, e.g. 0.04 mm Pb
Gap between strips: *D*, e.g Al or C-fiber
Grid ratio: *h*/*D*, e.g. 8 or 15
Grid frequency: 1/(*D*+*d*), e.g. 40/cm
Geometrical efficiency: *D*/(*D*+*d*)
Height of interspace material: *H*

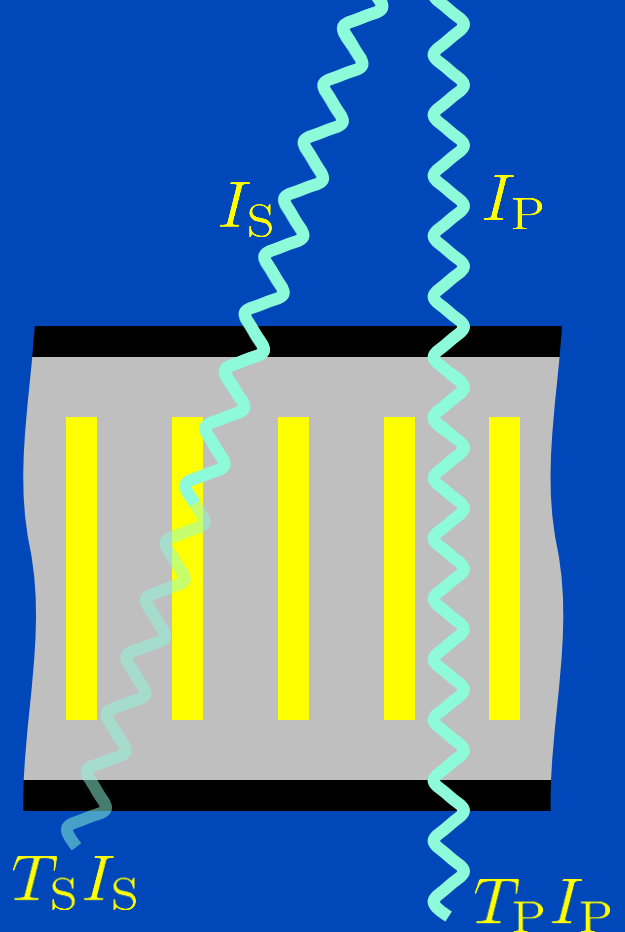

Primary intensity: I_P
Scatter intensity: I_S
Primary transmission: $T_P < 1$, e.g. 75%
Scatter transmission: $T_S > 0$, e.g. 30%

No grid: $T_P = T_S = 1$
Ideal grid: $T_P = 1$, $T_S = 0$

Drawn to grid ratio 4:1 and infinite focus distance.

dkfz.

To Grid or not to Grid?

- Only primary counts for the signal, but primary and scatter count for noise. Thus,

$$\mathrm{SNR} = \frac{T_\mathrm{P} I_\mathrm{P}}{\sqrt{T_\mathrm{P} I_\mathrm{P} + T_\mathrm{S} I_\mathrm{S}}}$$

- SNR improvement factor (SNR with grid / SNR no grid)

$$\mathrm{SNR}_\mathrm{if} = T_\mathrm{P} \frac{\sqrt{I_\mathrm{P} + I_\mathrm{S}}}{\sqrt{T_\mathrm{P} I_\mathrm{P} + T_\mathrm{S} I_\mathrm{S}}}$$

- The case $T_S = 0$ is instructive and yields

$$\mathrm{SNR}_\mathrm{if} \leq \sqrt{T_\mathrm{P}} \sqrt{1 + \mathrm{SPR}}$$

  with SPR being the scatter-to-primary ratio.

- Use a grid only for cases with $\mathrm{SNR}_\mathrm{if} \geq 1$.
- Scatter correction and noise reduction algorithms are to be used complementary and not as an alternative to grids!

Detector Technology

Clinical CT Detector Module

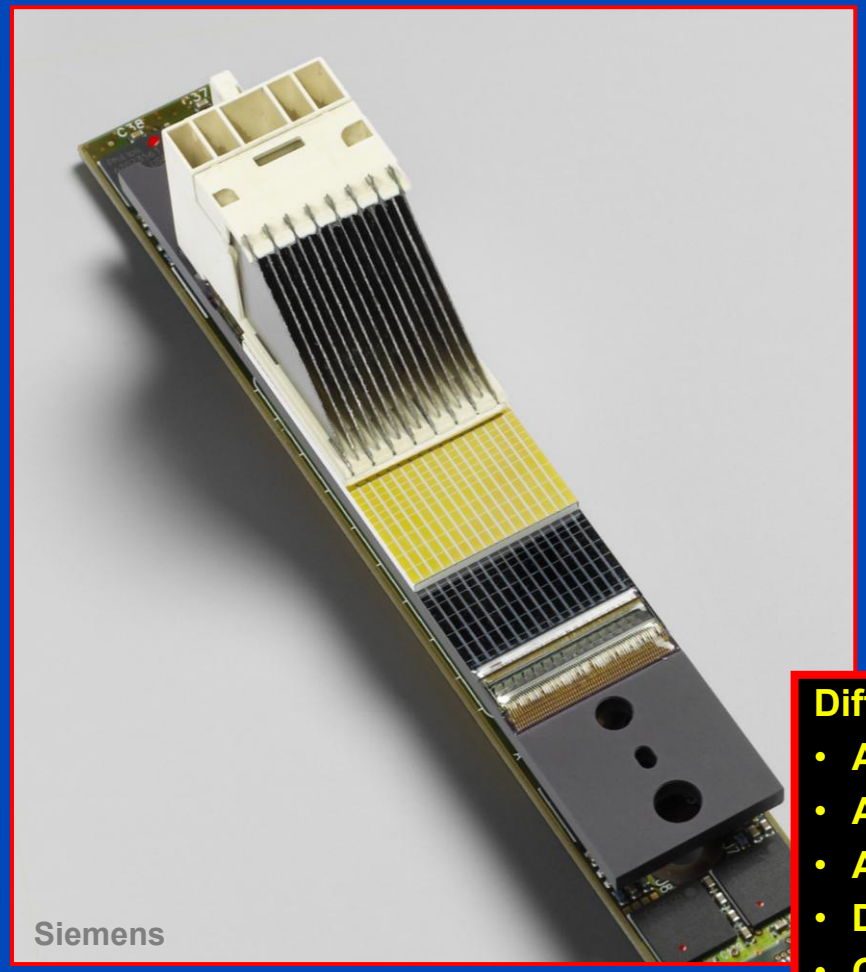

Siemens

Flat Detector (e.g. 40 × 30 cm)

Varex

Differences in:

- Absorption efficiency
- Afterglow
- Anti scatter grid
- Dynamic range
- Cross-talk
- Framerate
- …

dkfz.

Scatter estimation with the help of a pre patient modulator

PRIMARY MODULATOR

Existing Scatter Correction Methods

- Remove or prevent scattered radiation
  - anti scatter grid, slit scan, large detector distance, …
- Compute scatter to subtract it
  - convolution-based, Monte Carlo-based, …
- Measure scatter distribution and subtract it
  - collimator shadow, beam blockers, primary modulators, …

- Literature:
  - E.-P. Rührnschopf and K. Klingenbeck, “A general framework and review of scatter correction methods in x–ray cone–beam computerized tomography. Part 1: Scatter compensation approaches,” Med. Phys., vol. 38, pp. 4296–4311, July 2011.
  - E.-P. Rührnschopf and K. Klingenbeck, “A general framework and review of scatter correction methods in x–ray cone beam CT. Part 2: Scatter estimation approaches,” Med. Phys., vol. 38, pp. 5186–5199, Sept. 2011.

Primary Modulation-based Scatter Estimation (PMSE)

- Idea: Insert a high frequency modulation pattern between the source and the object scanned
- Rationale: The primary intensity is modulated. The scatter is created in the object and only consists of low frequency components.
- Method: Estimate low frequency primary without scatter by Fourier filtering techniques

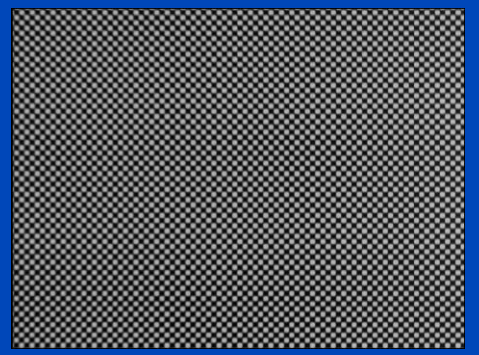

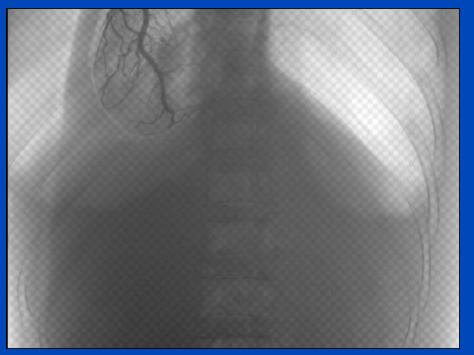

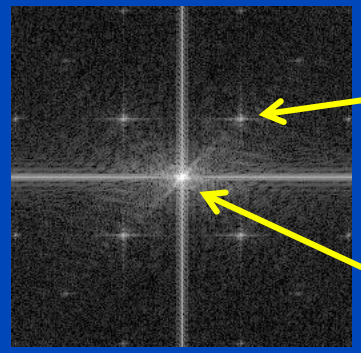

L. Zhu, R. N. Bennett, and R. Fahrig, "Scatter correction method for x–ray CT using primary modulation: Theory and preliminary results," IEEE Transactions on Medical Imaging, vol. 25, pp. 1573–1587, Dec. 2006.

dkfz.

Primary Modulation-based Scatter Estimation (PMSE)

Key hypothesis: Low-frequency components dominate the scatter distribution even if high-frequency components are present in the incident x-ray intensity distribution.

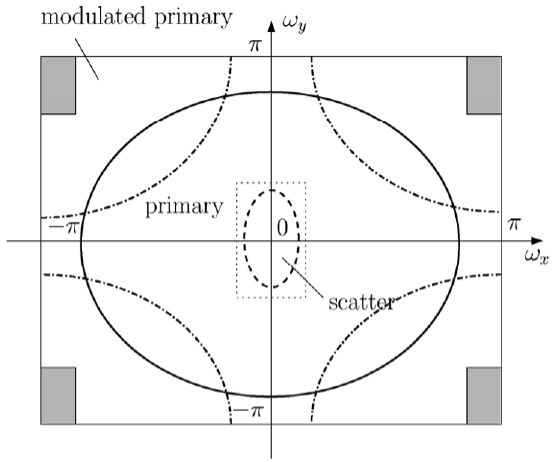

Fig. 3. Conceptual illustration of the primary and scatter distributions in the Fourier domain, with the primary modulator in place. The solid line indicates the primary distribution before modulation; the dot-dashed line indicates the modulated primary; the dashed line around the origin indicates the scatter distribution, which is mainly concentrated in the low-frequency region before and after primary modulation; the center region encompassed by the dotted line indicates the support of the low-pass filter used in Step 3.3 of the scatter correction algorithm proposed in Section II-D; the shaded region indicates the support of the high-pass filter used in Step 3.4.

The measurement with a modulator can be expressed in Fourier space with:

$$P'(\omega) = \frac{1+\alpha}{2}P(\omega) + \frac{1-\alpha}{2}P(\omega-\pi) + S(\omega), \qquad (1)$$

where P and S denote the Fourier transforms of primary and scatter, respectively, and $\omega \in [-\pi,\pi]\times[-\pi,\pi]$ is the 2D coordinate of (ω_x,ω_y) in the Fourier domain. Parameter $\alpha \in (0,1)$ is the transmission factor of the modulator blocker,

Scatter *S* can be estimated by

$$S_{\text{est}}(\omega) = P'(\omega)H(\omega) - \frac{1+\alpha}{1-\alpha}P'(\omega-\pi)H(\omega). \qquad (8)$$

with $H(\omega)$ being a low-pass filter

L. Zhu, R. N. Bennett, and R. Fahrig, "Scatter correction method for x–ray CT using primary modulation: Theory and preliminary results," IEEE Transactions on Medical Imaging, vol. 25, pp. 1573–1587, Dec. 2006.

dkfz.

Primary Modulation-based Scatter Estimation (PMSE)

- **Advantages:**
  - Non-destructive measurement of the scatter distribution
  - Works with high accuracy on laboratory setups
  - Corrected projection data can be used for projective imaging (fluoroscopy) or for tomographic reconstruction
- **Drawbacks:**
  - Sensitive to non-linearities due to polychromaticity of x-rays. Ring artifacts are introduced[1]. Can be resolved using ECCP[2].
  - Requires exact rectangular pattern on the detector. Very sensitive to non-idealities of the projected modulation pattern (blurring, distortion, manufacturing errors of the modulator). Can be resolved using iPMSE (this work).

[1]H. Gao, L. Zhu, and R. Fahrig. Modulator design for x-ray scatter correction using primary modulation: Material selection. Med. Phys. 37:4029–4037, 2010.
[2]R. Grimmer, R. Fahrig, W. Hinshaw, H. Gao, and M. Kachelrieß. Empirical cupping correction for CT scanners with primary modulation (ECCP). Med. Phys. 39:825-831, 2012.

Aim

Create a robust scatter estimation method which is able to estimate the scatter distribution with high accuracy using a modulator with an arbitrary high frequency pattern.

“Ideal” modulator
(projection of a copper modulator)

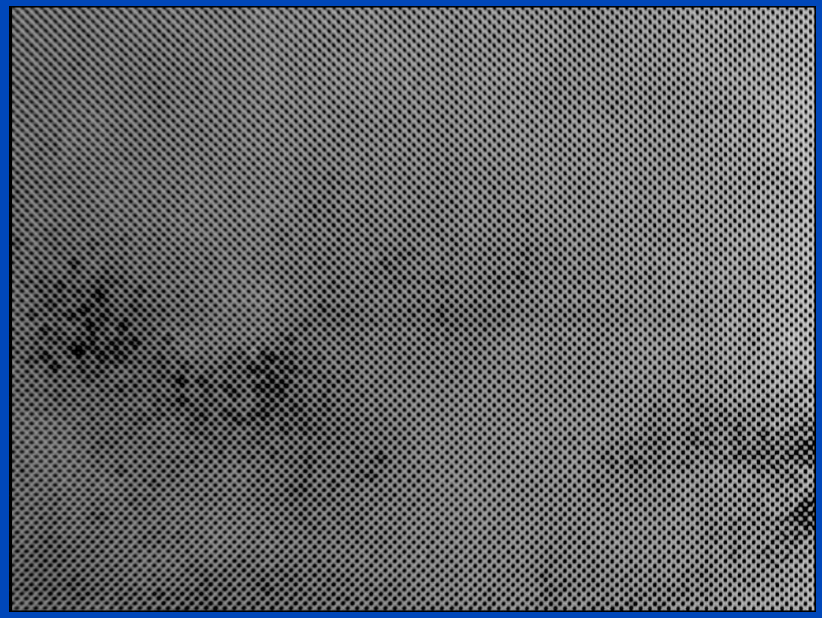

Non-ideal modulator
(projection of the erbium modulator)

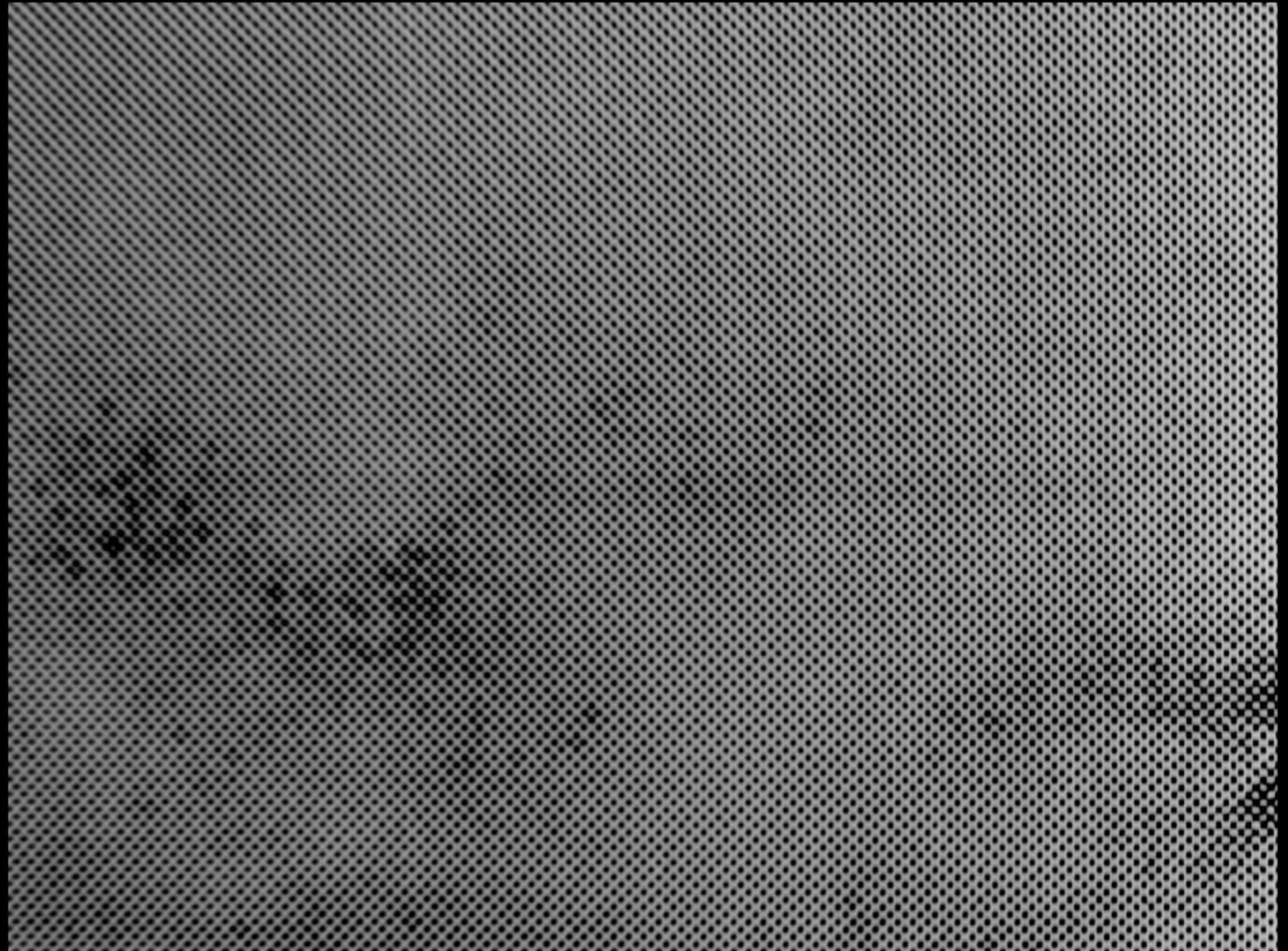

Modulation Process in the Rawdata Domain

- **Measured data:**

$$c_\mathrm{m} = M c_\mathrm{p} + c_\mathrm{s}$$

Primary intensity

Measured intensity

Modulation pattern

Scatter intensity

- **Solving for the primary intensity:**

$$c_\mathrm{p} = M^{-1}(c_\mathrm{m} - c_\mathrm{s})$$

- **Error of primary estimate:**

$$\begin{aligned} c_\mathrm{p}^\mathrm{est} &= M^{-1}(c_\mathrm{m} - c_\mathrm{s}^\mathrm{est}) \\ &= c_\mathrm{p} + M^{-1}(c_\mathrm{s} - c_\mathrm{s}^\mathrm{est}) \end{aligned}$$

Scatter estimate error

The modulation pattern remains visible as long as the scatter estimation error is not zero.

L. Ritschl, R. Fahrig, M. Knaup, J. Maier, and M. Kachelrieß. Robust primary modulation-based scatter estimation for cone-beam CT. Med. Phys. 42(1):469-478, January 2015.

Is there a cost function which is sensitive to the modulation pattern?

Regard the image sequence $c_\mathrm{p}(t) = M^{-1}(c_\mathrm{m} - t)$:

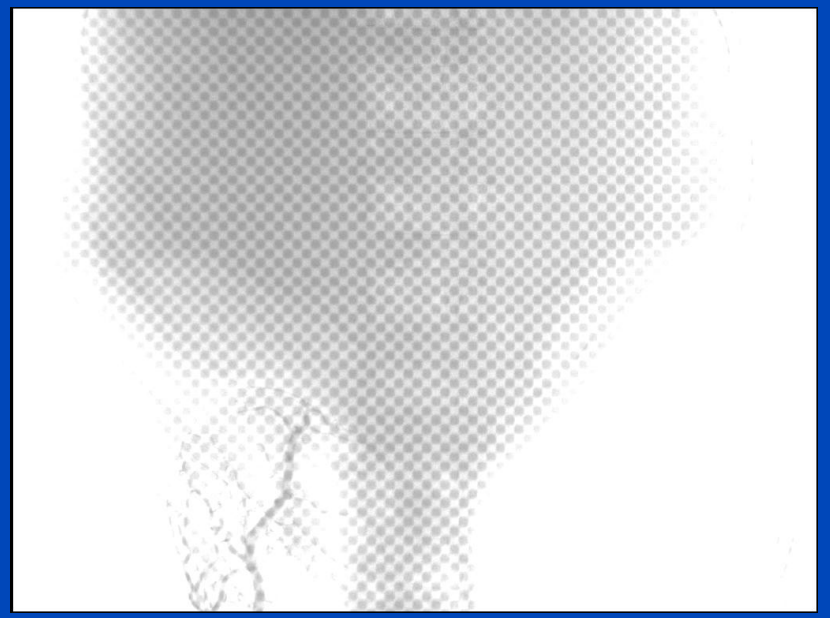

$c_\mathrm{p}(t)$

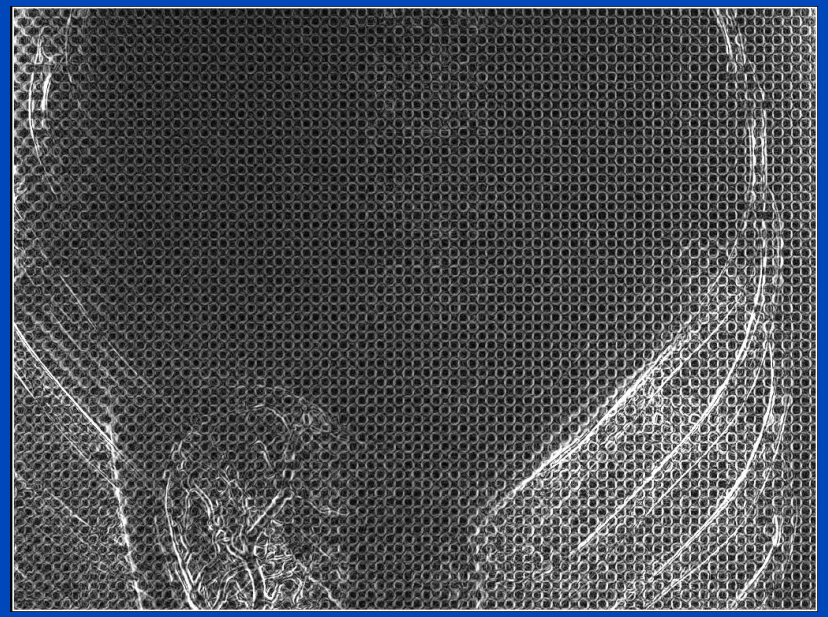

$|\nabla \cdot c_\mathrm{p}(t)|$

L. Ritschl, R. Fahrig, M. Knaup, J. Maier, and M. Kachelrieß. Robust primary modulation-based scatter estimation for cone-beam CT. Med. Phys. 42(1):469-478, January 2015.

dkfz.

Optimization Problem

- **Subject to** $H \cdot \boldsymbol{c}_{\mathrm{s}}^{\mathrm{est}} = 0$ **solve:**

$$C(\boldsymbol{c}_{\mathrm{p}}^{\mathrm{est}}) = \|\nabla \cdot \boldsymbol{c}_{\mathrm{p}}^{\mathrm{est}}\|_1 = \|\nabla \cdot M^{-1}(\boldsymbol{c}_{\mathrm{m}} - \boldsymbol{c}_{\mathrm{s}}^{\mathrm{est}})\|_1$$

- **Assumption:**
  In a sufficiently small and sufficiently large sub image the constraint can be satisfied by assuming c_s = const.

- **Solution:**
  Solve cost function for each possible sub image separately.

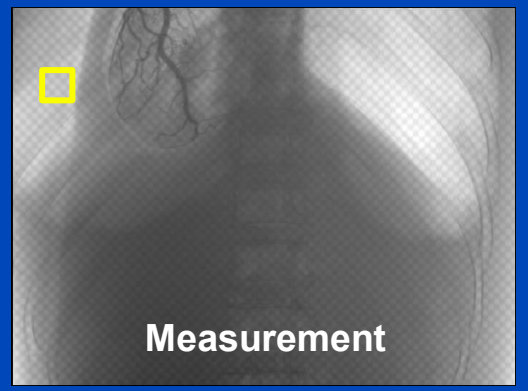

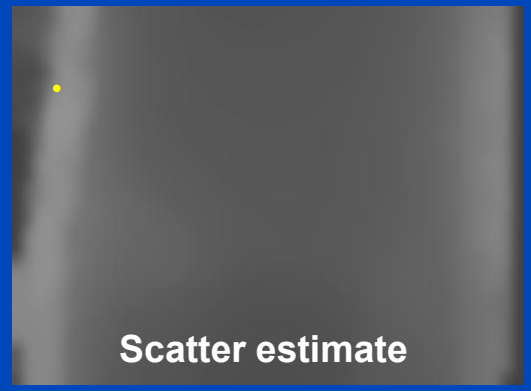

L. Ritschl, R. Fahrig, M. Knaup, J. Maier, and M. Kachelrieß. Robust primary modulation-based scatter estimation for cone-beam CT. Med. Phys. 42(1):469-478, January 2015.

dkfz.

Measured Intensity

L. Ritschl, R. Fahrig, M. Knaup, J. Maier, and M. Kachelrieß. Robust primary modulation-based scatter estimation for cone-beam CT. Med. Phys. 42(1):469-478, January 2015.

dkfz.

iPMSE Estimation

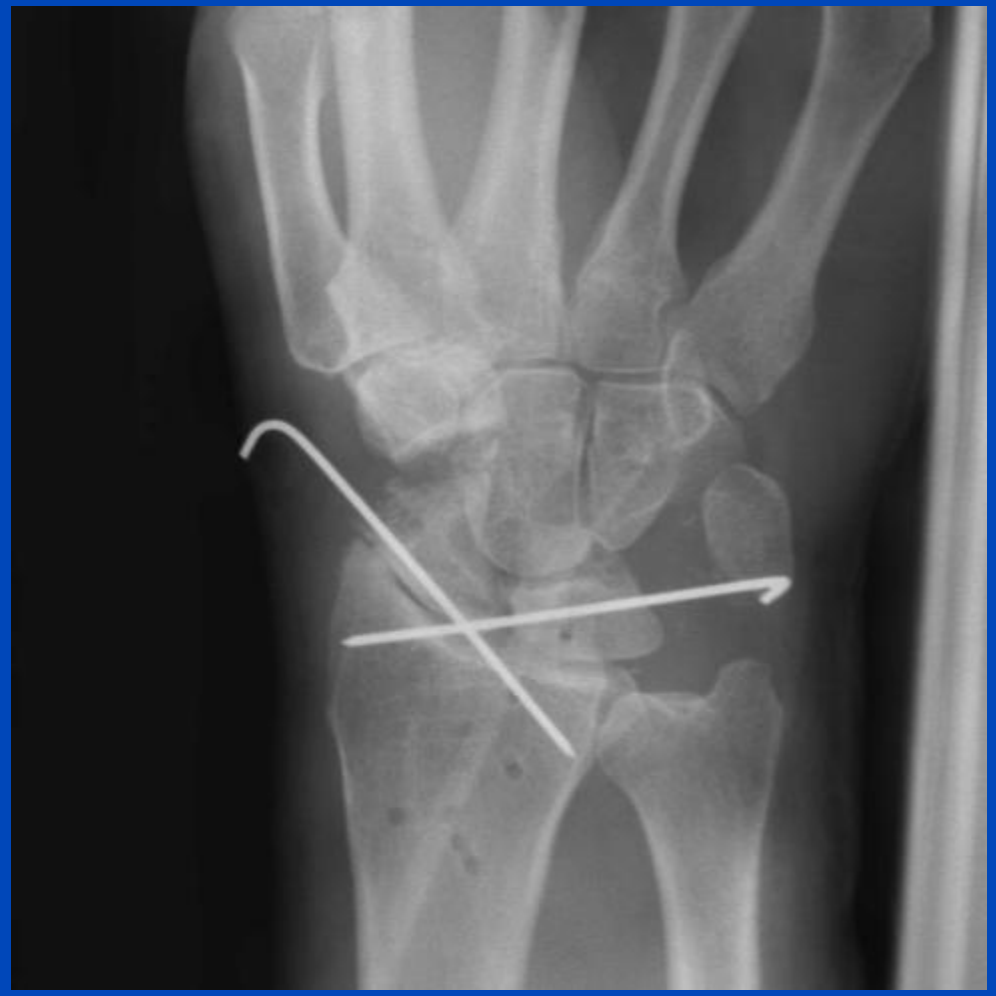

L. Ritschl, R. Fahrig, M. Knaup, J. Maier, and M. Kachelrieß. Robust primary modulation-based scatter estimation for cone-beam CT. Med. Phys. 42(1):469-478, January 2015.

dkfz.

Cadaver Head and Lung Phantom

- Scan parameters
  - 80 kV
  - 30 mA
  - 13 ms pulse length
  - 625 projections of 360°
  - 244 mAs
- No antiscatter grid
- Modulator
  - Material: Erbium
  - Thickness: 0.0254 mm
  - Pattern size: 0.457 mm
- ECCP[1] preprocessing
- iPMSE scatter removal
- FDK reconstruction

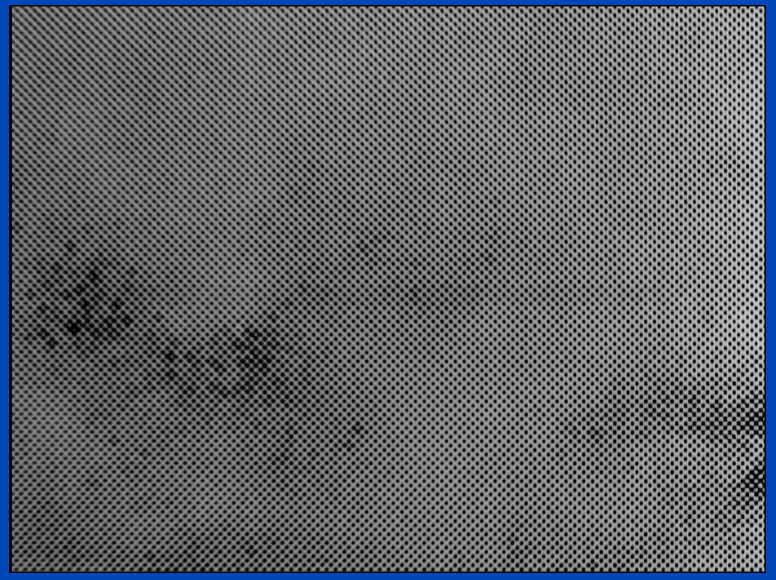

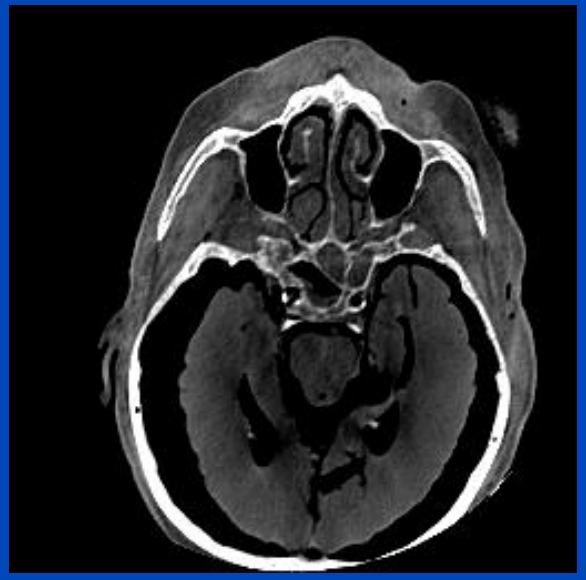

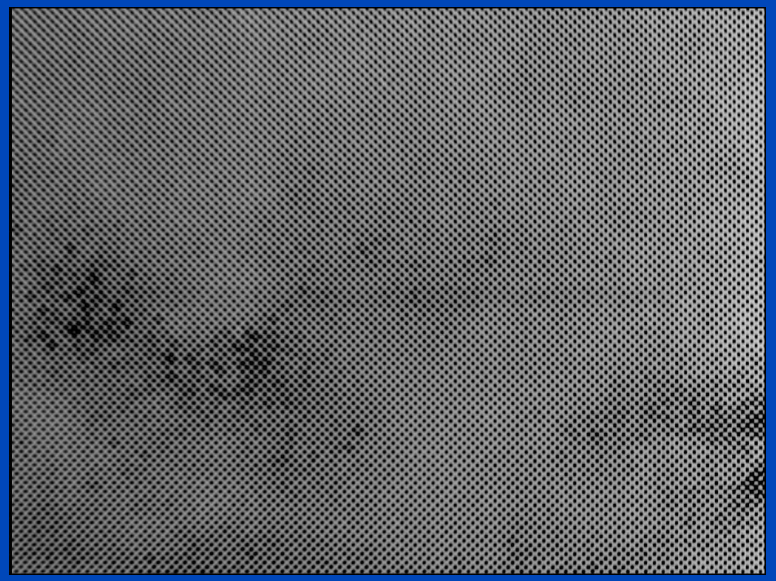

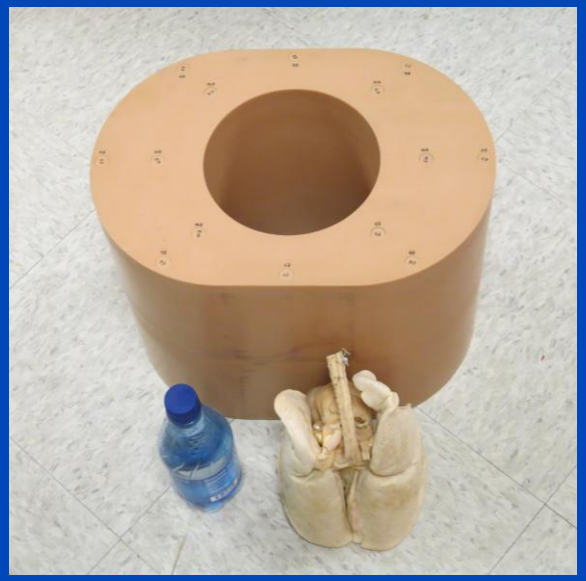

[1]R. Grimmer, R. Fahrig, W. Hinshaw, H. Gao, and M. Kachelrieß. Empirical cupping correction for CT scanners with primary modulation (ECCP). Med. Phys. 39:825-831, 2012.

dkfz.

Cadaver Head Axial Slice

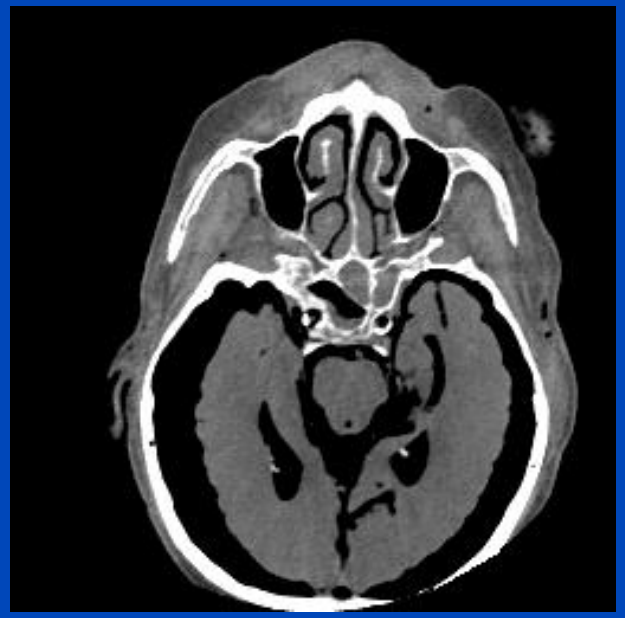

Slit scan

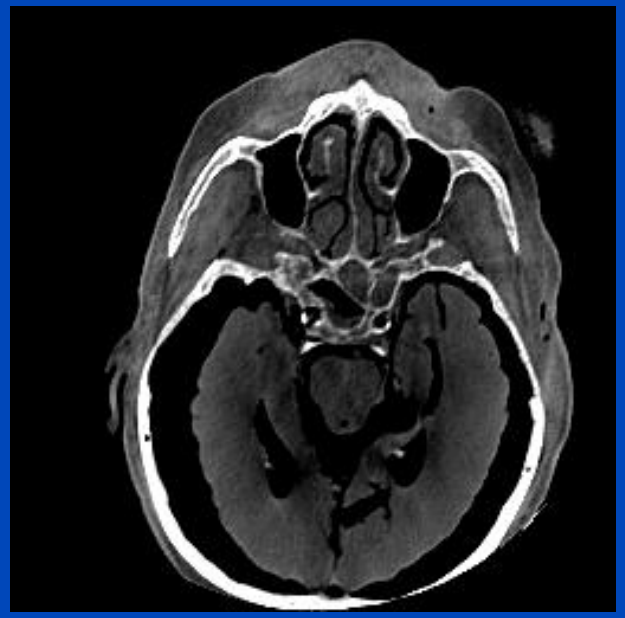

Uncorrected

iPMSE

C = 200 HU, *W* = 800 HU

L. Ritschl, R. Fahrig, M. Knaup, J. Maier, and M. Kachelrieß. Robust primary modulation-based scatter estimation for cone-beam CT. Med. Phys. 42(1):469-478, January 2015.

dkfz.

Lung Phantom Scan

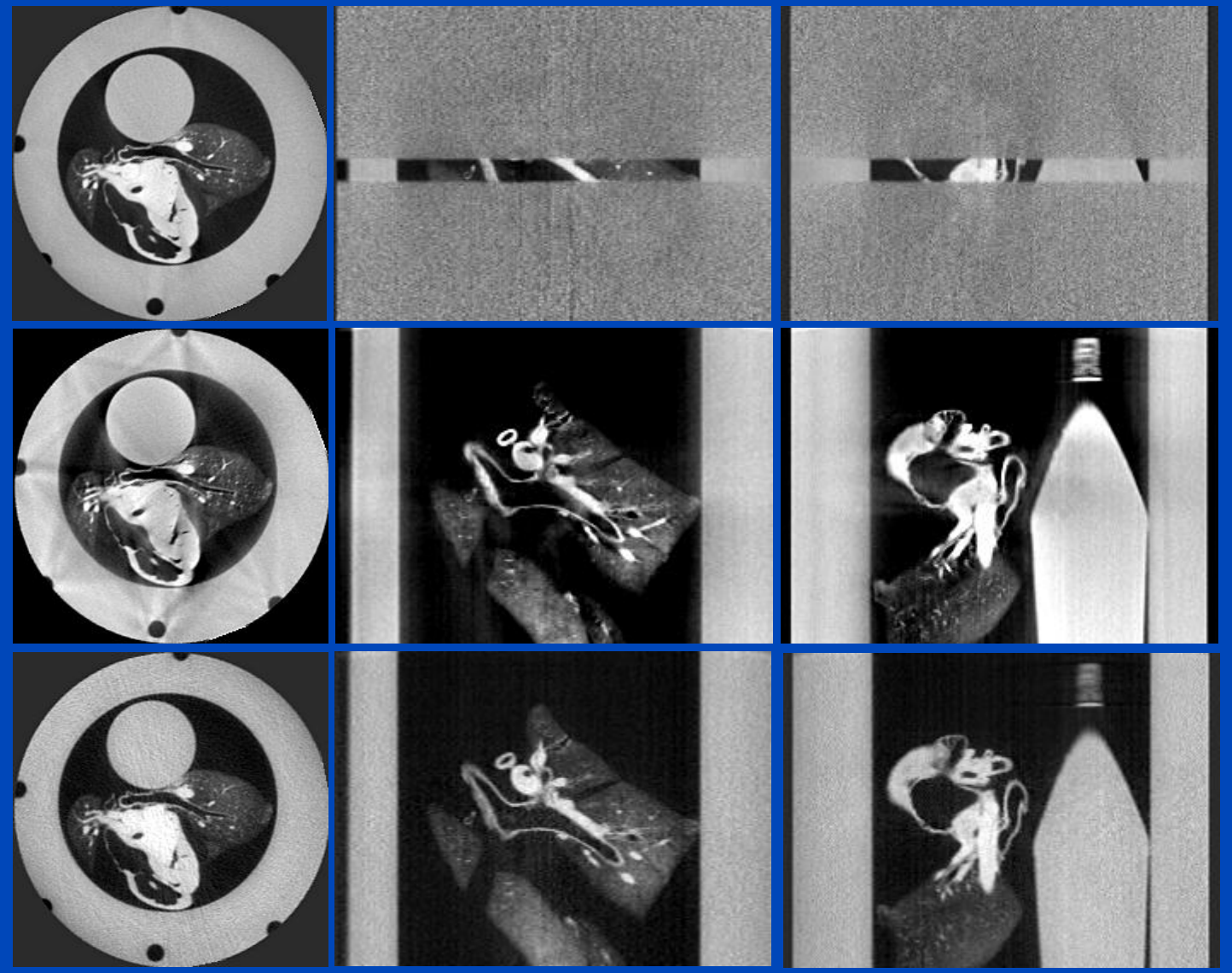

C = 0 HU, *W* = 1000 HU

L. Ritschl, R. Fahrig, M. Knaup, J. Maier, and M. Kachelrieß. Robust primary modulation-based scatter estimation for cone-beam CT. Med. Phys. 42(1):469-478, January 2015.

dkfz.

Discussion

- Highly accurate scatter estimation and removal is also possible using irregular modulation patterns.
- Non-idealities of the modulation pattern and penumbra effects are optimally handled with iPMSE.
- The combination ECCP and iPMSE guarantees quantitative flat detector images without scatter artifacts.
- Accurate scatter correction opens the field of quantitative flat detector CT.

L. Ritschl, R. Fahrig, M. Knaup, J. Maier, and M. Kachelrieß. Robust primary modulation-based scatter estimation for cone-beam CT. Med. Phys. 42(1):469-478, January 2015.

The gold standard for scatter estimation

MONTE CARLO

Monte Carlo Scatter Estimation

- Simulation of photon trajectories according to physical interaction probabilities.
- Simulating a large number of photon trajectories well approximates the actual scatter distribution.

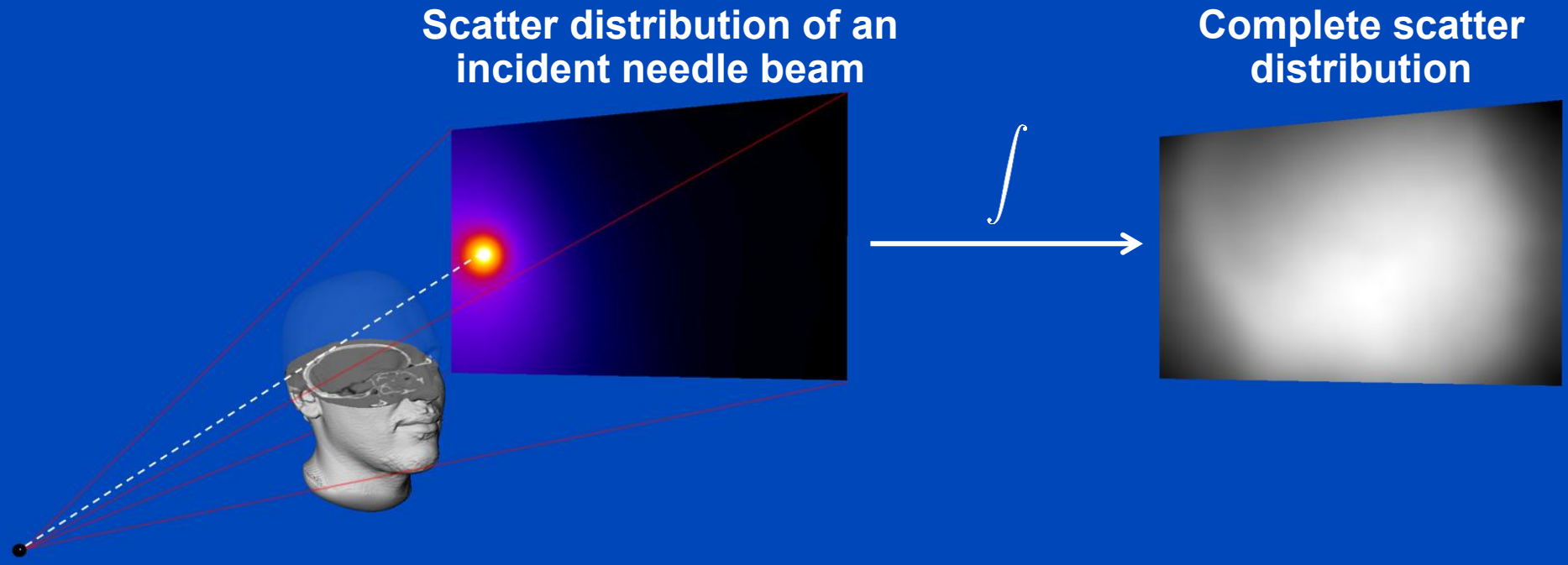

Monte Carlo Simulation of Radiation Transport

- The quantity *Q* of interest could be the number of photons reaching the detector or the energy deposited in the detector.

$$\mathrm{E}Q = \int Q\, p(Q)\, dQ,$$

- However, the probability density *p*(*Q*) is usually unknown.
- Simulation of individual photon tracks (= random walk from source to detector) yields a practical method to sample Q_i

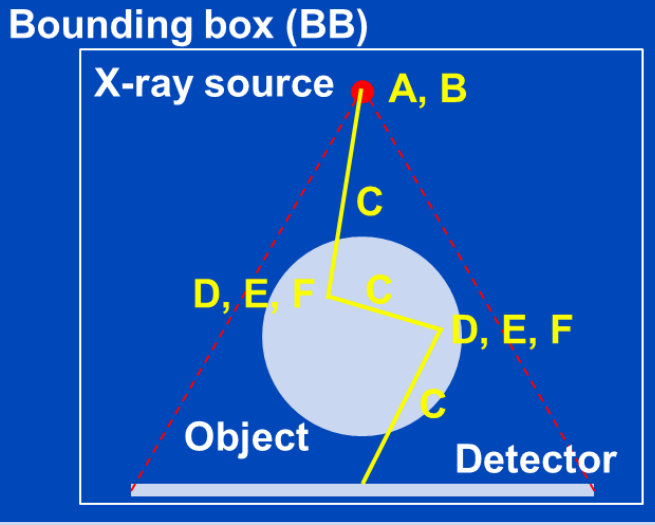

for(Number of tracks)
- A. Sample x-ray energy
- B. Sample initial flight direction

while(Energy > 0 && x-ray inside BB)
- C. Sample path length
- D. Sample interaction effect
- E. Sample flight direction
- F. Update energy

Sampling of the X-Ray Energy

- The spectral distribution of x-rays $w(E)$ can be determined using theoretical models (e.g. the model of Tucker[1]).
- Normalizing the x-ray spectrum to unit area allows to interpret it as probability density function:

$$p_{\mathrm{E}}(E) = \frac{w(E)}{\int dE\, w(E)}$$

- Sampling from cumulative distribution, e.g. with the upsampling method.

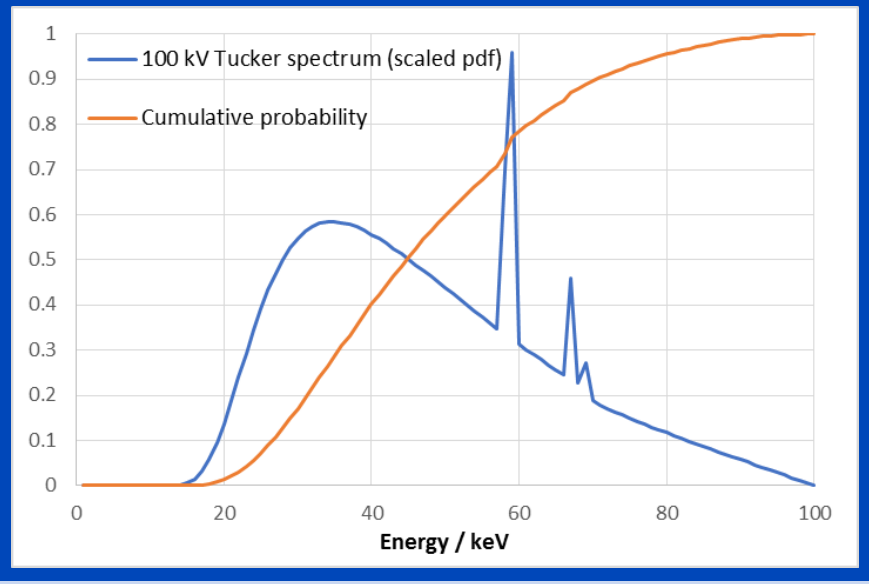

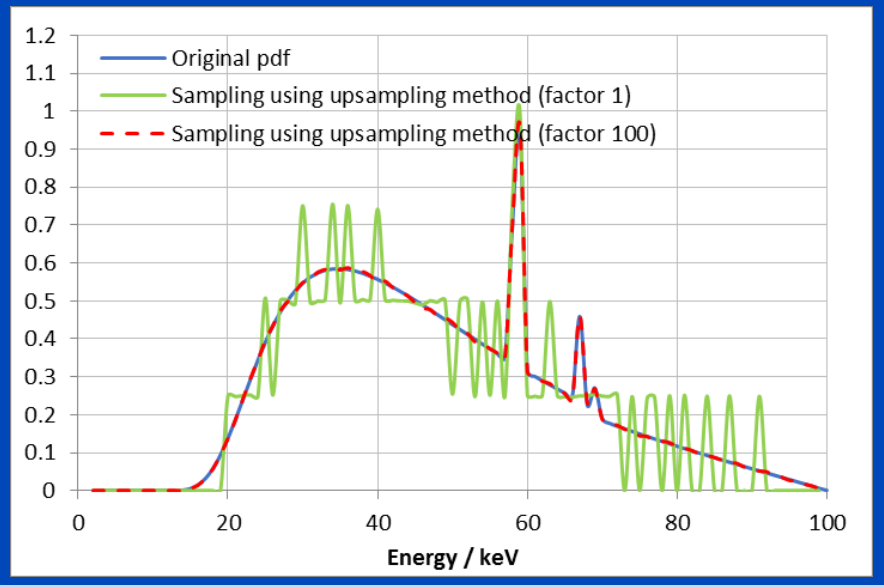

[1]Tucker D. M., Barnes G.T., Chakraborty D.P. (1991), Semiempirical model for generating tungsten target x-ray spectra. Med. Phys. 18, 211–218.

dkfz.

Sampling of the Initial Flight Direction

- Assuming an isotropic emission of the x-ray source, the probability density function of the azimuthal angle θ and the polar angle φ are given as

$$p_\theta = \frac{1}{\pi}, \qquad p_\varphi = \frac{1}{2\pi}$$

- The inverse transform method yields

$$\theta = \pi \cdot \xi_1$$
$$\varphi = 2\pi \cdot \xi_2$$

- The initial flight direction is given by

$$t_x = \sin\theta \cdot \cos\varphi$$
$$t_y = \sin\theta \cdot \sin\varphi$$
$$t_z = \cos\theta$$

Path Length Sampling

- The probability $p_R(r)dr$ of an interaction between r and $r + dr$ is

$$\begin{aligned} p_{\mathrm{R}}(r)dr &= \frac{1}{I_0}(I(r) - I(r+dr)) \\ &= e^{-\int_0^r \mu(r')dr'} - e^{-\int_0^{r+dr} \mu(r')dr'} \\ &= e^{-\int_0^r \mu(r')dr'}(1 - e^{-\int_r^{r+dr} \mu(r')dr'}) \\ &= e^{-\int_0^r \mu(r')dr'}(1 - e^{-\mu(r)dr}) \\ &= e^{-\int_0^r \mu(r')dr'}\mu(r)dr \end{aligned}$$

- The cumulative probability distribution is

$$P_{\mathrm{R}}(r) = 1 - e^{-\int_0^r dr' \mu(r')}$$

- The path length r is sampled using the inverse transform method:

$$\ln(\xi) \stackrel{!}{=} -\int_0^r dr' \mu(r')$$

Path Length Sampling

Woodcock sampling

- **Numerical inversion of** $\ln(\xi) \stackrel{!}{=} -\int_0^r dr' \mu(r')$ **might be computationally expensive.**
- **Woodcock sampling is a faster alternative:**
  1. **Sample path length according to maximum attenuation (for a single material there is an analytical inverse)**

$$r = r - \frac{1}{\mu_{\max}} \ln(\xi)$$

  2. **Sample uniform random number** ξ**:**

$$\text{if } (\mu(r)/\mu_{\max} < \xi) \text{ goto } 1.$$
$$\text{else return } r$$

Path Length Sampling
Woodcock sampling

- **Numerical inversion of** $\ln(\xi) \stackrel{!}{=} -\int_0^r dr' \mu(r')$ **might be computationally expensive.**
- **Woodcock sampling is a faster alternative:**
  1. **Sample path length according to maximum attenuation (for a single material there is an analytical inverse)**

$$r = r - \frac{1}{\mu_{\max}} \ln(\xi)$$

  2. **Sample uniform random number** ξ**:**

$$\text{if } (\mu(r)/\mu_{\max} < \xi) \text{ goto 1.}$$
$$\text{else return } r$$

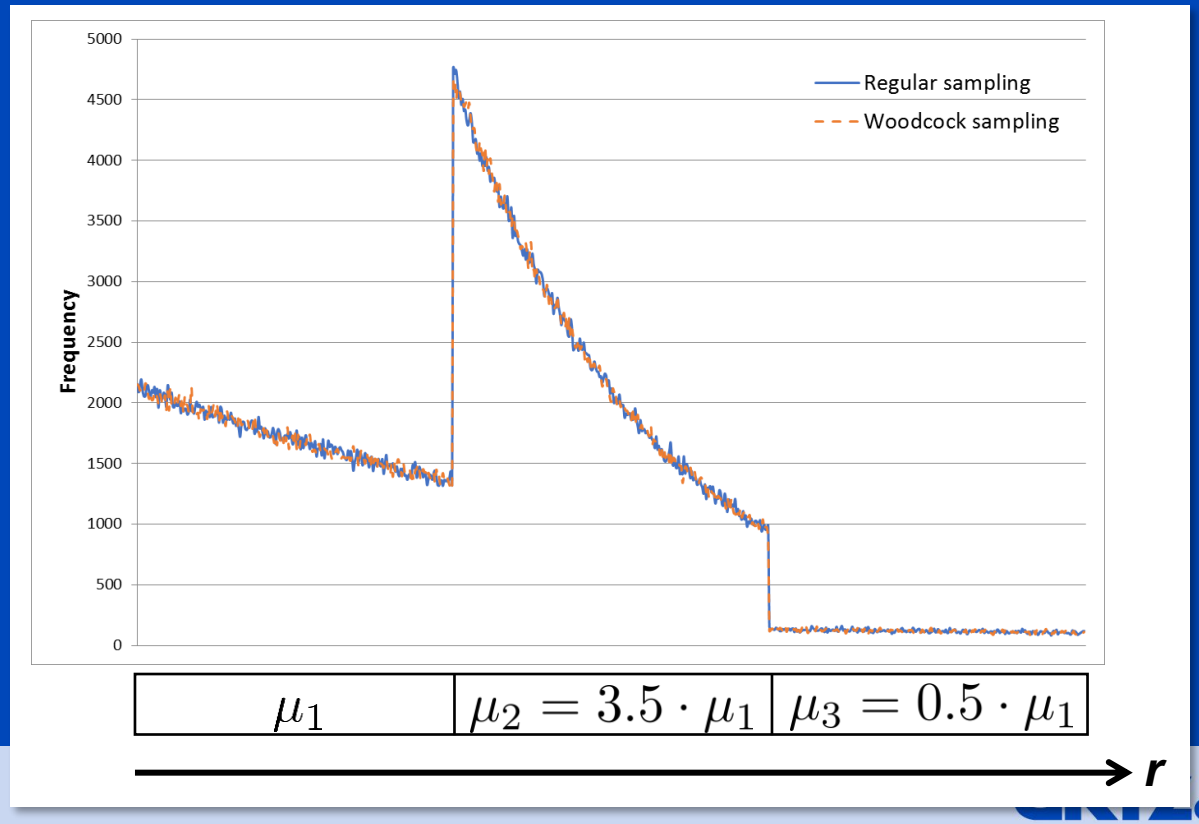

Sampling of Interaction Effect

- Considering x-ray eneries used for medical imaging, there are three relevant interaction effects: photoelectric absorption (P), Compton scattering (C) and Rayleigh scattering (R).
- Interaction probabilities[1]:

$$p_{\mathrm{P}} = \frac{\mu_{\mathrm{P}}}{\mu_{\mathrm{P}} + \mu_{\mathrm{C}} + \mu_{\mathrm{R}}}, \quad p_{\mathrm{C}} = \frac{\mu_{\mathrm{C}}}{\mu_{\mathrm{P}} + \mu_{\mathrm{C}} + \mu_{\mathrm{R}}}, \quad p_{\mathrm{R}} = \frac{\mu_{\mathrm{R}}}{\mu_{\mathrm{P}} + \mu_{\mathrm{C}} + \mu_{\mathrm{R}}}$$

- Cumulative probability:

$$P[3] = \{\ p_{\mathrm{P}}, \quad p_{\mathrm{P}} + p_{\mathrm{C}}, \quad p_{\mathrm{P}} + p_{\mathrm{C}} + p_{\mathrm{R}}\ \}$$

- Sampling:
  - Sample uniform random number ξ:

$$\begin{aligned} \text{if } (\xi \leq P[0]) &: \text{ Photo effect} \\ \text{else if } (\xi \leq P[1]) &: \text{ Compton effect} \\ \text{else if } (\xi \leq P[2]) &: \text{ Rayleigh effect} \end{aligned}$$

[1]Attenuation coefficients can be taken from EPDL library: Cullen D.E., Hubbell J.H., Kissel L. (1997), EPDL97: The Evaluated Photon Data Library, '97 version.

Sampling of Flight Direction

- The polar angle of the flight direction can be sampled using tabulated values of differential cross-sections[1]
- Normalization to unit area allows to interpret the cross-section as probability density function

$$p(\theta) = \frac{\frac{d\sigma}{d\theta}(\theta)}{\int d\theta \, \frac{d\sigma}{d\theta}(\theta)}$$

- Sampling using inverse transform method

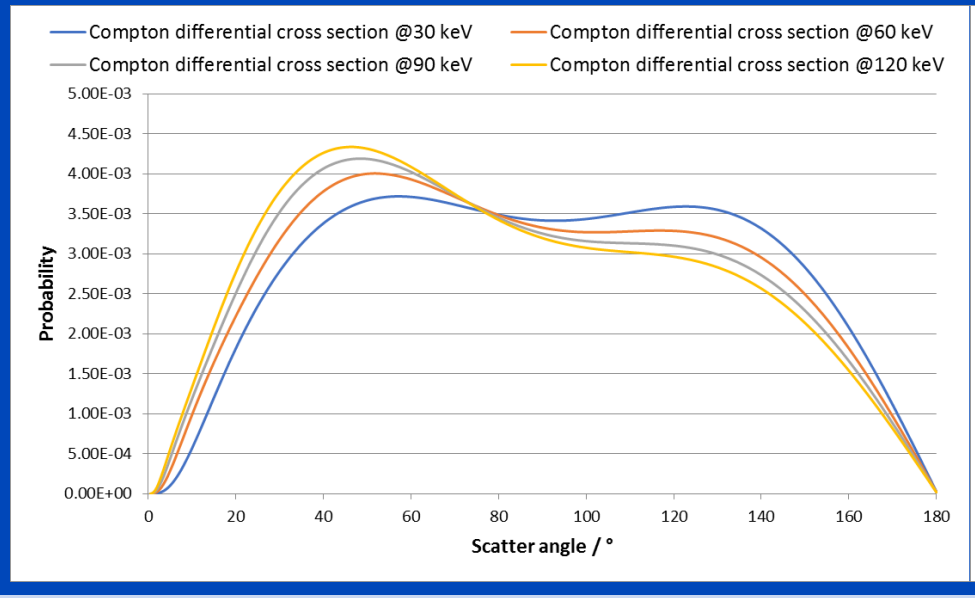

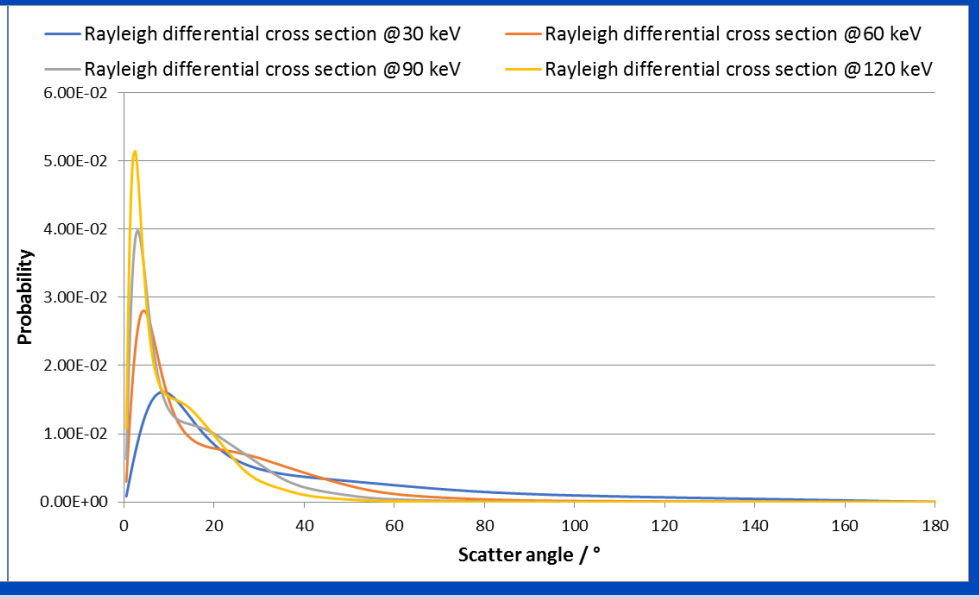

[1]Attenuation coefficients can be taken from EPDL library: Cullen D.E., Hubbell J.H., Kissel L. (1997), EPDL97: The Evaluated Photon Data Library, '97 version.

dkfz.

Updating the X-Ray Energy

- After any interaction, the energy *E* of the x-ray has to be updated ($E \rightarrow E'$) according to the interaction effect.
- Photoelectric effect
  - X-ray is absorbed: $E' = 0$ (neglecting K-escape)
- Compton scattering
  - Klein-Nishina:

$$E' = \frac{E}{1 + \frac{E}{m_e c^2}(1 - \cos\theta)}$$

where θ is the scatter angle with respect to the flight direction.

- Rayleigh scattering
  - Coherent scattering: $E' = E$

Variance Reduction

Biased sampling

- **Sample from a biased probability density function** $p_{\text{biased}}(q)$
- **Assign a weight** w_{bias} **to each particle to correct for the biased sampling:**

$$w_{\text{bias}} \cdot p_{\text{biased}}(q) = p_{\text{real}}(q)$$

- **The MC estimate is given as:**

$$\bar{Q} = \frac{1}{N} \sum_{n}^{N} q_{n,\text{real}} = \frac{1}{N} \sum_{n}^{N} w_{n,\text{bias}} \cdot q_{n,\text{biased}}$$

Variance Reduction

Biased sampling

- Sample from a biased probability density function $p_{\text{biased}}(q)$
- Assign a weight w_{bias} to each particle to correct for the biased sampling:

$$w_{\text{bias}} \cdot p_{\text{biased}}(q) = p_{\text{real}}(q)$$

- The MC estimate is given as:

$$\bar{Q} = \frac{1}{N}\sum_{n}^{N} q_{n,\text{real}} = \frac{1}{N}\sum_{n}^{N} w_{n,\text{bias}} \cdot q_{n,\text{biased}}$$

Example: sampling of initial flight direction of an isotropic emitter

- Real sampling: Sampling of a random angle $\varphi \in [0 : 2\pi]$
- Biased sampling: neglect all x-rays that are blocked by collimator
  → Sample $\varphi \in [0 : a]$

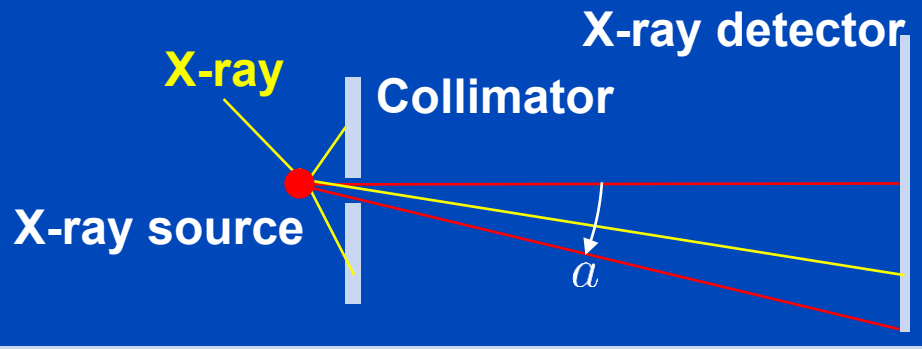

Real pdf: $p_{\text{real}}(\varphi) = \frac{1}{2\pi}$

Biased pdf: $p_{\text{biased}}(\varphi) = \frac{1}{a}$

Weight: $w_{\text{bias}} = \frac{a}{2\pi}$

Variance Reduction

Biased sampling

- Sample from a biased probability density function $p_{\text{biased}}(q)$
- Assign a weight w_{bias} to each particle to correct for the biased sampling:

$$w_{\text{bias}} \cdot p_{\text{biased}}(q) = p_{\text{real}}(q)$$

- The MC estimate is given as:

$$\bar{Q} = \frac{1}{N}\sum_{n}^{N} q_{n,\text{real}} = \frac{1}{N}\sum_{n}^{N} w_{n,\text{bias}} \cdot q_{n,\text{biased}}$$

Example: sampling of the interaction effect

- Real sampling: sampling of photo effect, Compton and Rayleigh scatter.
- Biased sampling: neglect photo effect since absorbed photons do not contribute to the scatter distribution

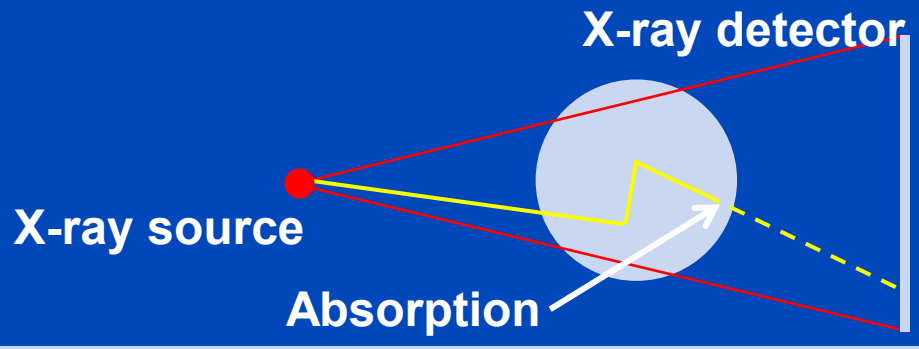

Real pdf: $p_{\text{i, real}} = \dfrac{\mu_i}{\mu_P + \mu_C + \mu_R}$

Biased pdf: $p_{\text{i, biased}} = \dfrac{\mu_i}{\mu_C + \mu_R}$

Weight: $w_{\text{bias}} = \dfrac{\mu_C + \mu_R}{\mu_P + \mu_C + \mu_R}$

Variance Reduction

Biased sampling

- Sample from a biased probability density function $p_{\text{biased}}(q)$
- Assign a weight w_{bias} to each particle to correct for the biased sampling:

$$w_{\text{bias}} \cdot p_{\text{biased}}(q) = p_{\text{real}}(q)$$

- The MC estimate is given as:

$$\bar{Q} = \frac{1}{N}\sum_{n}^{N} q_{n,\text{real}} = \frac{1}{N}\sum_{n}^{N} w_{n,\text{bias}} \cdot q_{n,\text{biased}}$$

Example: sampling of path lengths

- Real sampling: sampling from exponential distribution.
- Biased sampling: sampling from uniform distribution to increase number of interactions at higher depth

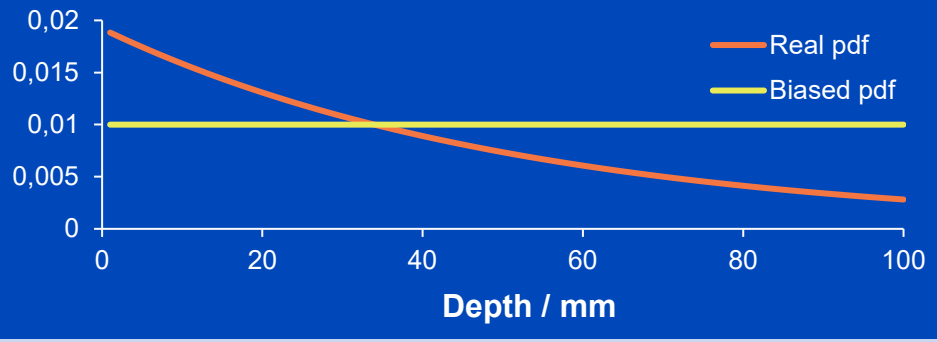

Real pdf: $p_{\text{real}}(r) = \mu \cdot e^{-\mu \cdot r}$

Biased pdf: $p_{\text{biased}}(r) = \frac{1}{r_{\max} - r_{\min}}$

Weight: $w_{\text{bias}}(r) = (r_{\max} - r_{\min})\mu \cdot e^{-\mu \cdot r}$

dkfz.

Variance Reduction

Particle splitting / Russian roulette

- **Particle splitting**
  - Split photon into *N* photons if it moves towards a region of interest (e.g. to the detector).
  - Assign a weight of $w_{\mathrm{split}} = \frac{w_0}{N}$ to each split photon.
- **Russian roulette**
  - Kill a photon with probability *K* if it moves away from the region of interest (i.e. to the detector).
  - Assign a weight of $w_{\mathrm{RR}} = \frac{1}{1-K}$ if the photon survives the Russian roulette.

Variance Reduction

Forced Detection

- X-ray may leave the volume without hitting the detector → Simulated track does not contribute to the
- Score the probability of hitting the detector at every interaction point
- Apply a weight that corresponds to this probability

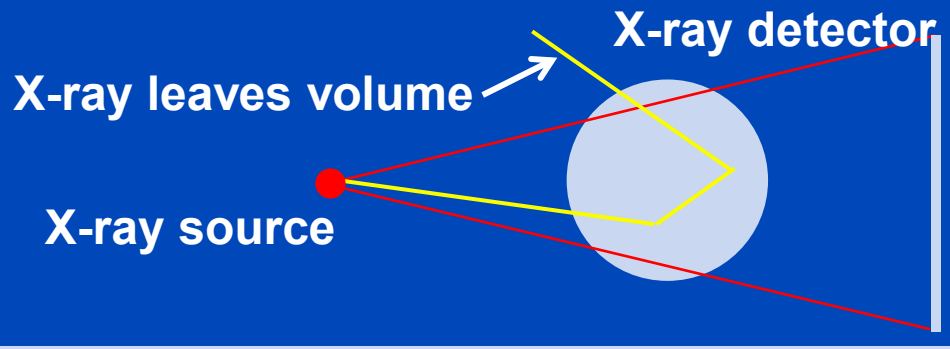

Literature

- Bank, D.: P ENELOPE – A Code System for Monte Carlo Simulation of Electron and Photon Transport A Code System for Monte Carlo. (2001)
- James, F.: Monte Carlo theory and practice. Reports Prog. Phys. 43, 1145–1189 (1980).
- Mainegra-Hing, E., Kawrakow, I.: Variance reduction techniques for fast Monte Carlo CBCT scatter correction calculations. Phys. Med. Biol. 55, 4495–4507 (2010).

Fast, but not very accurate

KERNEL-BASED SCATTER ESTIMATION

Kernel-Based Scatter Estimation

2D scatter kernels
(low complexity)

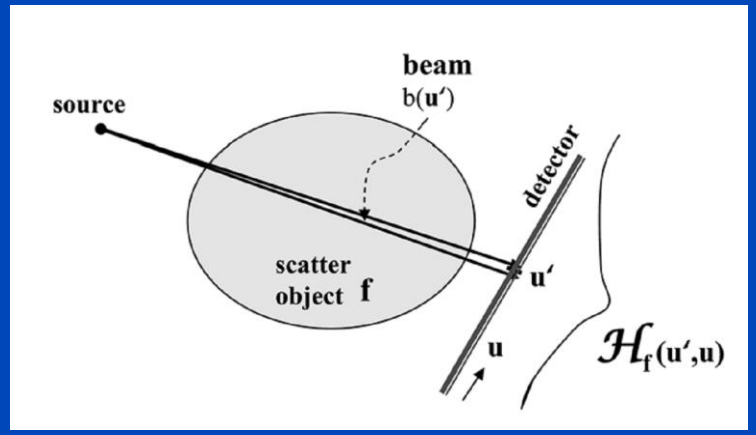

$$S(\boldsymbol{u}) = \int d^2\hat{u}\, T\big(I(\hat{\boldsymbol{u}})\big) K_{\boldsymbol{c}}(\boldsymbol{u}, \hat{\boldsymbol{u}})$$

3D scatter kernels
(high complexity)

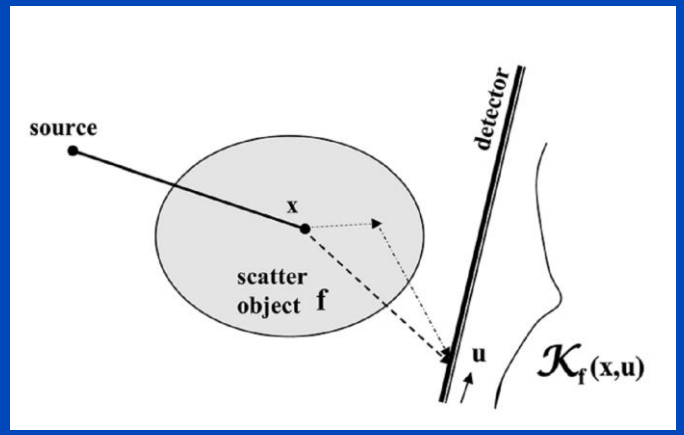

$$S(\boldsymbol{u}) = \int d^3 r\, T\big(I(\boldsymbol{r})\big) K_{\boldsymbol{c}}(\boldsymbol{u}, \boldsymbol{r})$$

- **The intensities (typically primary plus scatter) I, either at the detector or in the volume, undergo a pointwise transfer function T, also known as the scatter potential. Then they are convolved with the scatter kernel.**
- **The scatter kernels *K* may be shift variant (general case) or shift invariant (special case) and they depend on many parameters *c*, such as the tube voltage, projection angle, object size and composition, scatter geometry, anti scater grids, …**

2D (Beam Spread) Scatter Kernels

- **Typical scatter potentials**

$$T(I) = I_0$$

$$T(I) = I$$

$$T(I) = -\frac{I}{I_0} \ln \frac{I}{I_0} = pe^{-p}$$

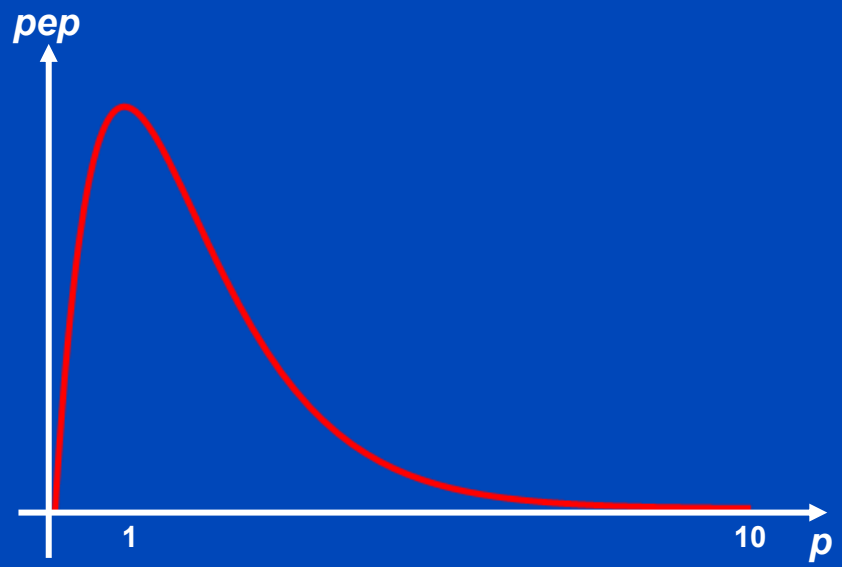

- **Typical scatter kernels**
  - Shift invariant scatter kernels, e.g. Gaussian, sum of Gaussians, exponentials …
  - Shift variant kernels
    - » Kernels as a function of the water equivalent thickness at both points
    - » Kernels can be Gaussian, exponential, sums thereof, …
  - Asymmetric kernels

PEP

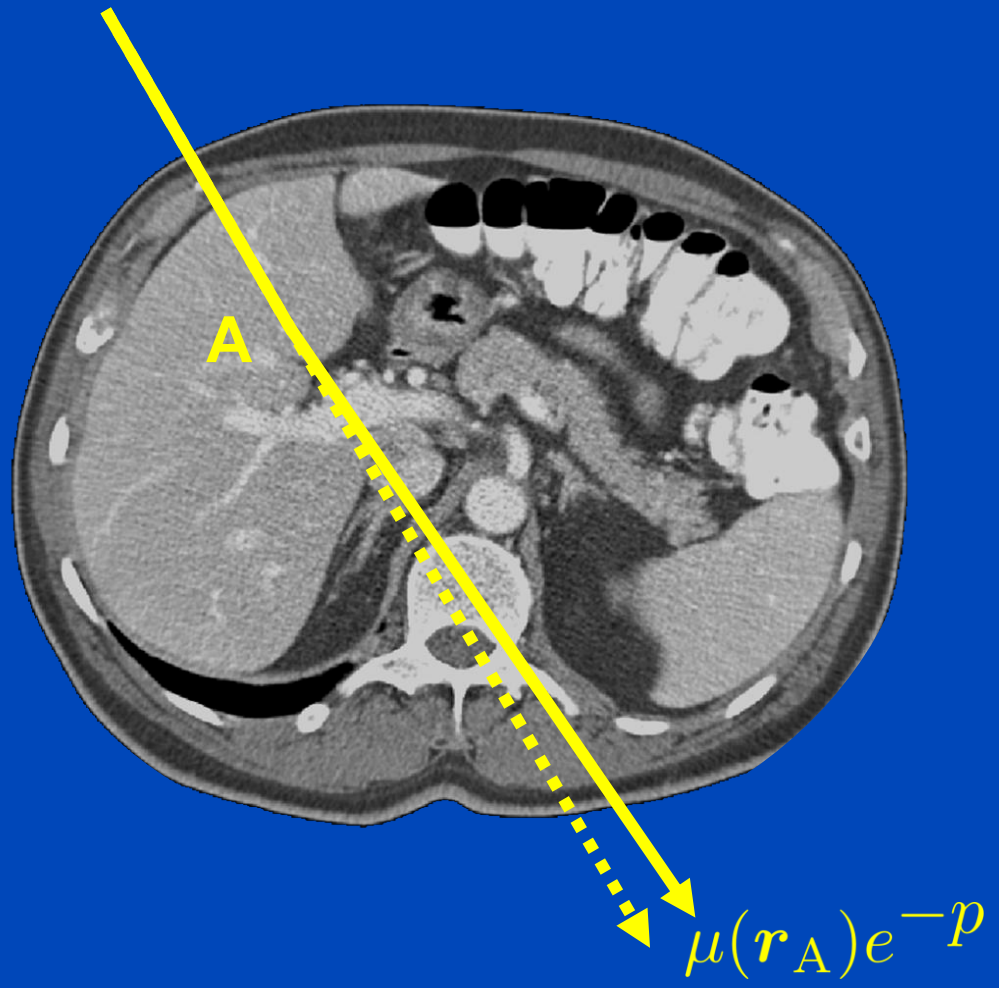

PEP

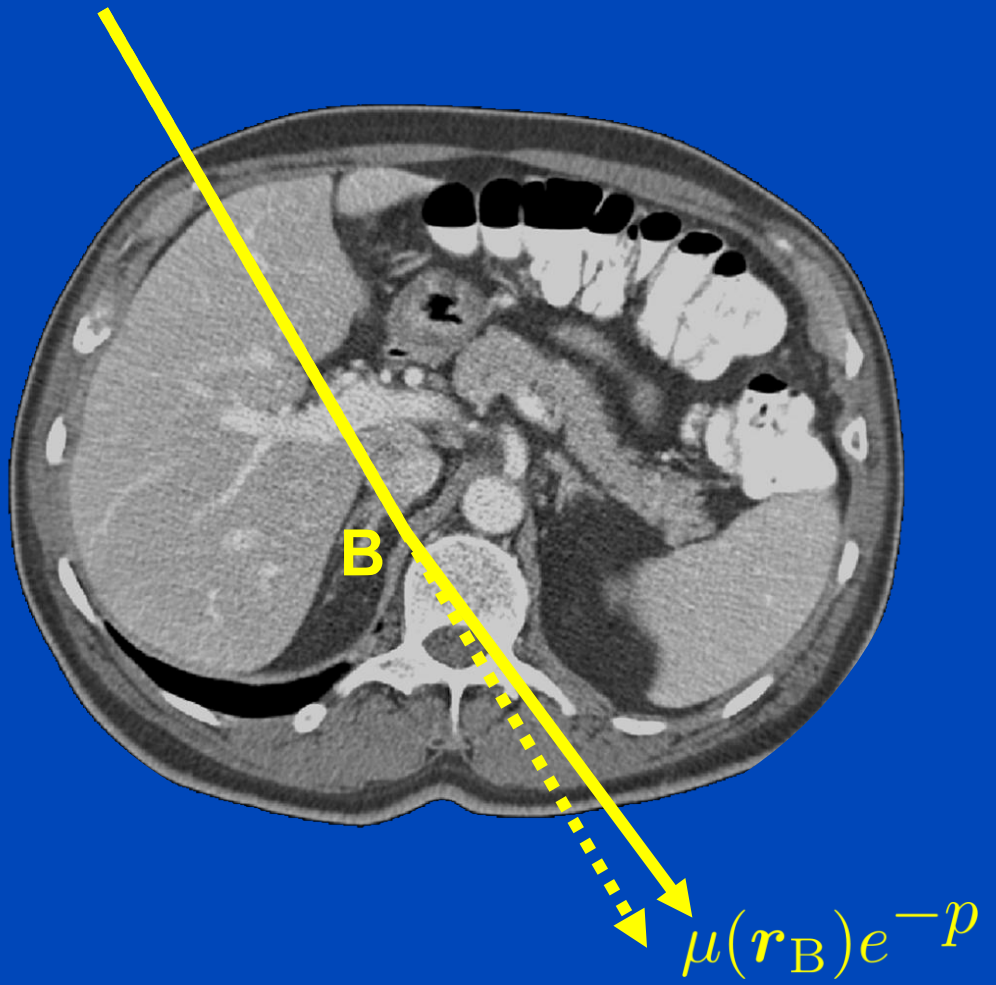

PEP

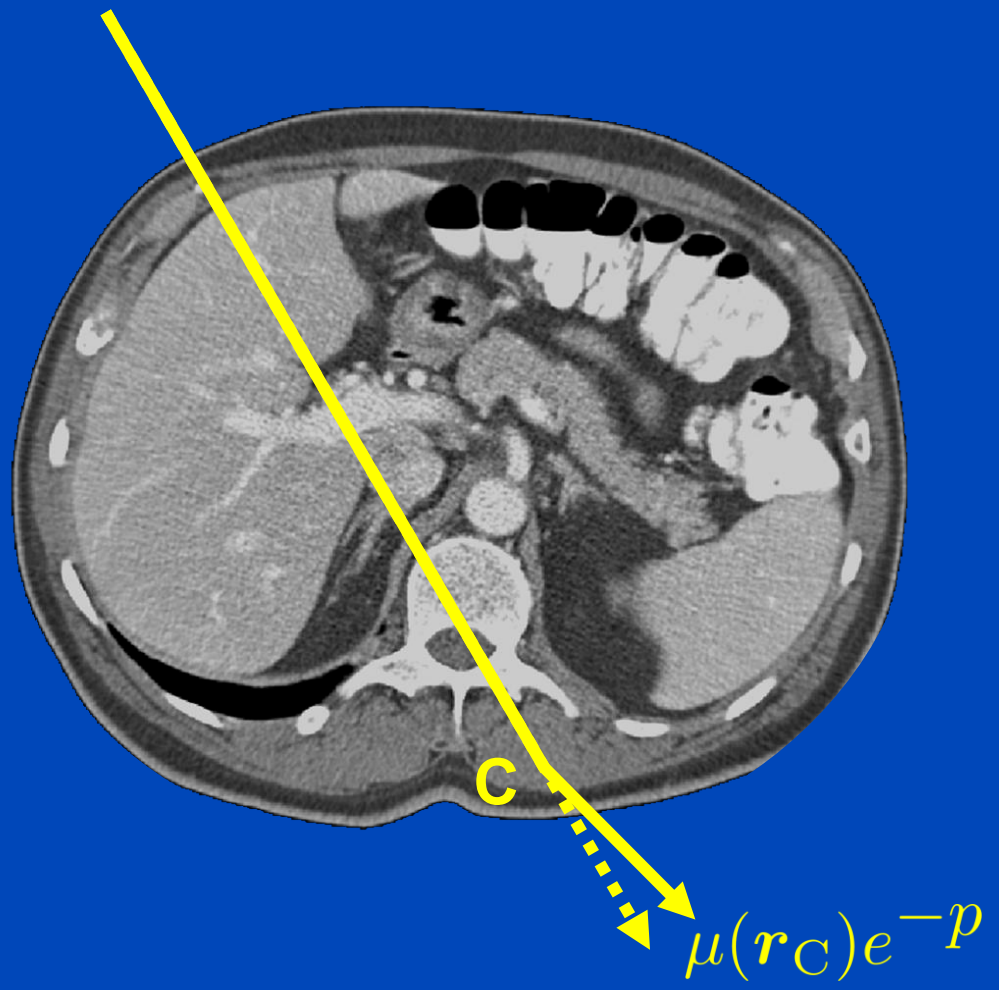

PEP

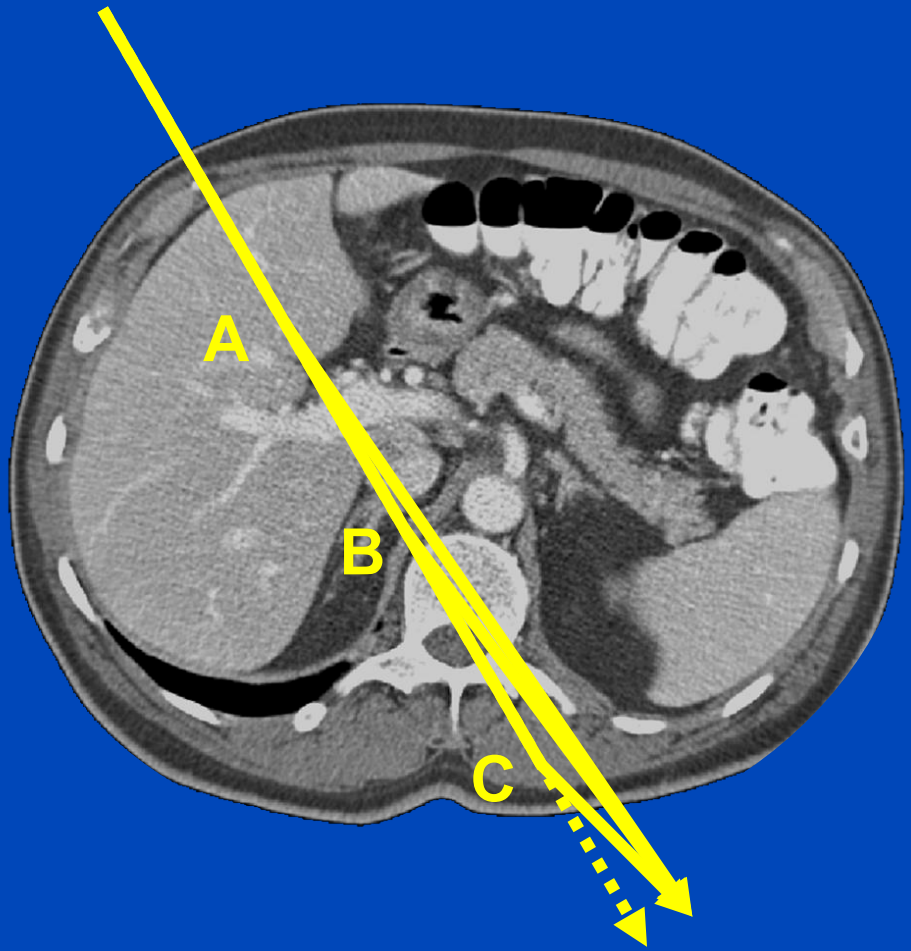

$$\big(\mu(\boldsymbol{r}_\mathrm{A}) + \mu(\boldsymbol{r}_\mathrm{B}) + \mu(\boldsymbol{r}_\mathrm{C})\big)e^{-p} = p\,e^{-p}$$

PEP for CT

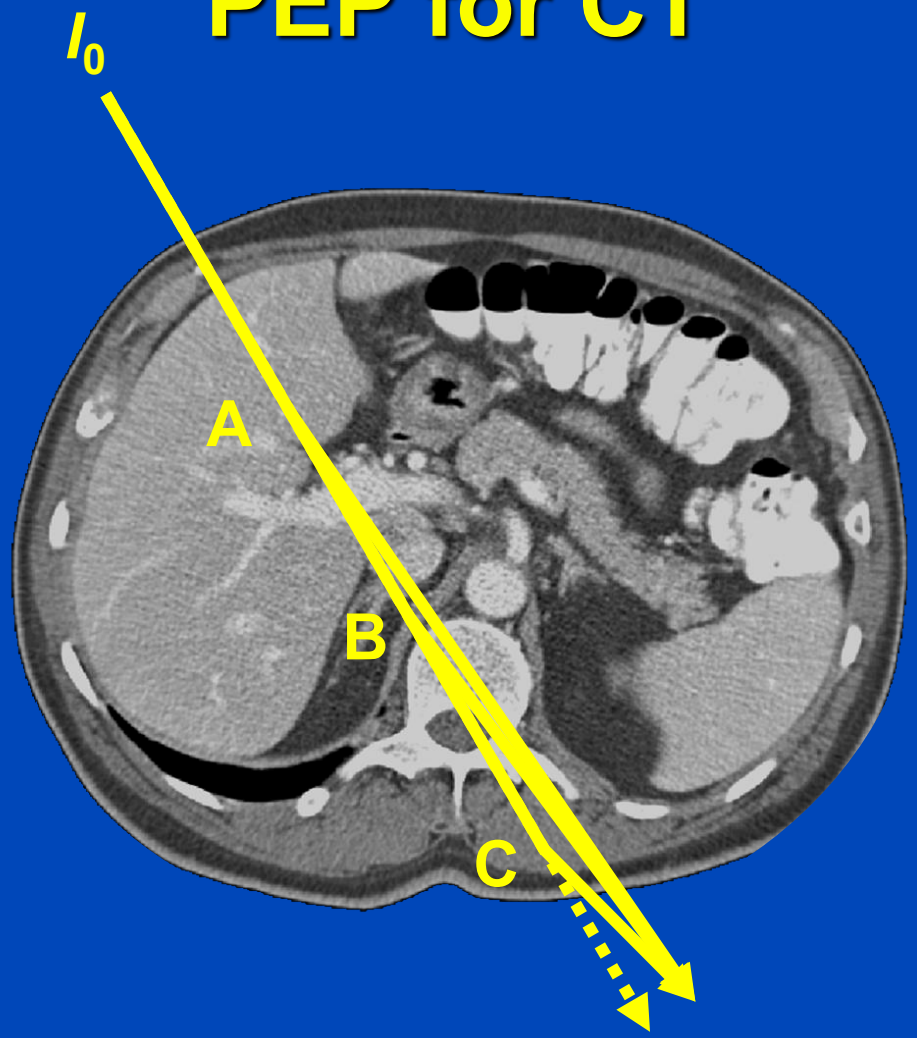

$$I_0\big(\mu(\boldsymbol{r}_\mathrm{A}) + \mu(\boldsymbol{r}_\mathrm{B}) + \mu(\boldsymbol{r}_\mathrm{C})\big)e^{-p} = I_0\, p\, e^{-p}$$

PEP for PET

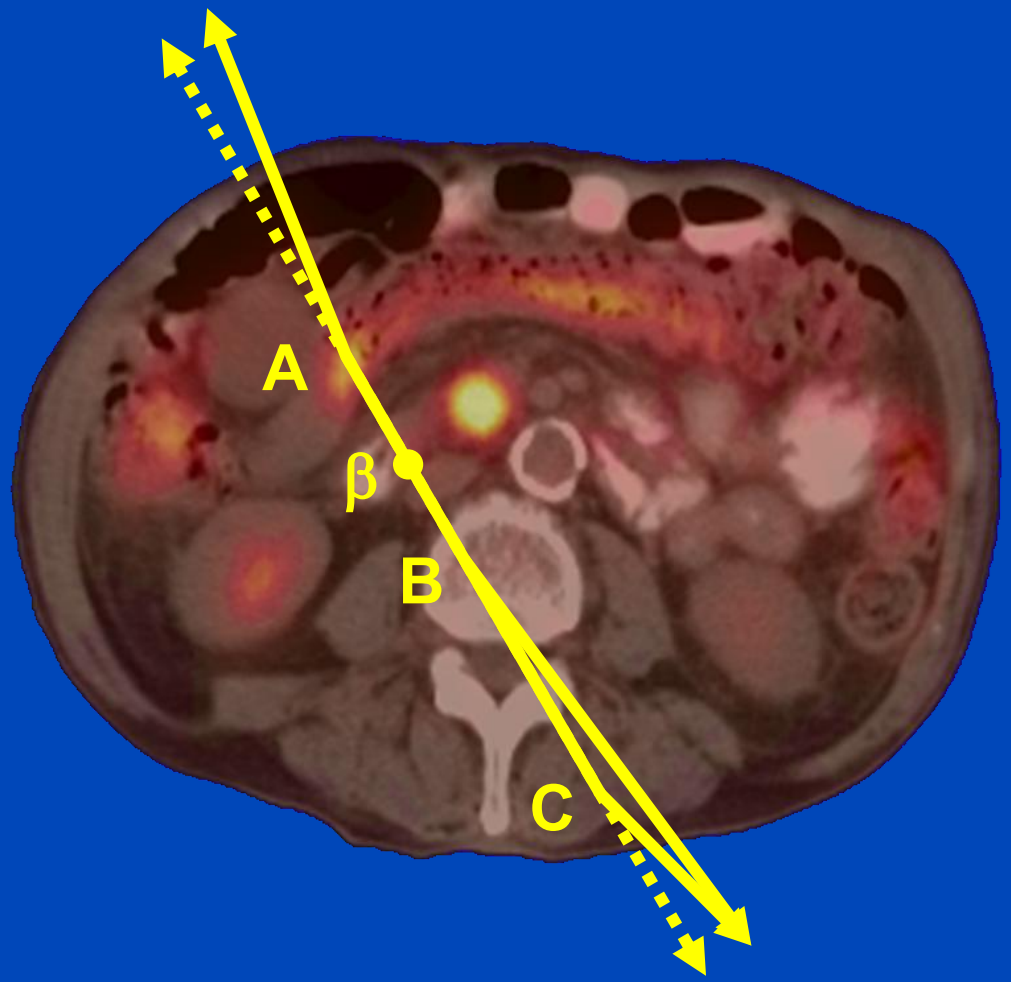

$$a(\boldsymbol{r}_\beta)\big(\mu(\boldsymbol{r}_\mathrm{A}) + \mu(\boldsymbol{r}_\mathrm{B}) + \mu(\boldsymbol{r}_\mathrm{C})\big)e^{-p} = a(\boldsymbol{r}_\beta)\,p\,e^{-p}$$

PEP for PET

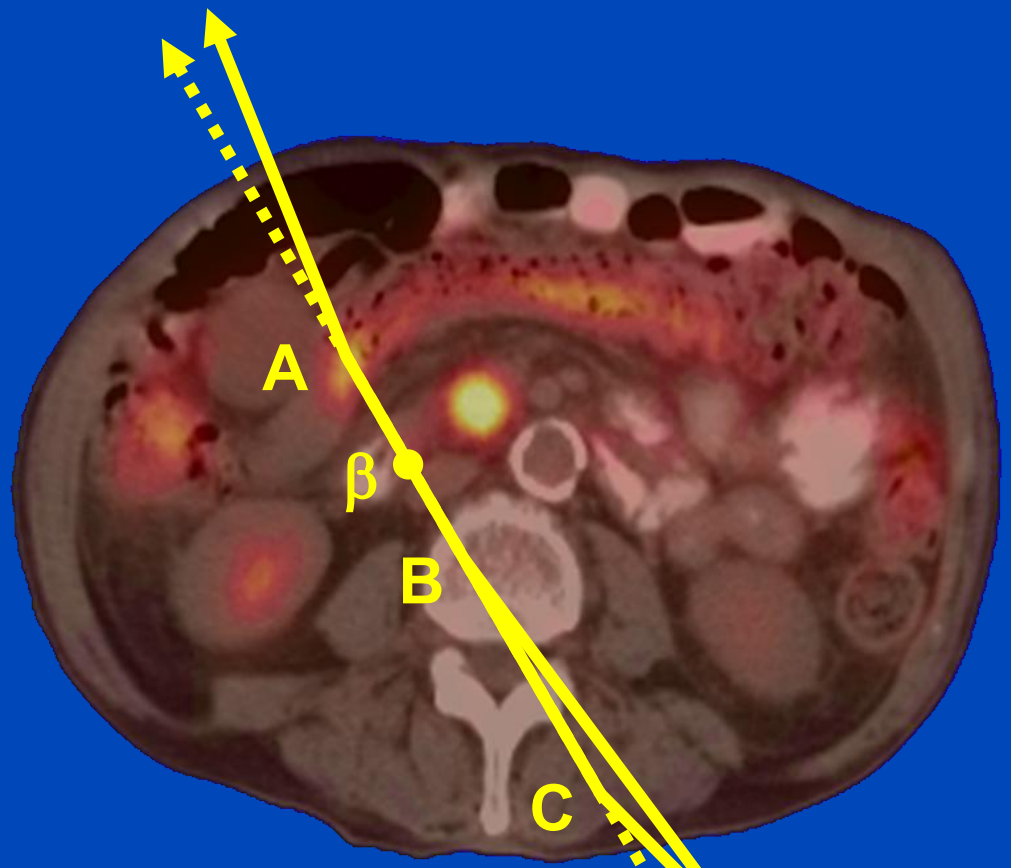

$$\sum_{\mathrm{LOR}} a(\boldsymbol{r})\, p\, e^{-p}$$

HYBRID SCATTER CORRECTION

IOP Publishing Physics in Medicine and Biology

Phys. Med. Biol. **57** (2012) 6849–6867 doi:10.1088/0031-9155/57/21/6849

Hybrid scatter correction for CT imaging

Matthias Baer[1,2] **and Marc Kachelrieß**[1,2]

[1] Institute of Medical Physics (IMP), University of Erlangen–Nürnberg, Henkestr. 91, D-91052 Erlangen, Germany
[2] German Cancer Research Center (DKFZ), Im Neuenheimer Feld 280, D-69120 Heidelberg, Germany

E-mail: matthias.baer@imp.uni-erlangen.de

Received 4 April 2012, in final form 17 July 2012
Published 5 October 2012
Online at stacks.iop.org/PMB/57/6849

Abstract

The purpose of this study was to develop and evaluate the hybrid scatter correction algorithm (HSC) for CT imaging. Therefore, two established ways to perform scatter correction, i.e. physical scatter correction based on Monte

Scatter Estimation

Monte Carlo-based

Measured intensities (primary plus scatter)

Reconstruction

Simulation of physical photon paths based on density and material distribution

Physical effects:
Photo effect
Compton scattering
Rayleigh scattering

Monte Carlo-based scatter estimate $\hat{I}_{\mathrm{s}}^{\mathrm{MC}}$

Patient-specific, many computations

Convolution-based

Measured intensities (primary plus scatter)

$$\hat{I}_{\mathrm{s}}^{\mathrm{CB}}(\boldsymbol{c}) = \Phi(I_{\mathrm{ps}}, \boldsymbol{c}) * K(\boldsymbol{c})$$

Convolution of the scatter potential Φ with scatter kernel K

I_{ps}: Primary plus scatter intensity

c (vector): Open coefficients

We used the convolution-based method of Ohnesorge et al.*

Convolution-based scatter estimate $\hat{I}_{\mathrm{s}}^{\mathrm{CB}}$

Not patient-specific, few computations

* Ohnesorge et al., Efficient scatter correction algorithm for third and fourth generation CT scanners, Eur. Radiol. 9:563-569, 1999.

dkfz.

Hybrid Scatter Correction

Measured intensities (Primary plus scatter)

Uncorrected

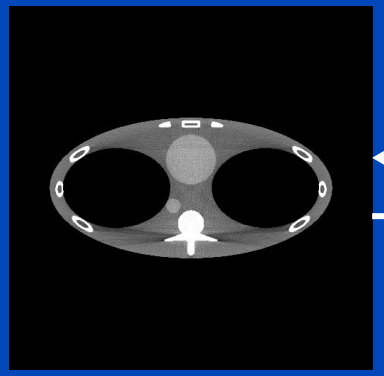

Reconstruct initial uncorrected CT image

Coarse Monte Carlo simulation

Noisy Monte Carlo scatter estimate $\hat{I}_{\mathrm{s}}^{\mathrm{MC}}$

Calibrate the open coefficients in the convolution−based model

$$\boldsymbol{c} = \arg\min_{\boldsymbol{c}} \int_{\text{Detector}} d\chi \left(\hat{I}_{\mathrm{s}}^{\mathrm{MC}}(\chi) - \hat{I}_{\mathrm{s}}^{\mathrm{CB}}(\chi, \boldsymbol{c})\right)^2$$

Compute scatter estimate with the convolution−based model

Convolution−based scatter estimate $\hat{I}_{\mathrm{s}}^{\mathrm{CB}}$

Subtract scatter from measured intensities and reconstruct corrected image

Corrected

M. Baer and M. Kachelrieß. Hybrid scatter correction for CT imaging. Phys. Med. Biol. 57(21):6849-6867, October 2012.

dkfz.

Number of Calibration Steps

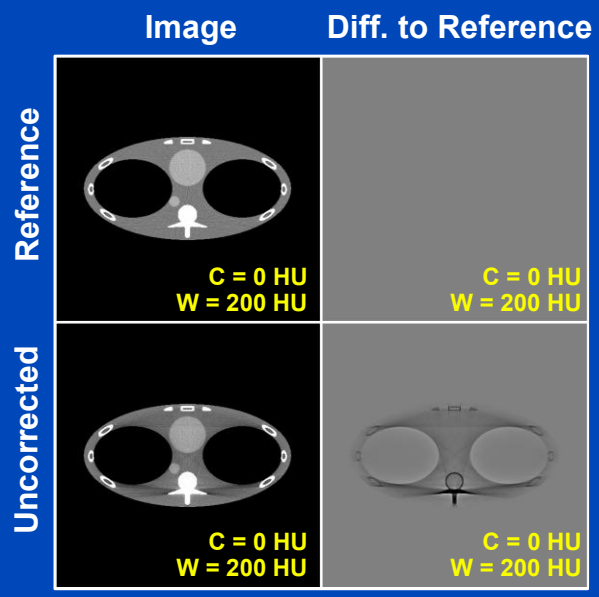

Monochromatic simulation study in clinical CT geometry
Scatter simulation by Monte Carlo

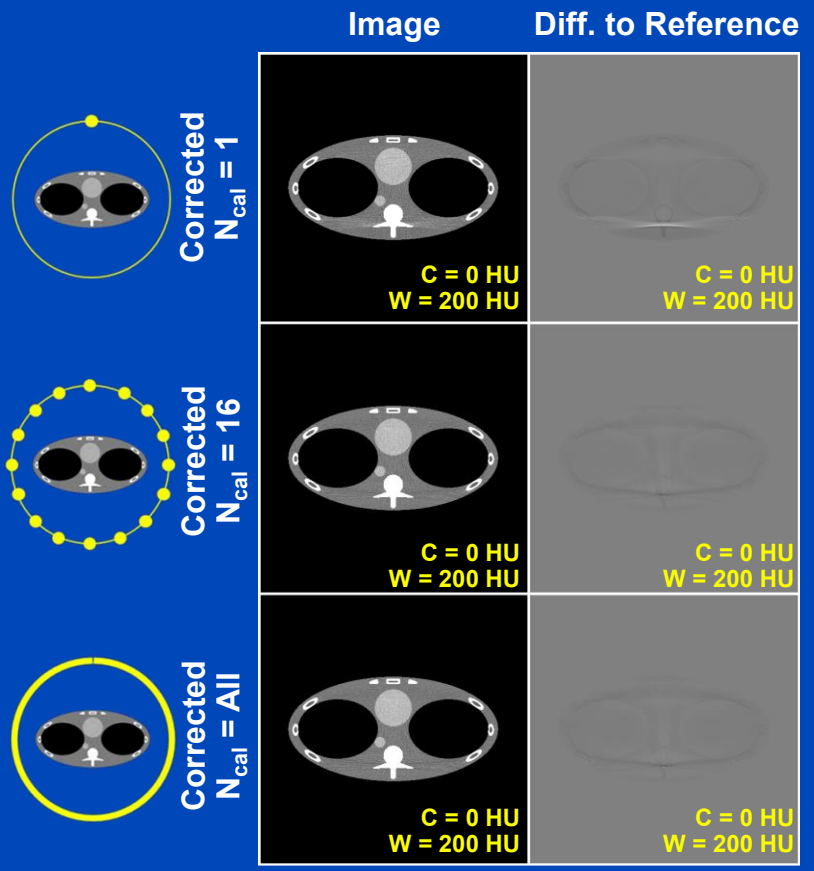

M. Baer and M. Kachelrieß. Hybrid scatter correction for CT imaging. Phys. Med. Biol. 57(21):6849-6867, October 2012.

dkfz.

Number of Photons

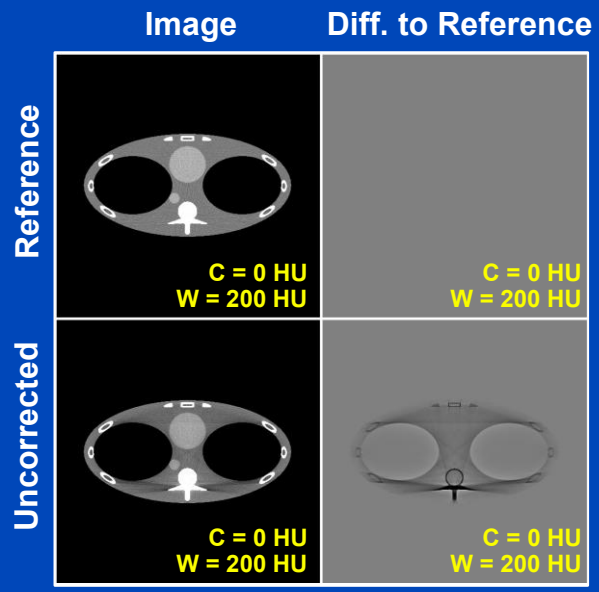

Monochromatic simulation study in clinical CT geometry
Scatter simulation by Monte Carlo

$N_{Ph,ref}$: Photon number for the low noise reference Monte Carlo simulation used for the uncorrected image

N_{cal} = 16

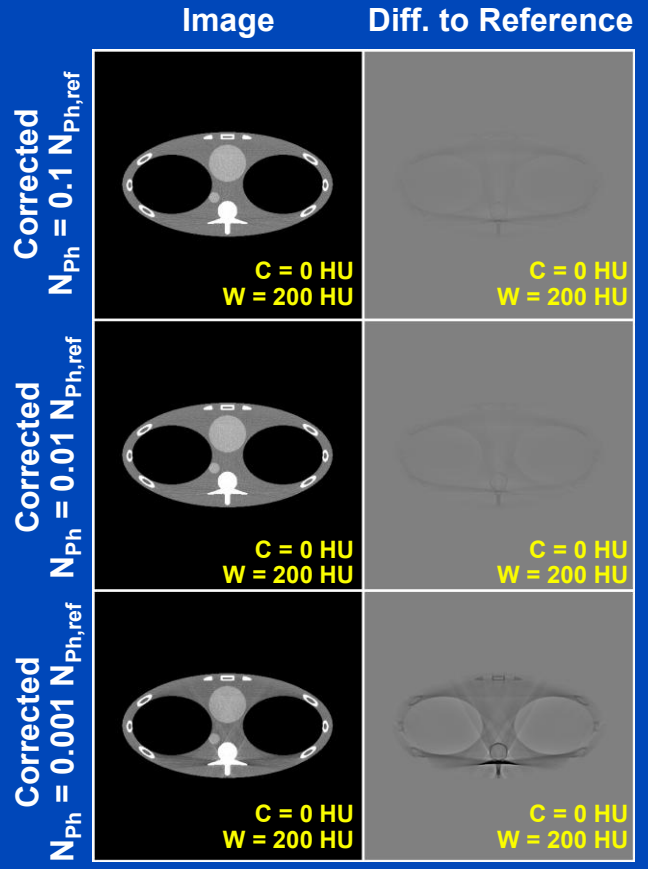

M. Baer and M. Kachelrieß. Hybrid scatter correction for CT imaging. Phys. Med. Biol. 57(21):6849-6867, October 2012.

dkfz.

Scatter Correction Results

- Measurements in cone-beam CT geometry
- Reference image:
  - Monte Carlo scatter correction and EBHC for beam hardening.
- Hybrid scatter correction (HSC):
  - Monte Carlo simulation for only 16 projections and 100 times less photons than in the reference Monte Carlo correction.
- HSC+EBHC:
  - Here we additionally applied the empirical beam-hardening correction (EBHC).

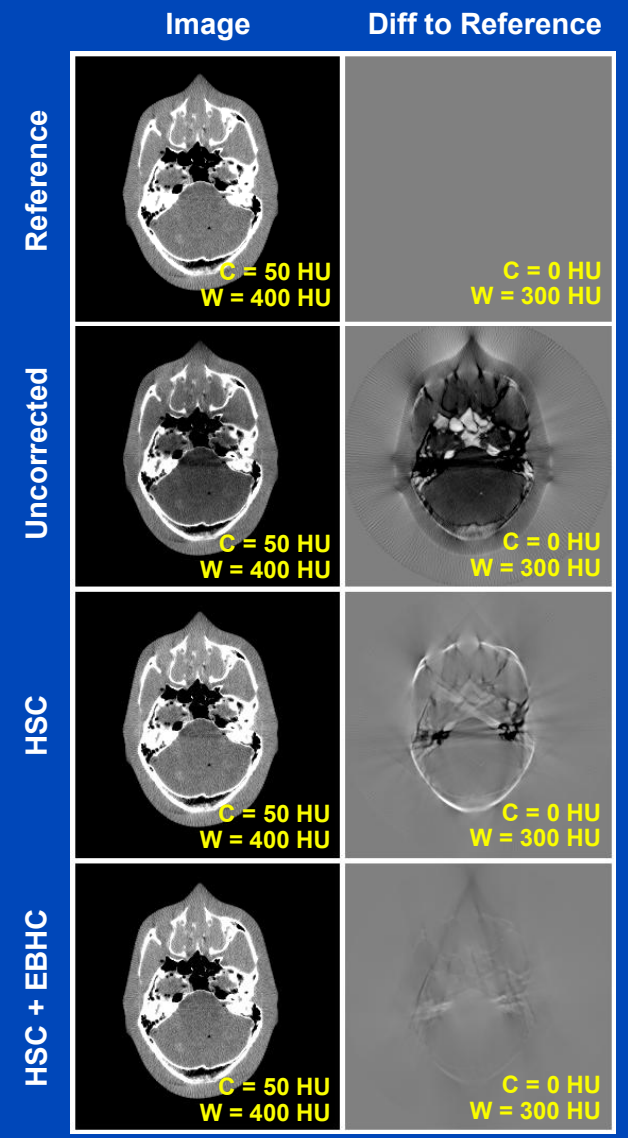

Scatter is Smooth only in Intensity Domain!

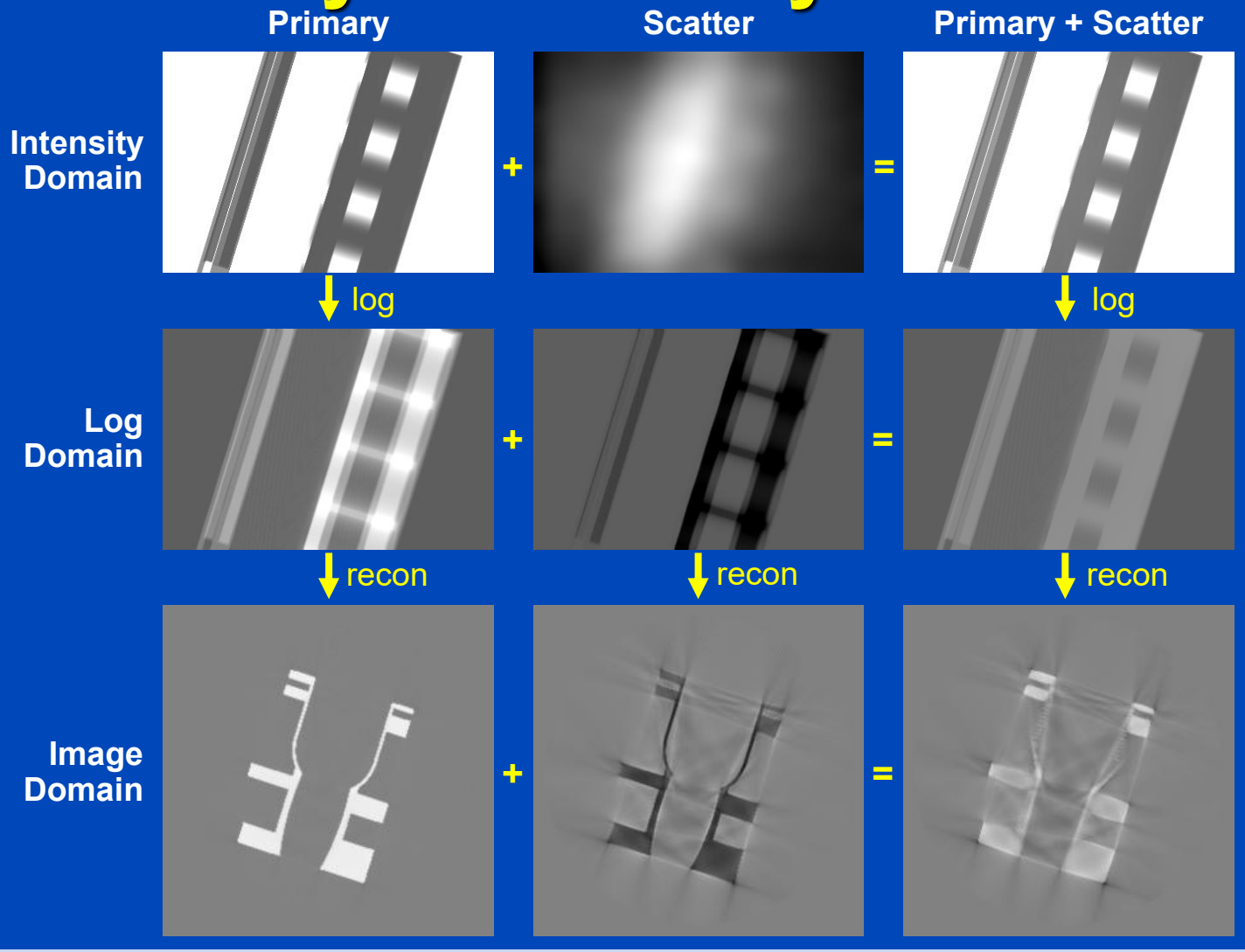

Scatter is Smooth only in Intensity Domain!

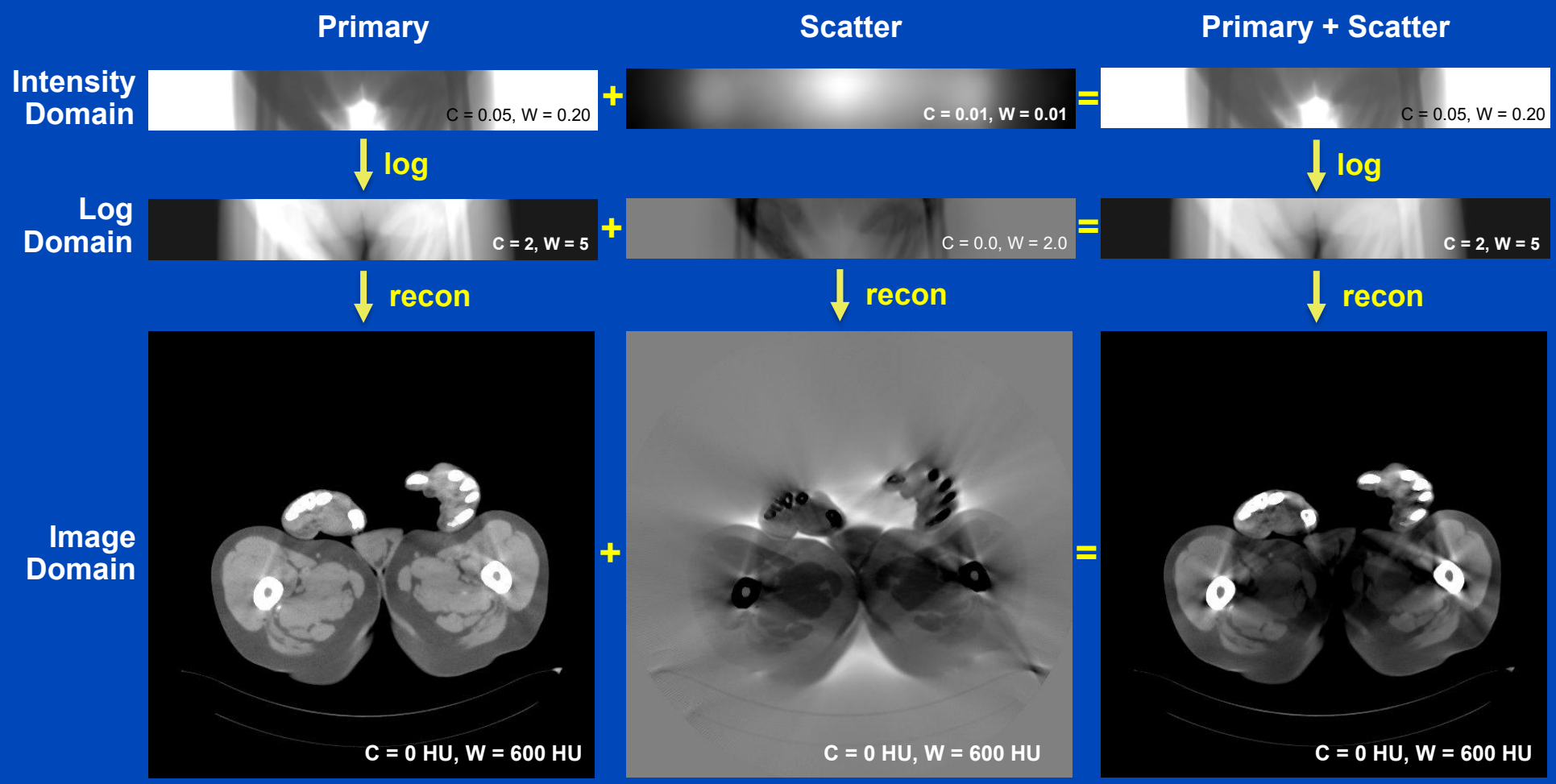

Scatter is Smooth only in Intensity Domain!

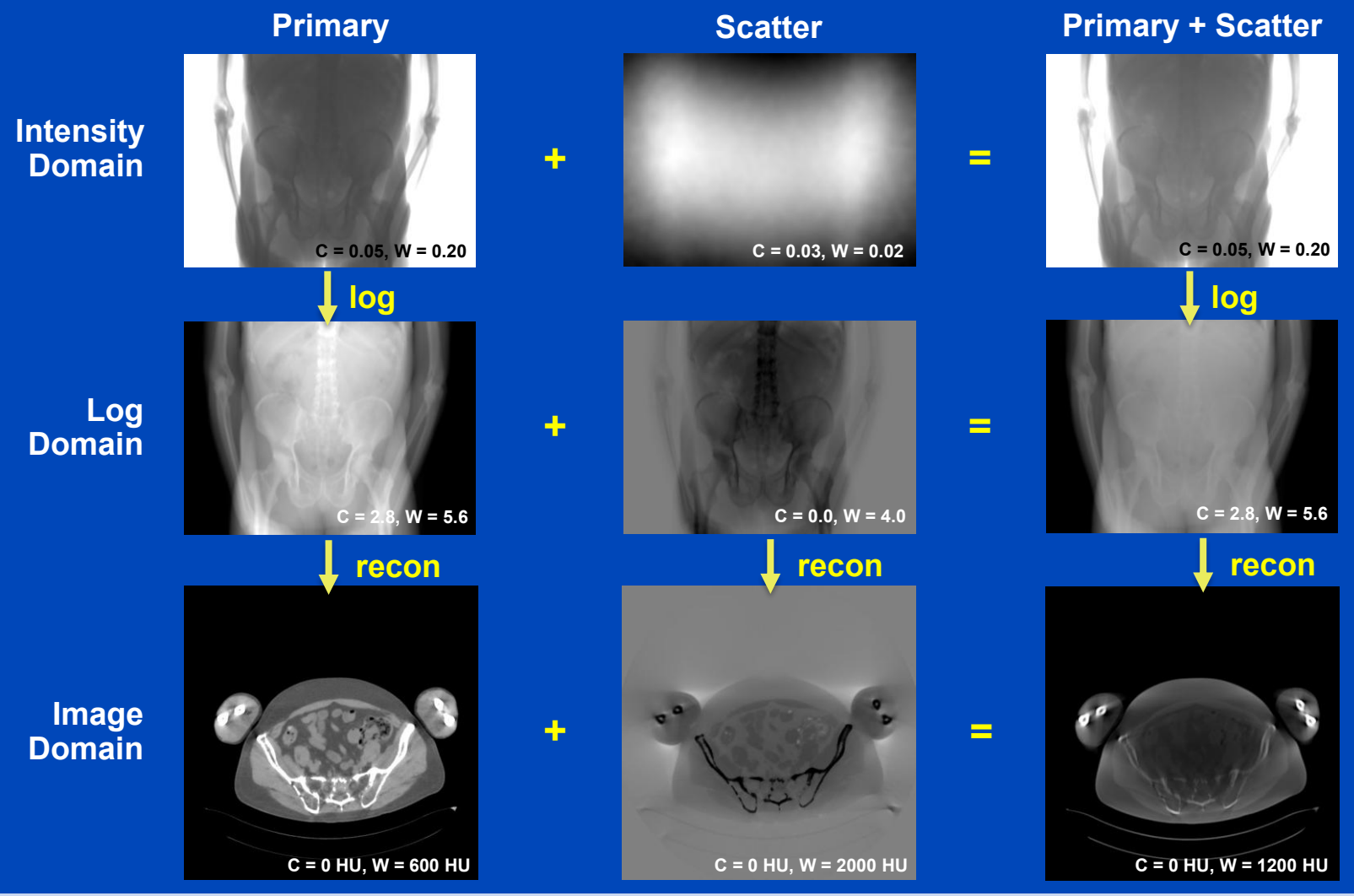

Further Reading

- Wei Zhao, Don Vernekohl, Jun Zhu, Luyao Wang, and Lei Xing. A model-based scatter artifacts correction for cone beam CT. Medical Physics 43 (1736), March2016.
- Ernst-Peter Rührnschopf and Klaus Klingenbeck. A General Framework and Review of Scatter Correction Methods in X-Ray Cone-Beam Computerized Tomography. Part 1: Scatter Compensation Approaches. Med. Phys. 38(7):4296-4311, July 2011.
- Ernst-Peter Rührnschopf and Klaus Klingenbeck. A General Framework and Review of Scatter Correction Methods in X-Ray Cone-Beam Computerized Tomography. Part 2: Scatter Estimation Approaches. Med. Phys. 38(9):5186-5199, September 2011.

Real-time scatter estimation with highest accuracy

DEEP SCATTER ESTIMATION (DSE)

Motivation

- X-ray scatter is a major cause of artifacts in CT and CBCT.
- Appropriate scatter correction is crucial to maintain the diagnostic value of the CT examination.

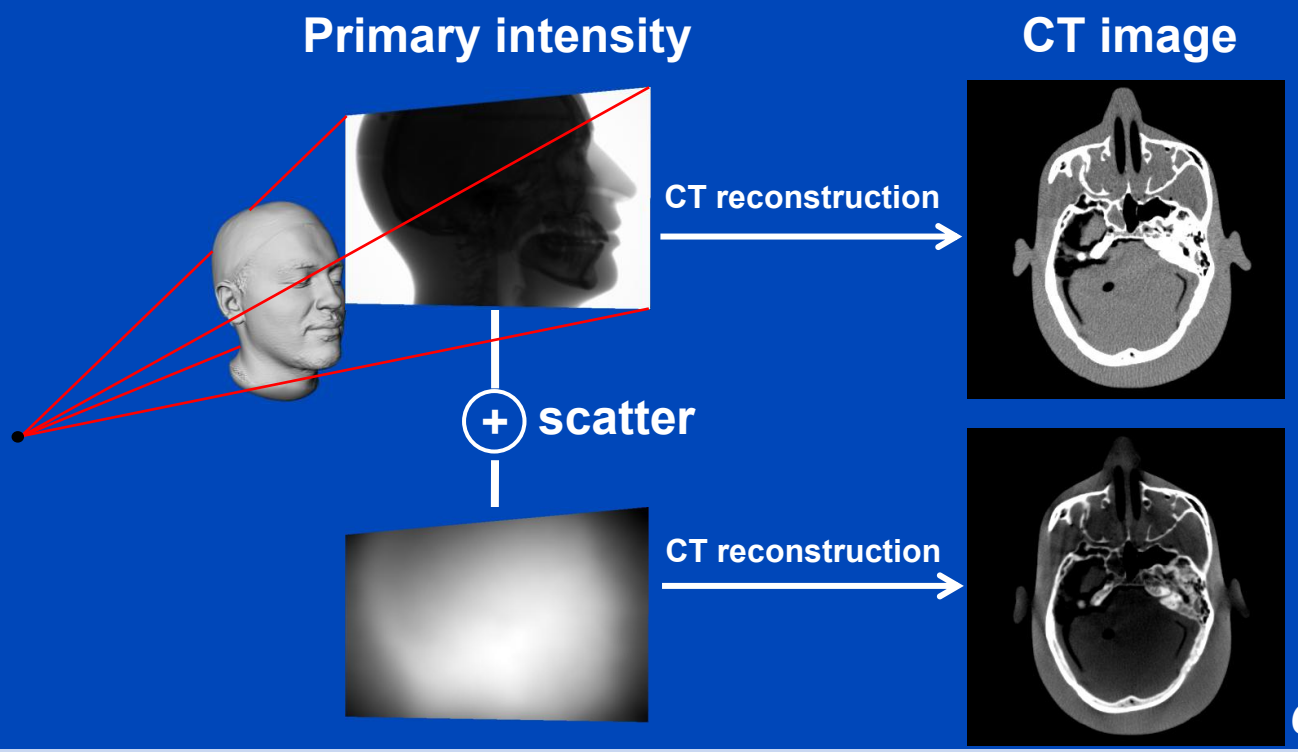

Scatter Correction

Scatter suppression

- Anti-scatter grids
- Collimators
- …

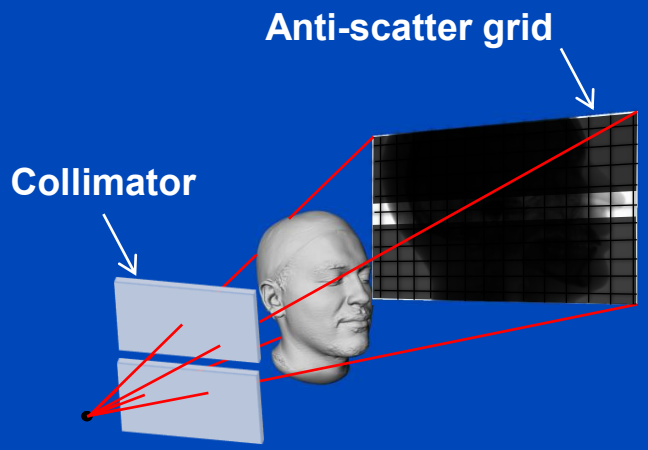

Scatter estimation

- Monte Carlo simulation
- Kernel-based approaches
- Boltzmann transport
- Primary modulation
- Beam blockers
- …

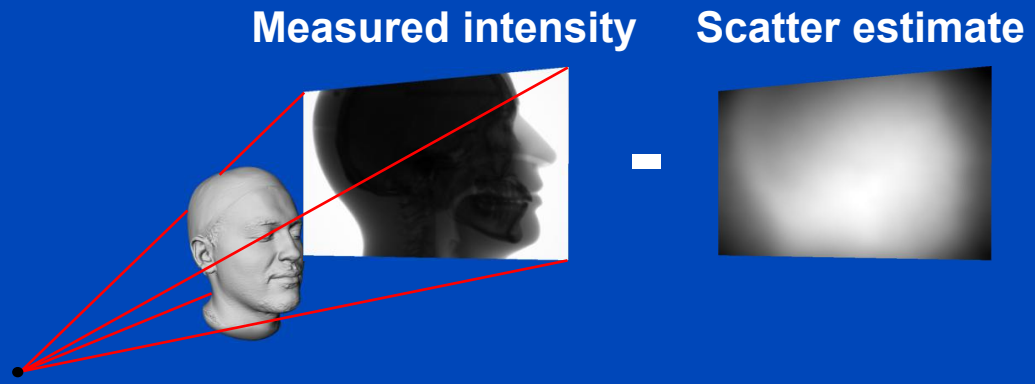

Monte Carlo Scatter Estimation

- Simulation of photon trajectories according to physical interaction probabilities.
- Simulating a large number of photon t… approximates the actual scatter distrib…

1 to 10 hours
per tomographic data set

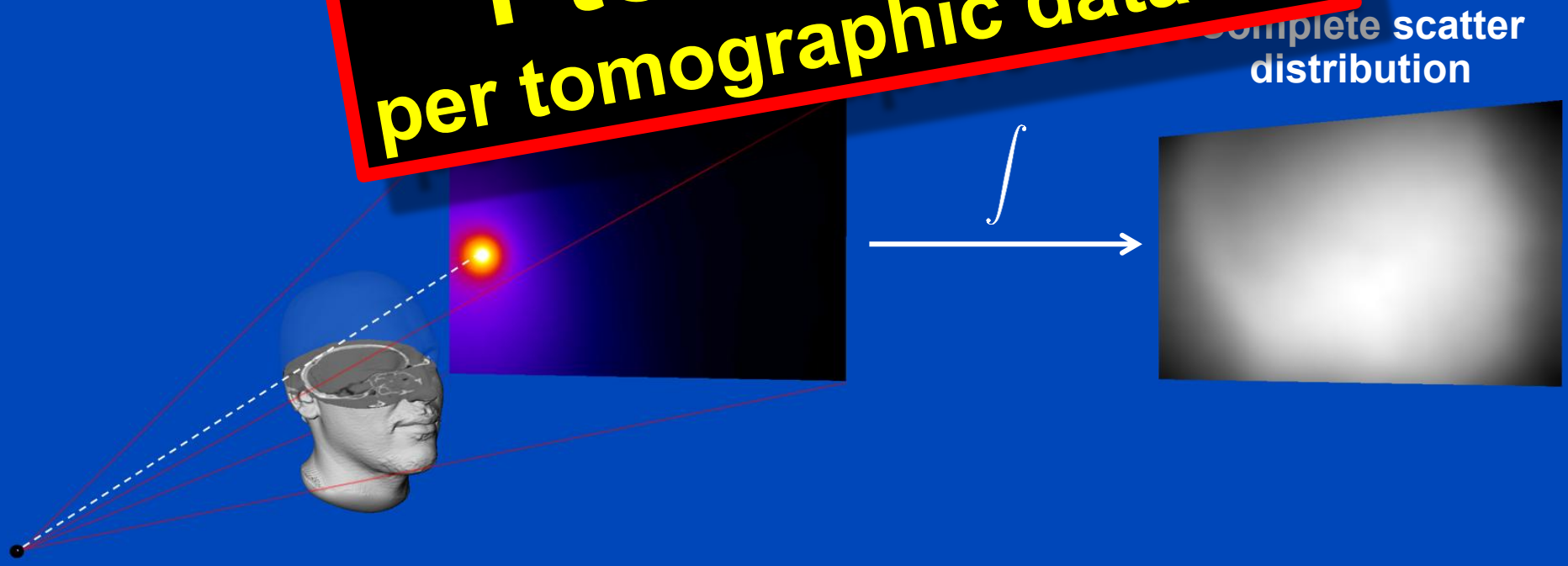

Deep Scatter Estimation

Network architecture & scatter estimation framework

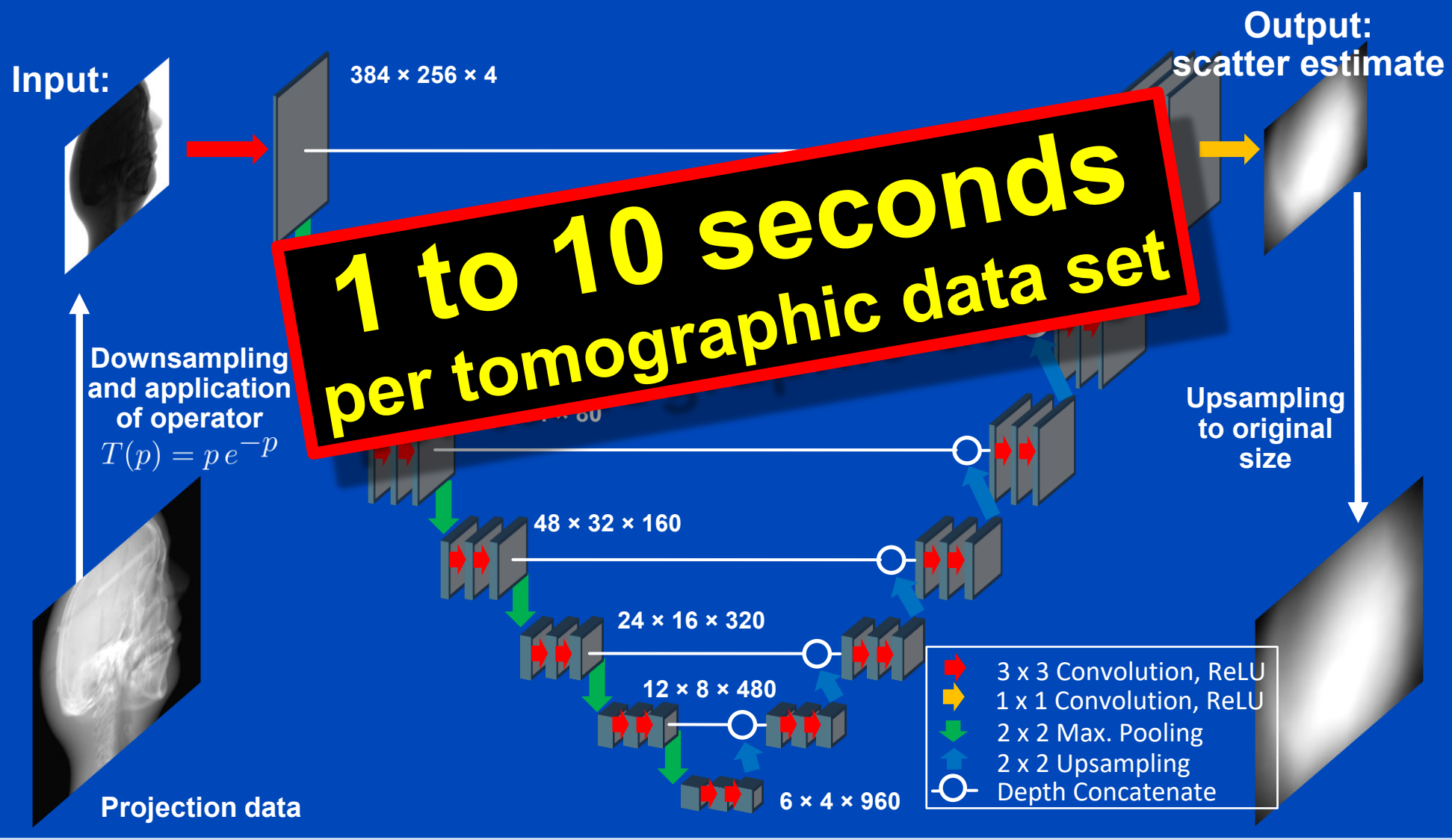

J. Maier, M. Kachelrieß et al. Deep scatter estimation (DSE). SPIE 2017 and Journal of Nondestructive Evaluation 37:57, July 2018.
J. Maier, M. Kachelrieß et al. Robustness of DSE. Med. Phys. 46(1):238-249, January 2019.

dkfz.

Training the DSE Network

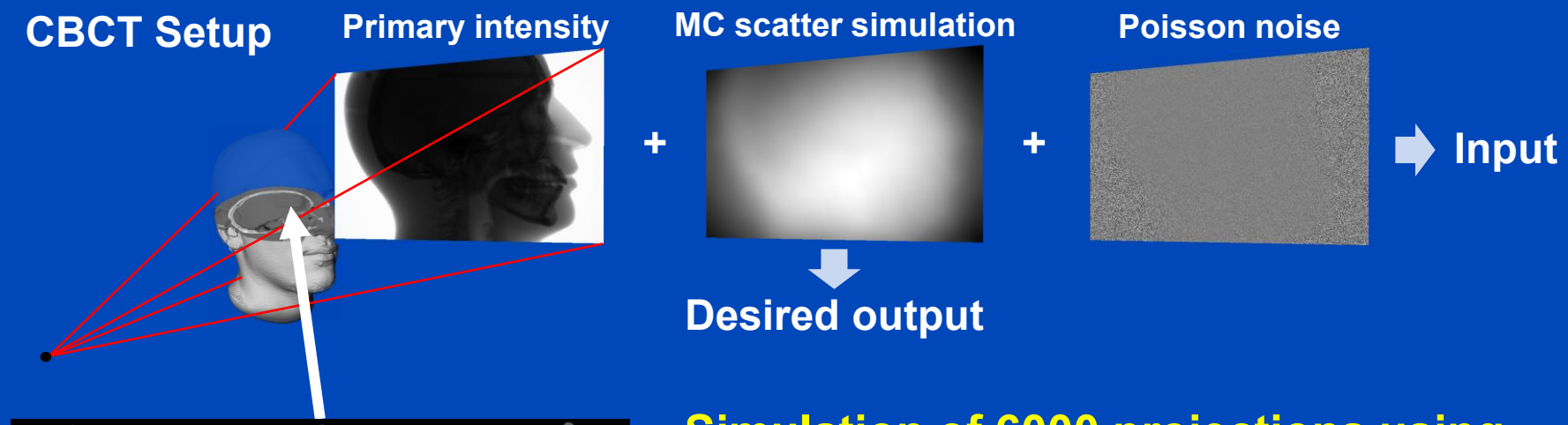

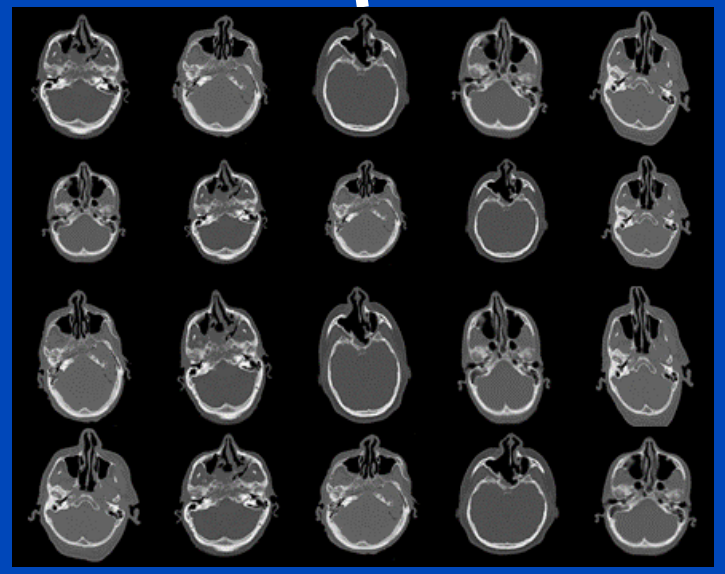

- Simulation of 6000 projections using different heads and acquisition parameters (80 kV, …, 140 kV in steps of 20 kV).
- Splitting into 80% training and 20% validation data.
- Mean *S/P* = 0.9
- 90th percentile *S/P* = 1.32
- Training minimizes MSE pixel-wise loss on a GeForce GTX 1080 for 80 epochs.

J. Maier, M. Kachelrieß et al. Deep scatter estimation (DSE). SPIE 2017 and Journal of Nondestructive Evaluation 37:57, July 2018.
J. Maier, M. Kachelrieß et al. Robustness of DSE. Med. Phys. 46(1):238-249, January 2019.

dkfz.

Testing of the DSE Network for Simulated Data (at 120 kV)

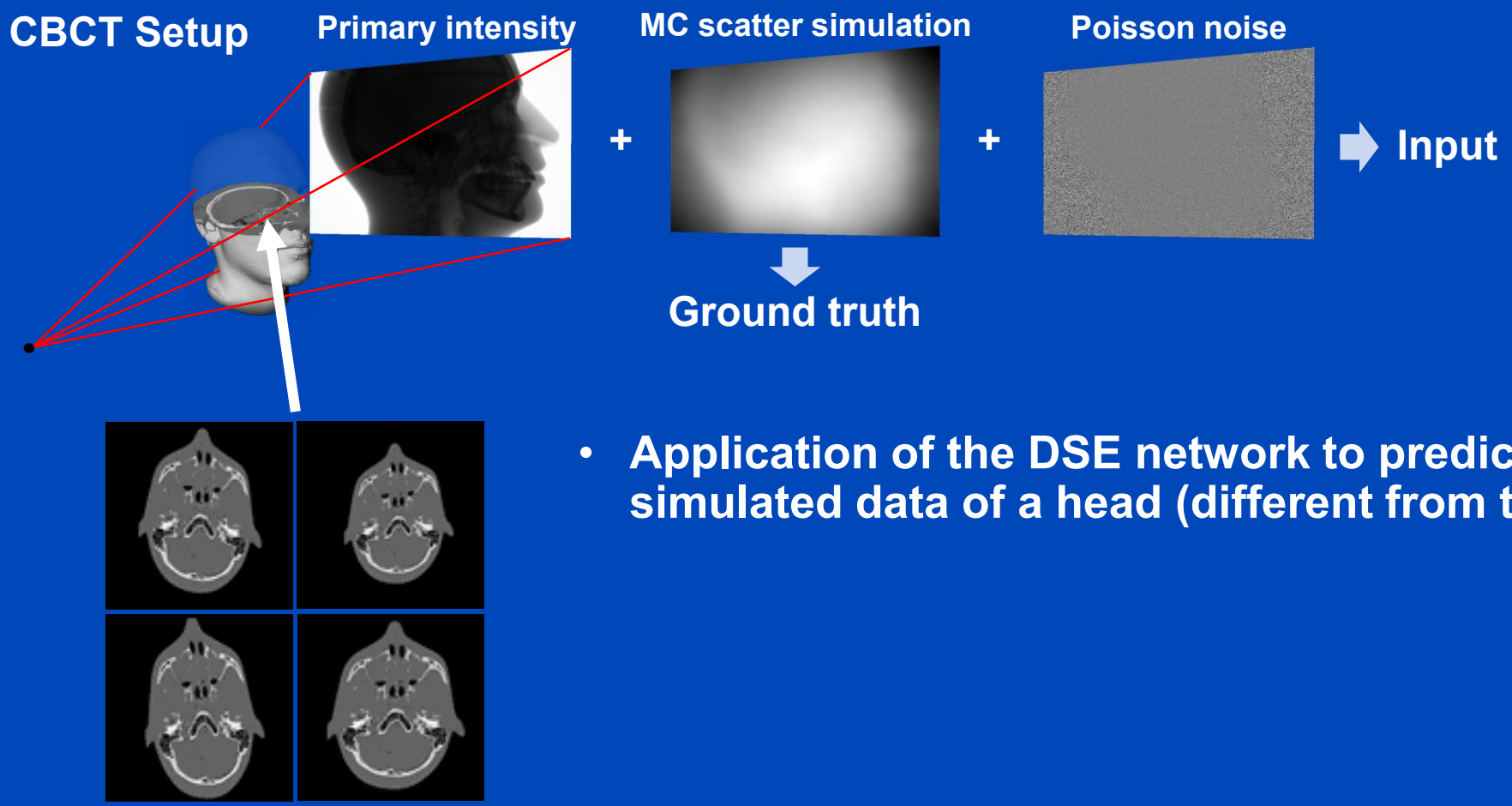

- Application of the DSE network to predict scatter for simulated data of a head (different from training data).

J. Maier, M. Kachelrieß et al. Deep scatter estimation (DSE). SPIE 2017 and Journal of Nondestructive Evaluation 37:57, July 2018.
J. Maier, M. Kachelrieß et al. Robustness of DSE. Med. Phys. 46(1):238-249, January 2019.

dkfz.

Training Performance for Different Inputs

$T(p) = e^{-p}$

$T(p) = p$

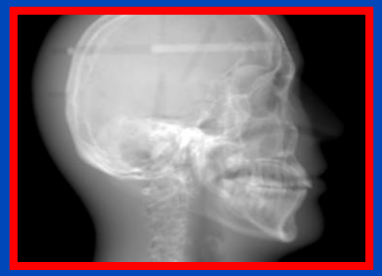

$T(p) = p \cdot e^{-p}$

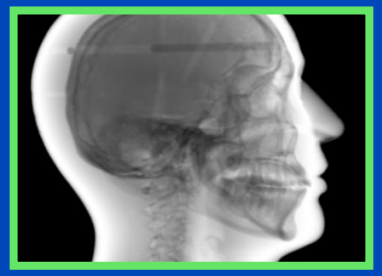

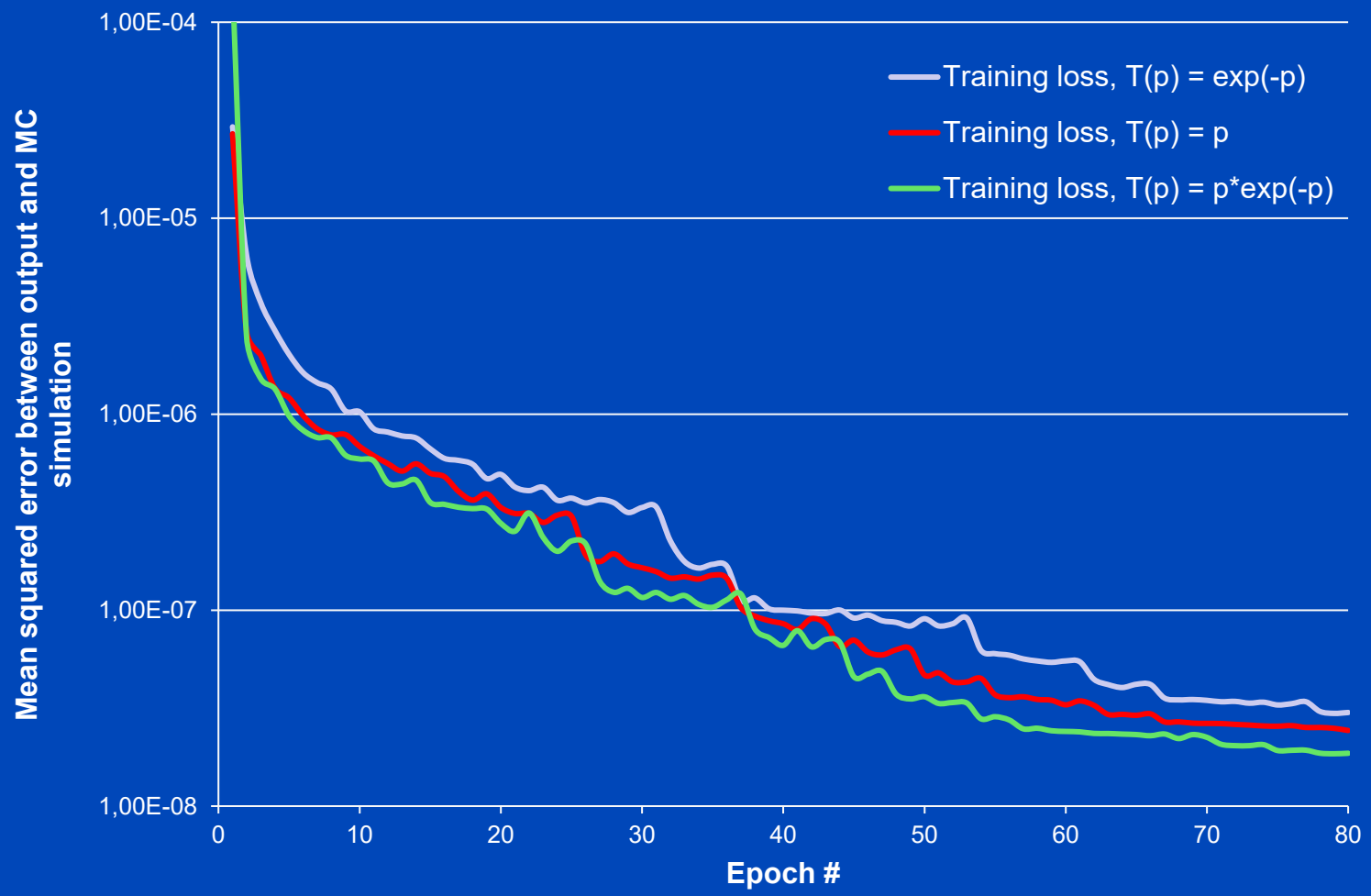

J. Maier, M. Kachelrieß et al. Deep scatter estimation (DSE). SPIE 2017 and Journal of Nondestructive Evaluation 37:57, July 2018.
J. Maier, M. Kachelrieß et al. Robustness of DSE. Med. Phys. 46(1):238-249, January 2019.

dkfz.

Validation Performance for Different Inputs

$T(p) = e^{-p}$

$T(p) = p$

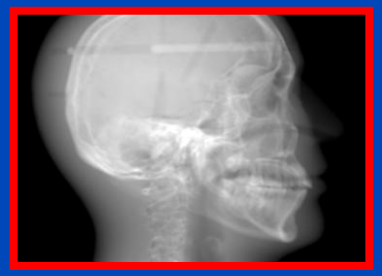

$T(p) = p \cdot e^{-p}$

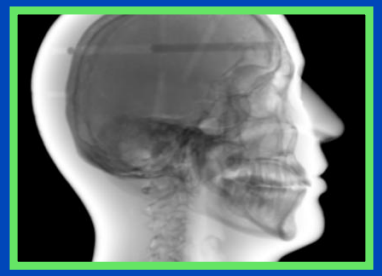

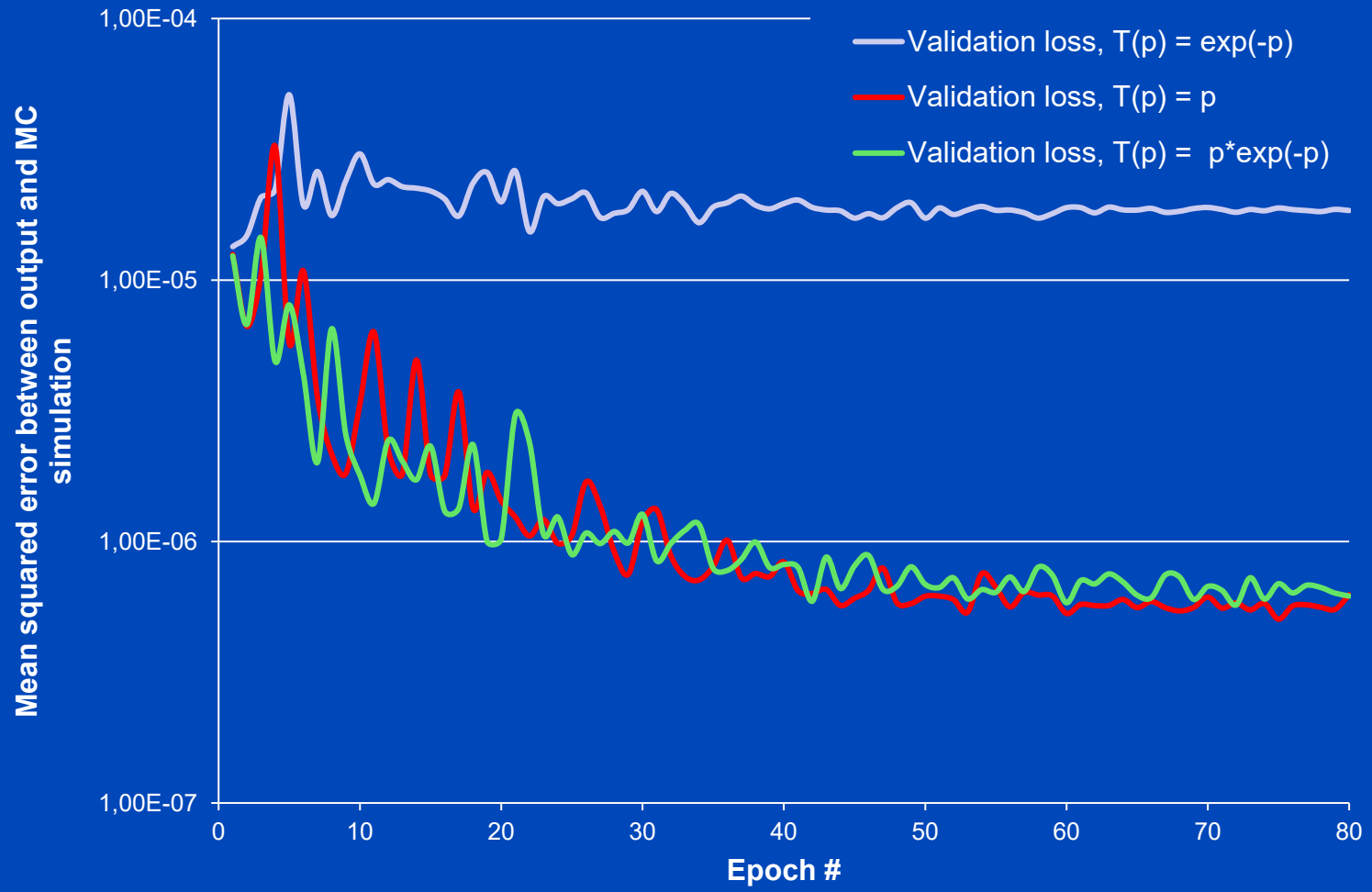

J. Maier, M. Kachelrieß et al. Deep scatter estimation (DSE). SPIE 2017 and Journal of Nondestructive Evaluation 37:57, July 2018.
J. Maier, M. Kachelrieß et al. Robustness of DSE. Med. Phys. 46(1):238-249, January 2019.

dkfz.

Ref 1: Kernel-Based Scatter Estimation

- **Kernel-based scatter estimation[1]:**
  - **Estimation of scatter by a convolution of the scatter source term *T*(*p*) with a scatter propagation kernel *G*(*u*, *c*):**

$$I_{\mathrm{s,\ est}}(\boldsymbol{u}) = \underbrace{\left(c_0 \cdot p(\boldsymbol{u}) \cdot e^{-p(\boldsymbol{u})}\right)}_{T(p)(\boldsymbol{u})} * \underbrace{\left(\sum_{\pm} e^{-c_1(\boldsymbol{u}\hat{\boldsymbol{e}}_1 \pm c_2)^2} \cdot \sum_{\pm} e^{-c_3(\boldsymbol{u}\hat{\boldsymbol{e}}_2 \pm c_4)^2}\right)}_{G(\boldsymbol{u},\boldsymbol{c})}$$

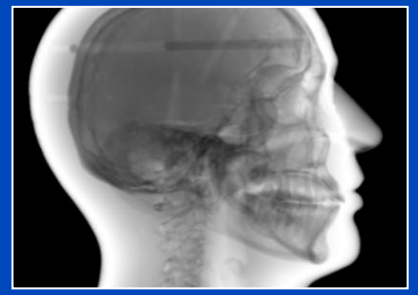

Open parameters: c_0

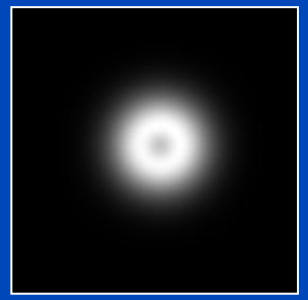

Open parameters: c_1, c_2, c_3, c_4

$$\{c_i\} = \operatorname{argmin} \sum_{n} \sum_{\boldsymbol{u}} \left\| I_{\mathrm{s,\ est}}(n, \boldsymbol{u}, \{c_i\}) - I_{\mathrm{s}}(n, \boldsymbol{u}) \right\|_2^2,$$

Samples of the training data set

Detector coordinate

Scatter estimate

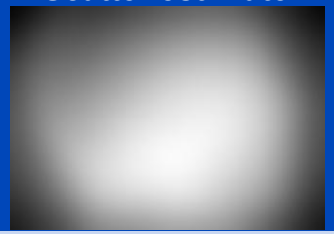

MC scatter simulation

[1] B. Ohnesorge, T. Flohr, K. Klingenbeck-Regn: Efficient object scatter correction algorithm for third and fourth generation CT scanners. Eur. Radiol. 9, 563–569 (1999).

dkfz.

Ref 2: Hybrid Scatter Estimation

- **Hybrid scatter estimation[2] :**
  - **Estimation of scatter by a convolution of the scatter source term *T*(*p*) with a scatter propagation kernel *G*(*u*, *c*):**

$$I_{\mathrm{s,\ est}}(\boldsymbol{u}) = \underbrace{\left(c_0 \cdot p(\boldsymbol{u}) \cdot e^{-p(\boldsymbol{u})}\right)}_{T(p)(\boldsymbol{u})} * \underbrace{\left(\sum_{\pm} e^{-c_1(\boldsymbol{u}\hat{\boldsymbol{e}}_1 \pm c_2)^2} \cdot \sum_{\pm} e^{-c_3(\boldsymbol{u}\hat{\boldsymbol{e}}_2 \pm c_4)^2}\right)}_{G(\boldsymbol{u},\boldsymbol{c})}$$

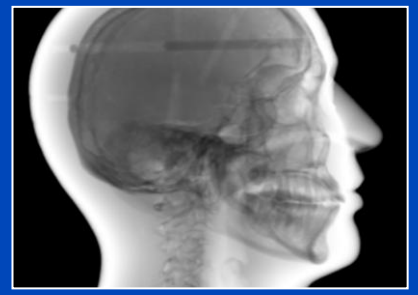

$T(p)(\boldsymbol{u})$

Open parameters: c_0

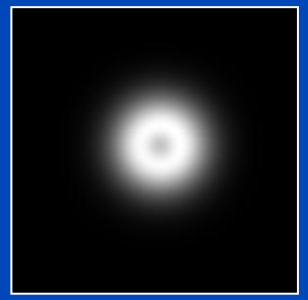

$G(\boldsymbol{u},\boldsymbol{c})$

Open parameters: c_1, c_2, c_3, c_4

$$\{c_i\}_n = \operatorname{argmin} \sum_{\boldsymbol{u}} \left\| I_{\mathrm{s,\ est}}(n, \boldsymbol{u}, \{c_i\}) - I_{\mathrm{s}}(n, \boldsymbol{u}) \right\|_2^2,$$

Samples of the test data set

Detector coordinate

Scatter estimate

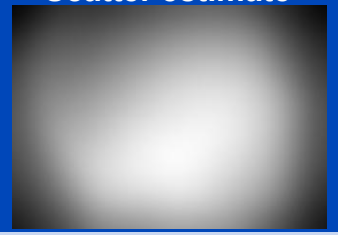

Coarse MC simulation

[2] M. Baer, M. Kachelrieß: Hybrid scatter correction for CT imaging. Phys. Med. Biol. 57, 6849–6867 (2012).

dkfz.

Results on Simulated Projection Data

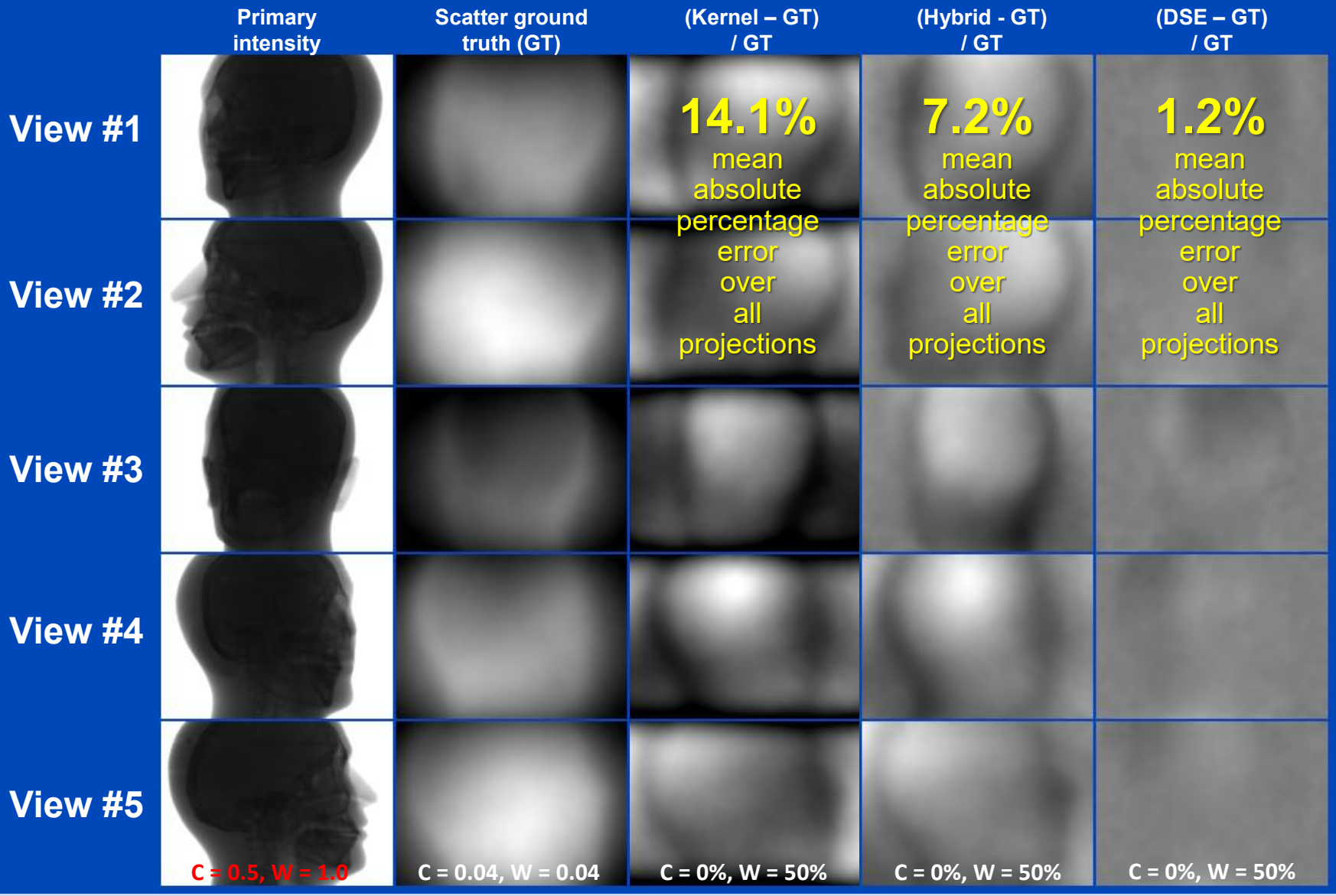

DSE trained to estimate scatter from **primary plus scatter**: High accuracy

dkfz.

Results on Simulated Projection Data

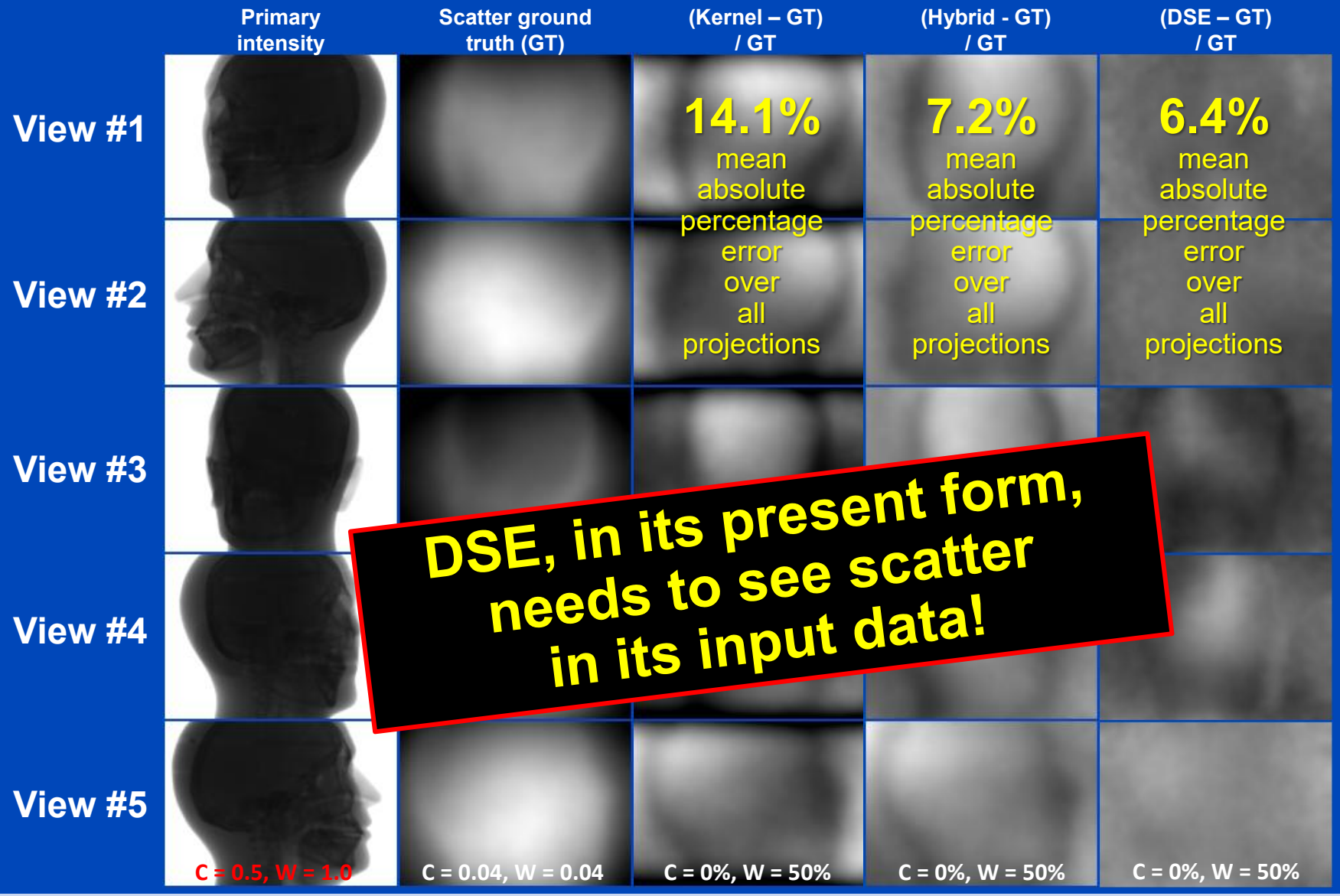

DSE trained to estimate scatter from **primary only**: Low accuracy

dkfz.

Results on Simulated Projection Data

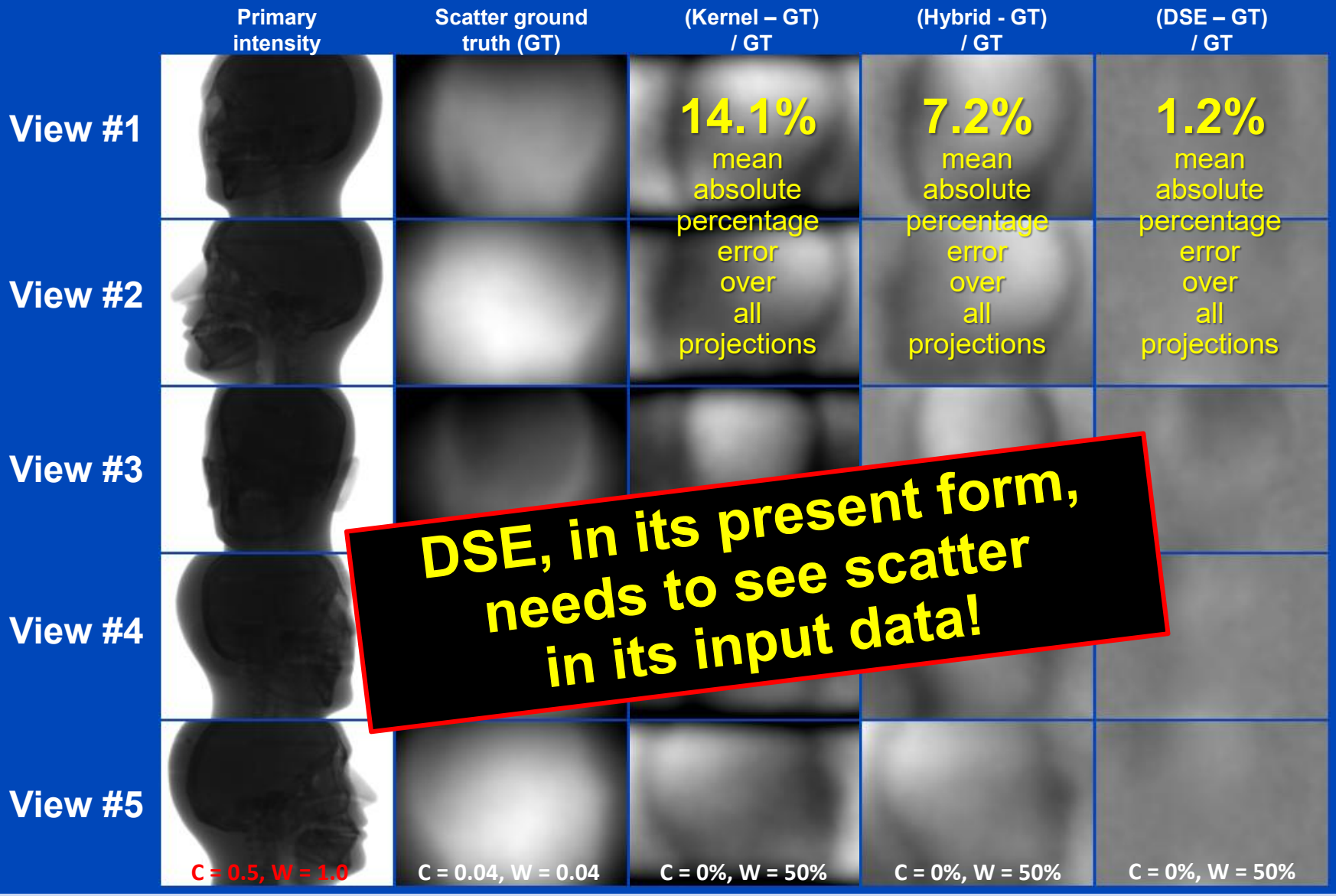

DSE trained to estimate scatter from **primary plus scatter**: High accuracy

dkfz.

Reconstructions of Simulated Data

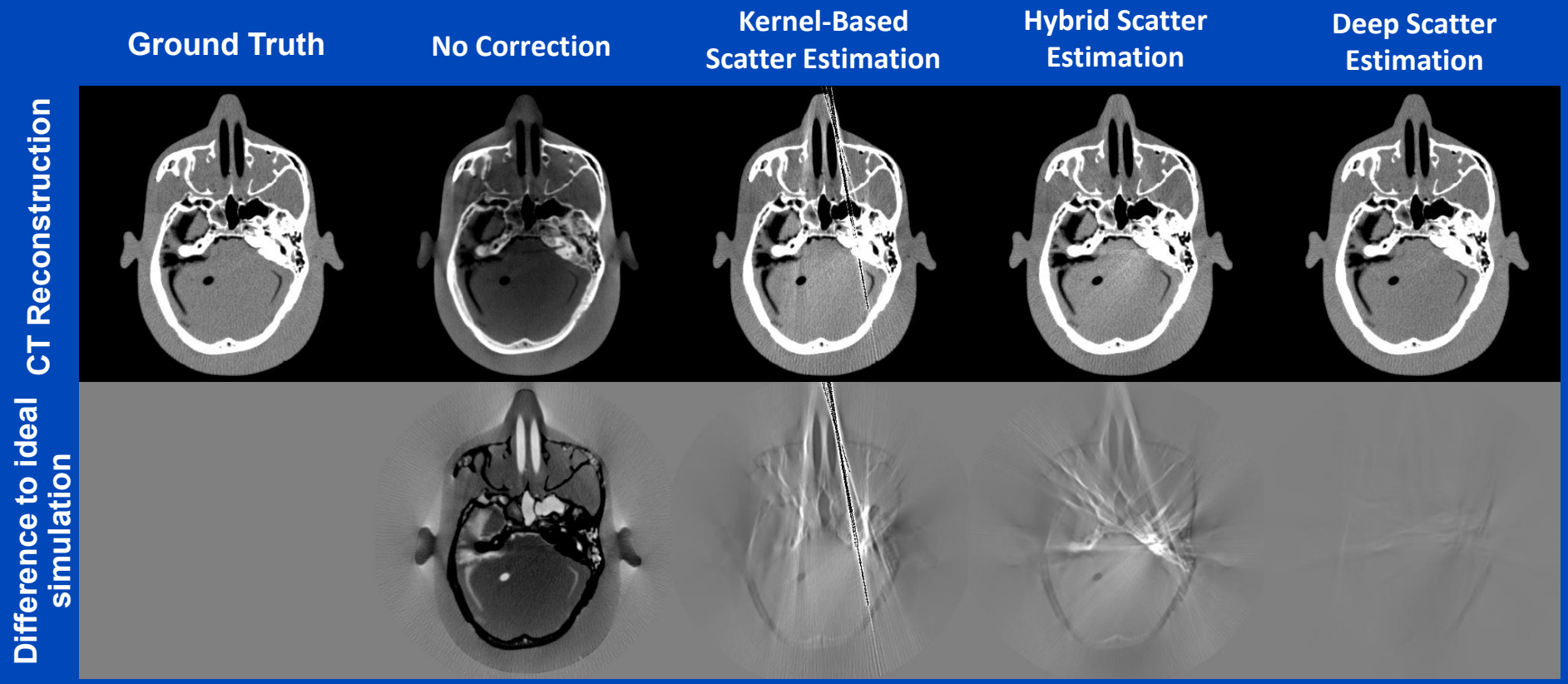

$C = 0$ HU, $W = 1000$ HU

J. Maier, M. Kachelrieß et al. Deep scatter estimation (DSE). SPIE 2017 and Journal of Nondestructive Evaluation 37:57, July 2018.
J. Maier, M. Kachelrieß et al. Robustness of DSE. Med. Phys. 46(1):238-249, January 2019.

dkfz.

Testing of the DSE Network for Measured Data (120 kV)

DKFZ table-top CT

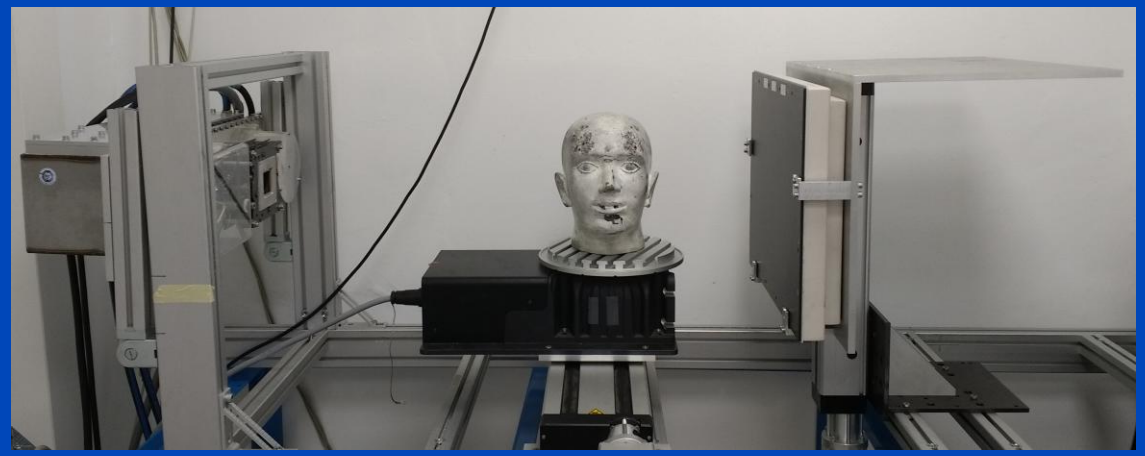

- Measurement of a head phantom at our in-house table-top CT.
- Slit scan measurement serves as ground truth.

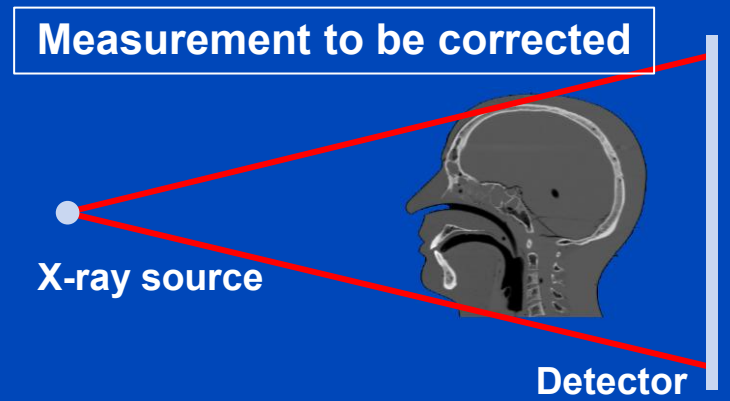

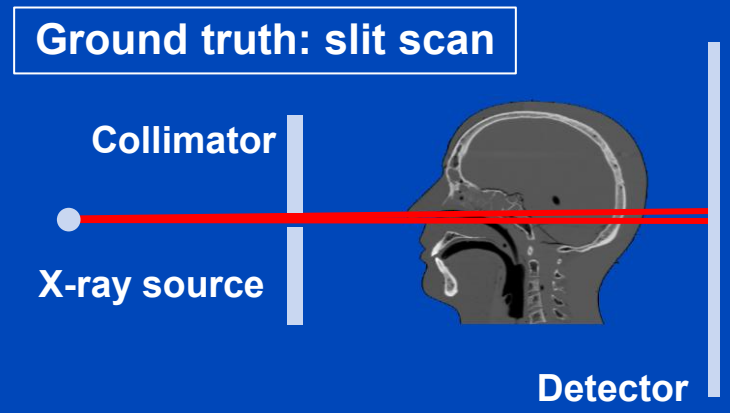

J. Maier, M. Kachelrieß et al. Deep scatter estimation (DSE). SPIE 2017 and Journal of Nondestructive Evaluation 37:57, July 2018.
J. Maier, M. Kachelrieß et al. Robustness of DSE. Med. Phys. 46(1):238-249, January 2019.

dkfz.

Reconstructions of Measured Data

Parameters of the two comparison methods trained in the same way as those of DSE: same data, same loss function, same optimization algorithm.

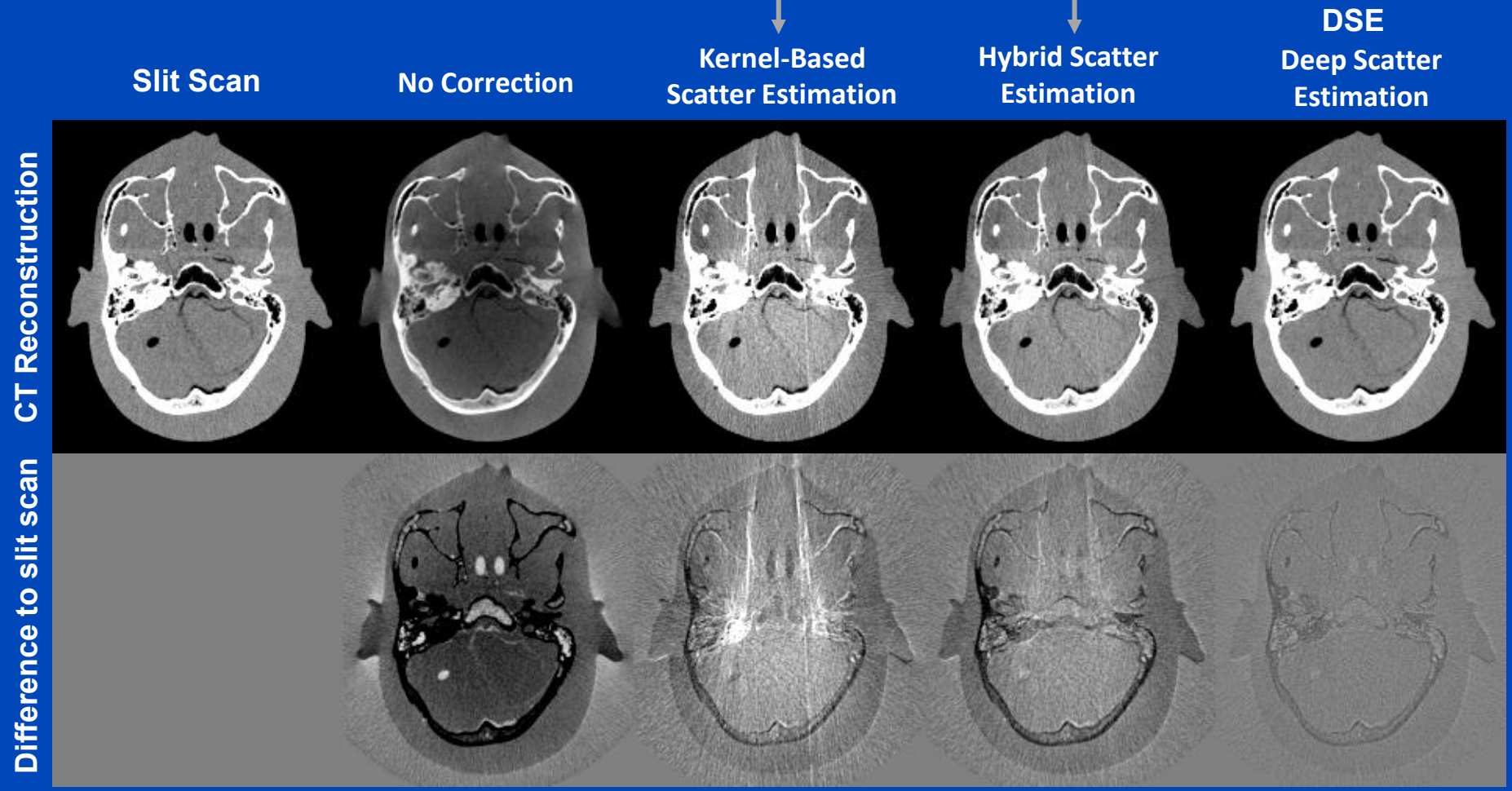

$C = 0$ HU, $W = 1000$ HU

J. Maier, M. Kachelrieß et al. Deep scatter estimation (DSE). SPIE 2017 and Journal of Nondestructive Evaluation 37:57, July 2018.
J. Maier, M. Kachelrieß et al. Robustness of DSE. Med. Phys. 46(1):238-249, January 2019.

dkfz.

Standard reconstruction

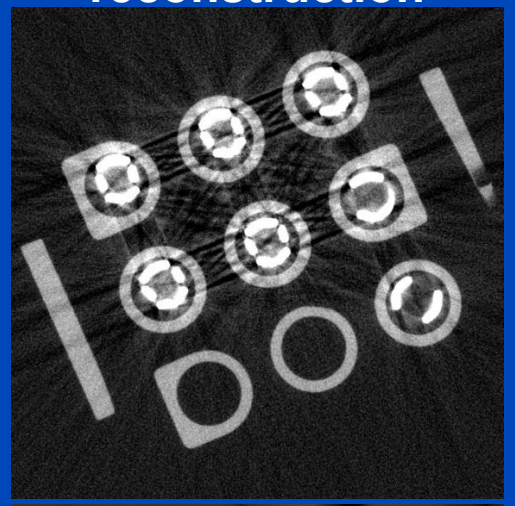

Simulation-based removal of
- beam hardening artifacts
- off-focal radiation artifacts
- focal spot blurring artifacts
- **scatter artifacts**
- …

Presented at iCT 2016

Simulation-based artifact correction

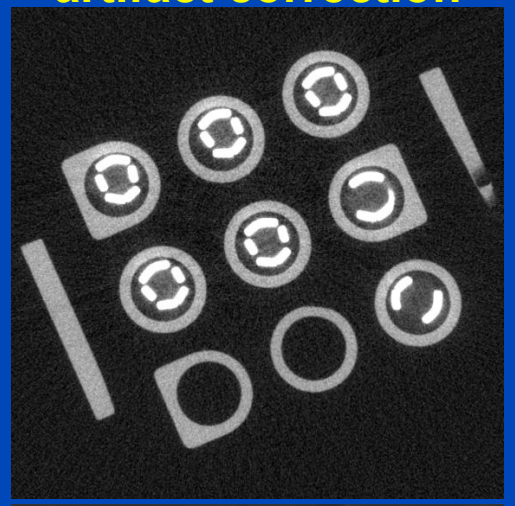

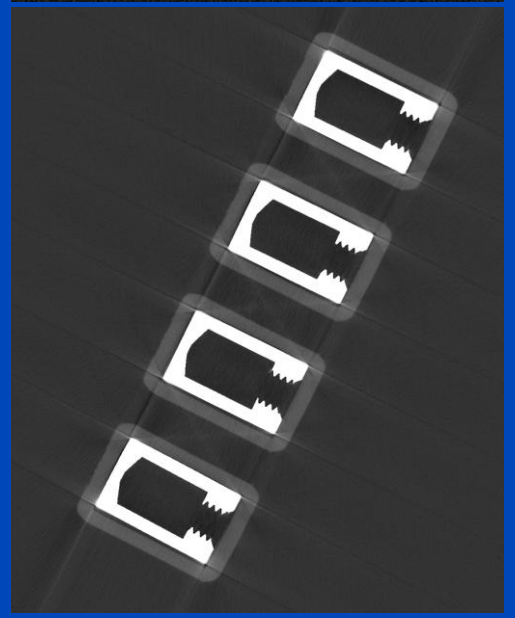

J. Maier, M. Kachelrieß et al. Simulation-based artifact correction (SBAC) for metrological computed tomography. Meas. Sci. Technol. 28(6):065011, May 2017.

Simulation Study: Training Data

- Simulation of 16416 projections using different objects and parameter settings to train the DSE network.
- Training on a GeForce GTX 1080 for 80 epochs using the Keras framework, an Adam optimizer and a mini-batch size of 16.

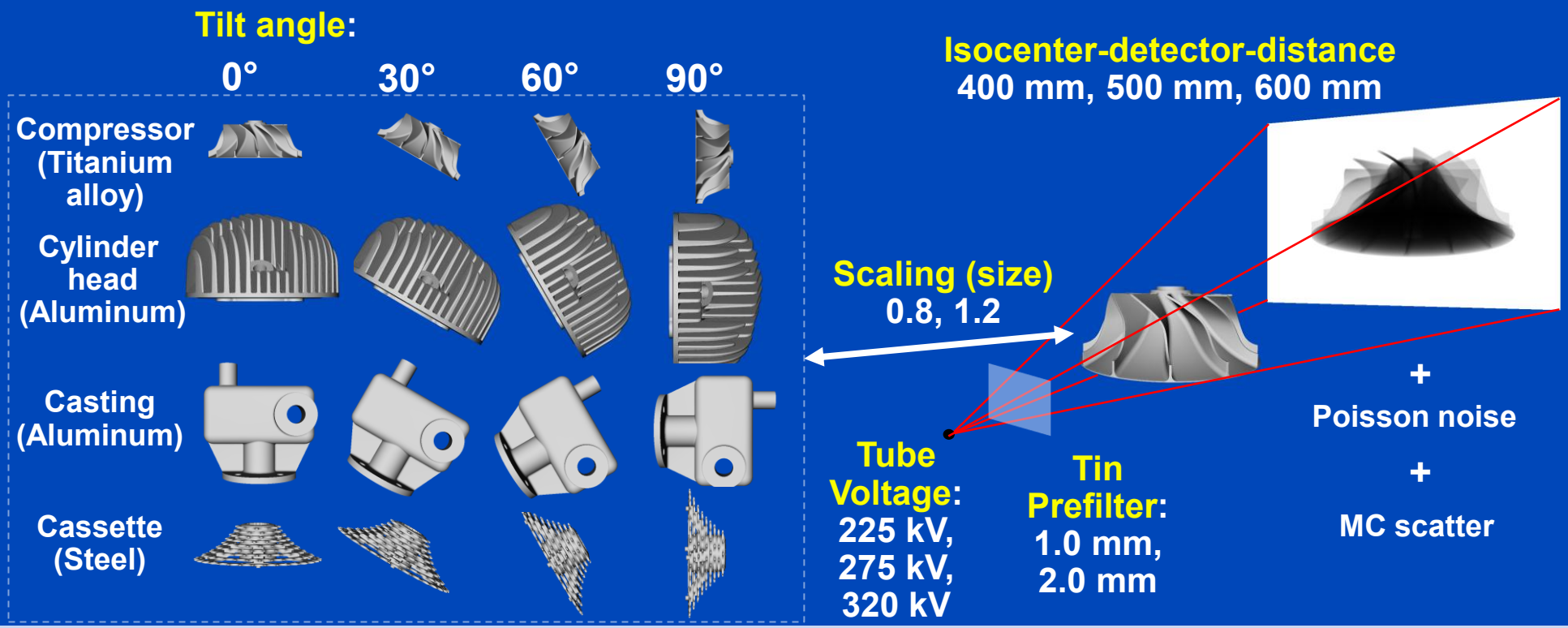

J. Maier, M. Kachelrieß et al. Deep scatter estimation (DSE). SPIE 2017 and Journal of Nondestructive Evaluation 37:57, July 2018.
J. Maier, M. Kachelrieß et al. Robustness of DSE. Med. Phys. 46(1):238-249, January 2019.

dkfz.

Simulation Study: Testing Data

- Simulation of a tomography (720 projection / 360°) of five components using acquisition parameters that differ from the ones used to generate the training data set.

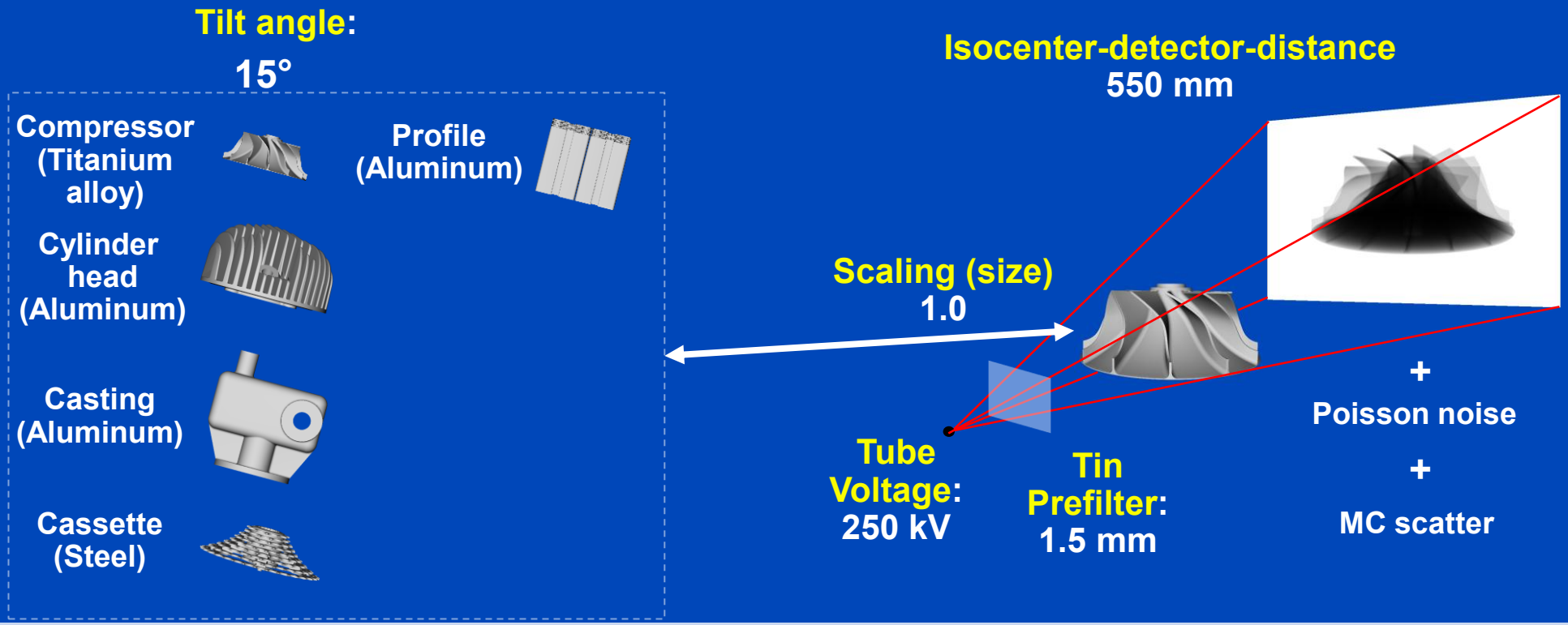

J. Maier, M. Kachelrieß et al. Deep scatter estimation (DSE). SPIE 2017 and Journal of Nondestructive Evaluation 37:57, July 2018.
J. Maier, M. Kachelrieß et al. Robustness of DSE. Med. Phys. 46(1):238-249, January 2019.

dkfz.

Test Performance for Different Inputs

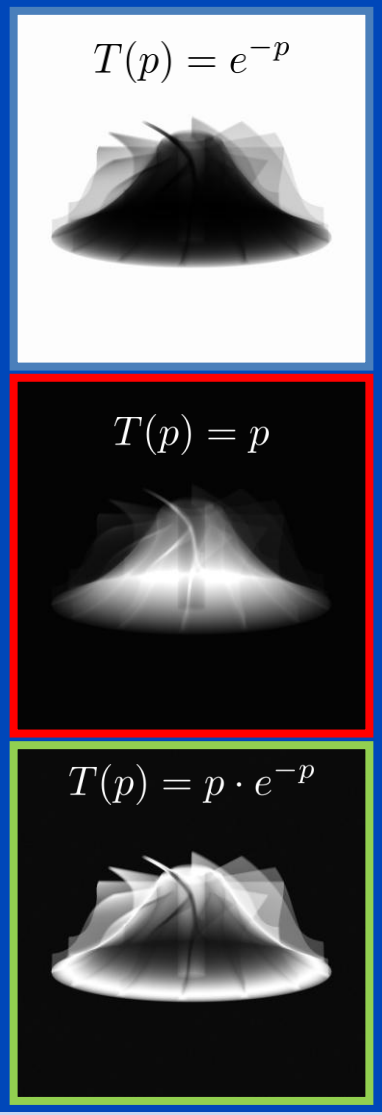

J. Maier, M. Kachelrieß et al. Deep scatter estimation (DSE). SPIE 2017 and Journal of Nondestructive Evaluation 37:57, July 2018.
J. Maier, M. Kachelrieß et al. Robustness of DSE. Med. Phys. 46(1):238-249, January 2019.

dkfz.

Results

Scatter estimates for simulated testing data

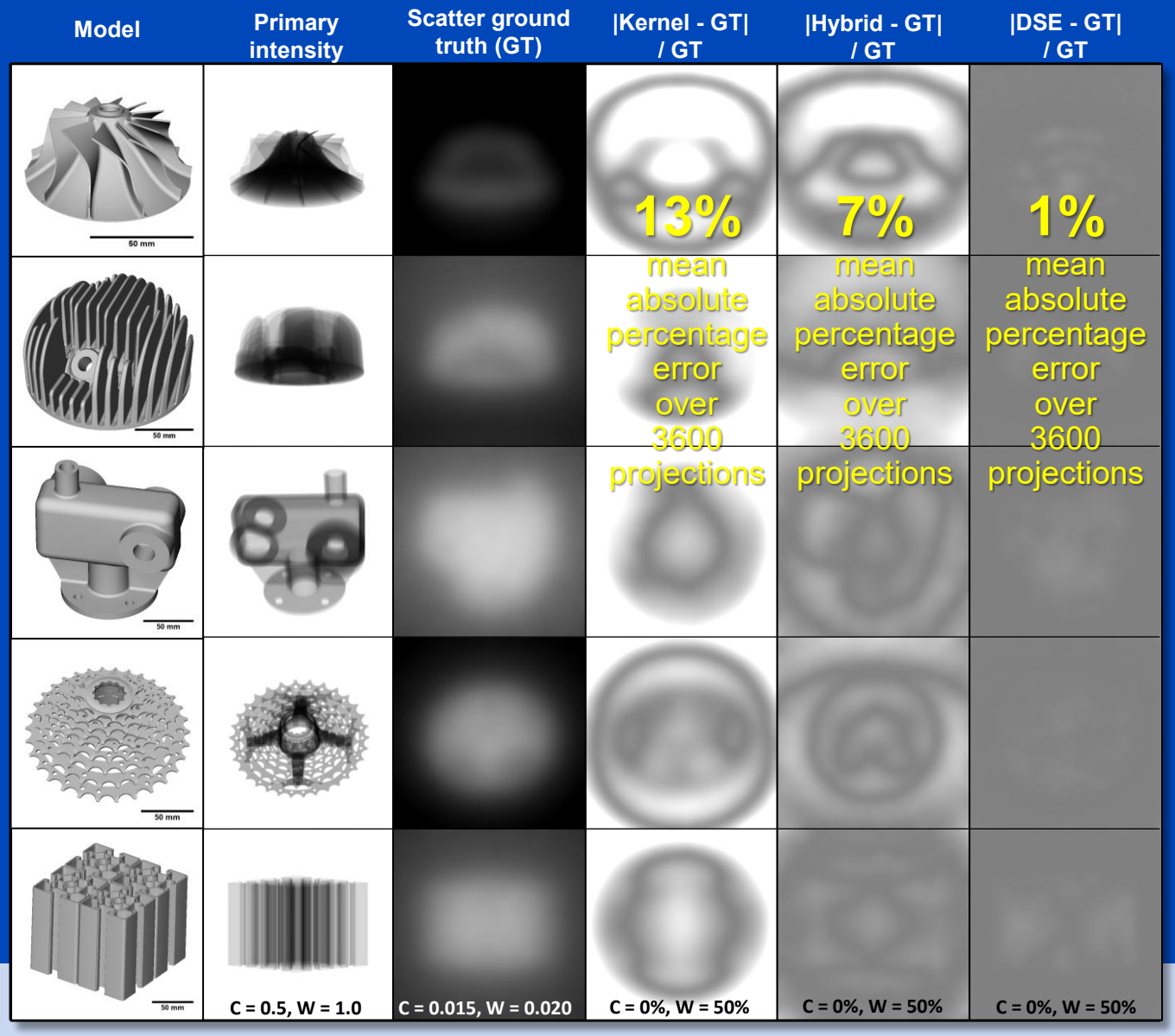

Results

CT reconstructions of scatter corrected testing data

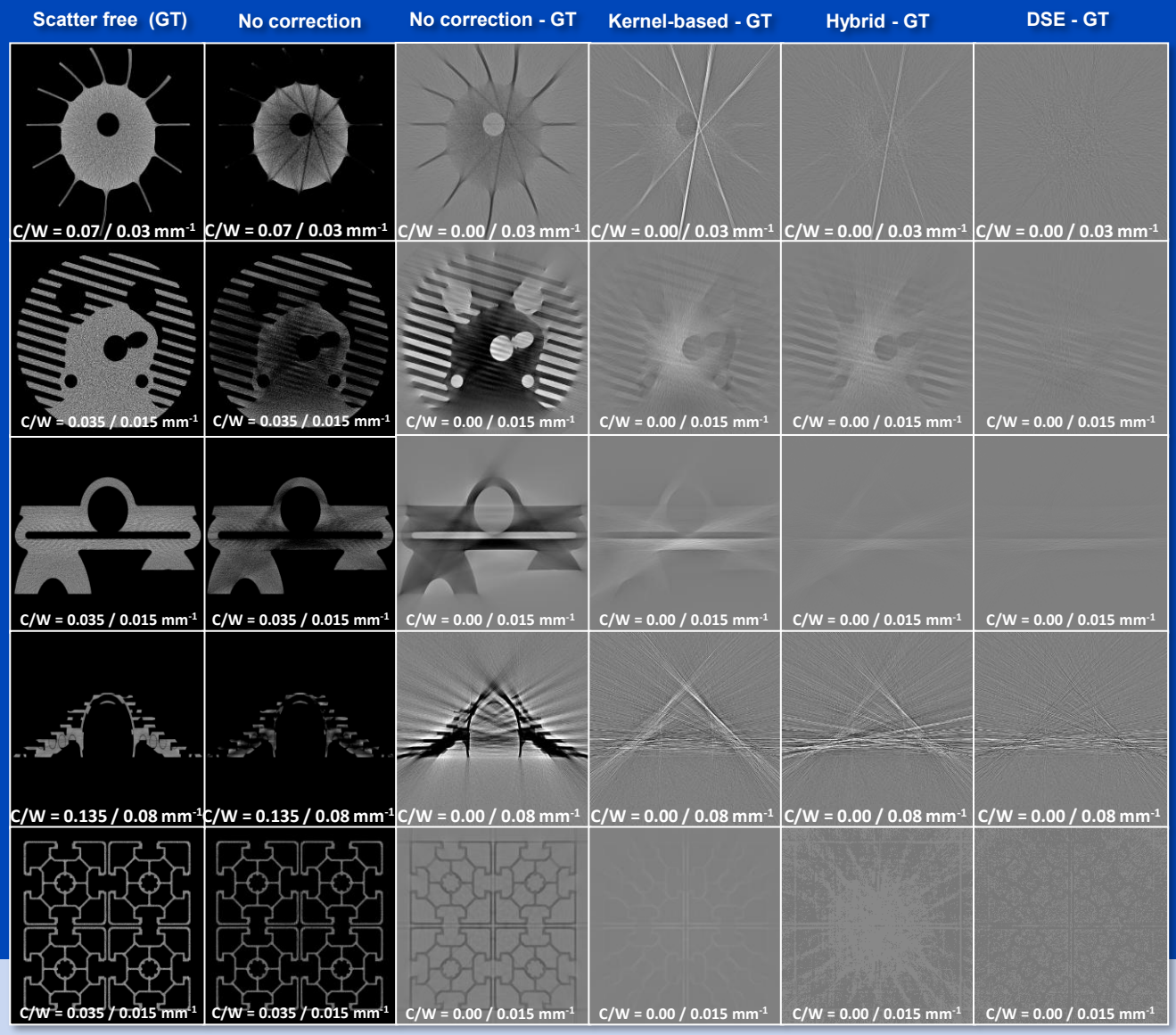

Application to Measured Data

- Measurement at DKFZ table-top CT
- Tomography of aluminum profile
- 720 projections, 360°
- 110 kV Hamamatsu micro-focus tube
- Varian flat detector

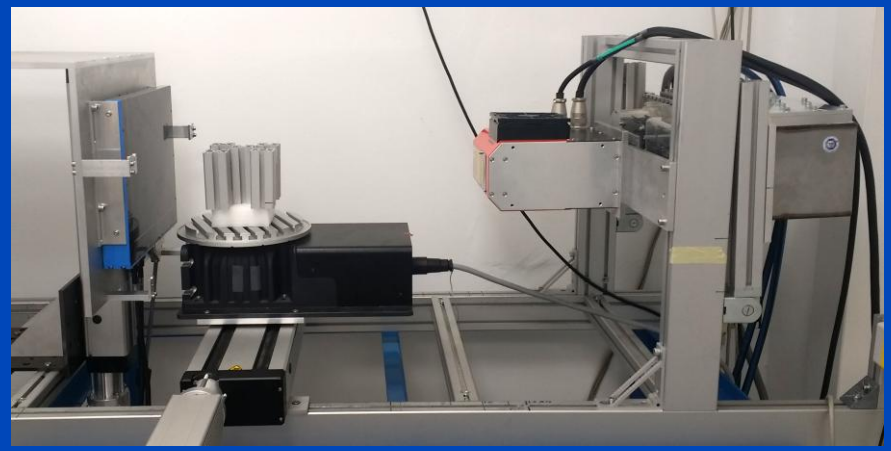

	Training	Testing
Components	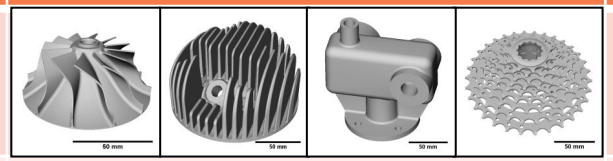	
Detector elements	768×768	768×768
Source-detector distance	580 mm	580 mm
Source-isocenter distance	100 mm, 110 mm, 120 mm	110 mm
Tilt angle	0°, 30°, 60°, 90°	0°
Tube voltage	100 kV, 110 kV, 120 kV	110 kV
Copper prefilter	1.0 mm, 2.0 mm	2.0 mm
Scaling	1.0	-
Number of projections	8208	720

Results

Performance of DSE for measured data

Projection data

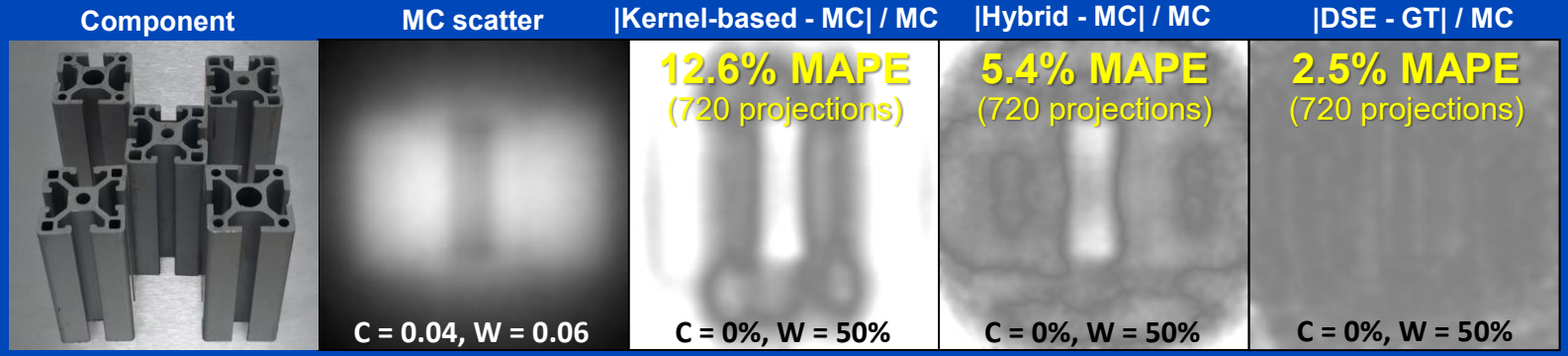

Reconstructions

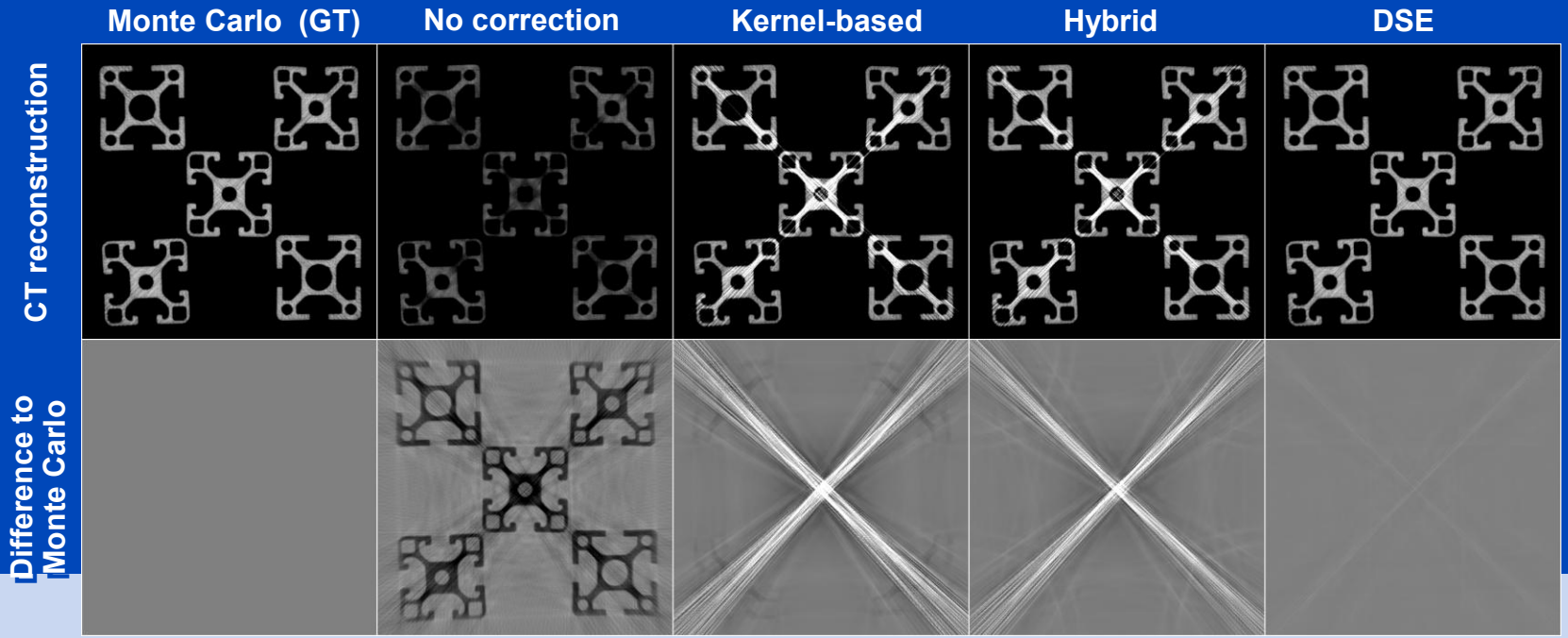

A simple detruncation was applied to the rawdata before reconstruction. Images were clipped to the FOM before display. *C* = -200 HU, *W* = 1000 HU.

Truncated DSE

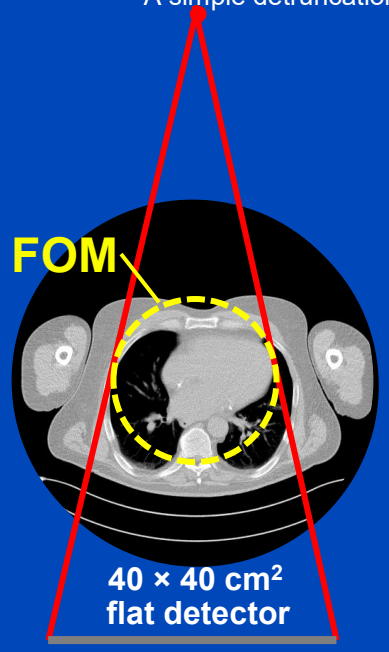

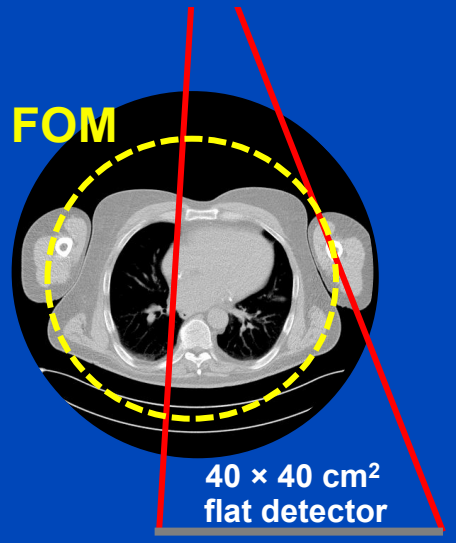

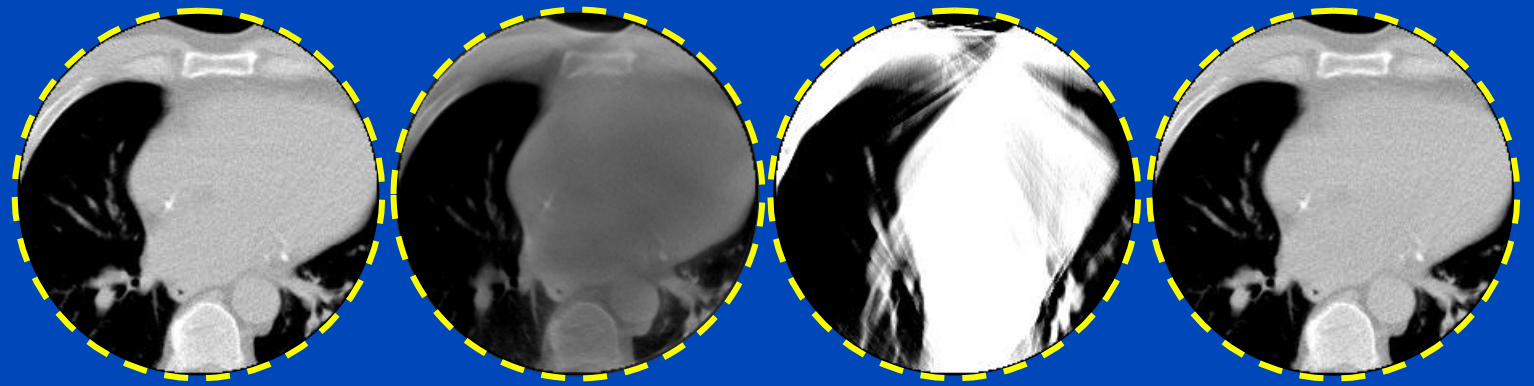

Ground truth | Uncorrected | MC-corrected | DSE

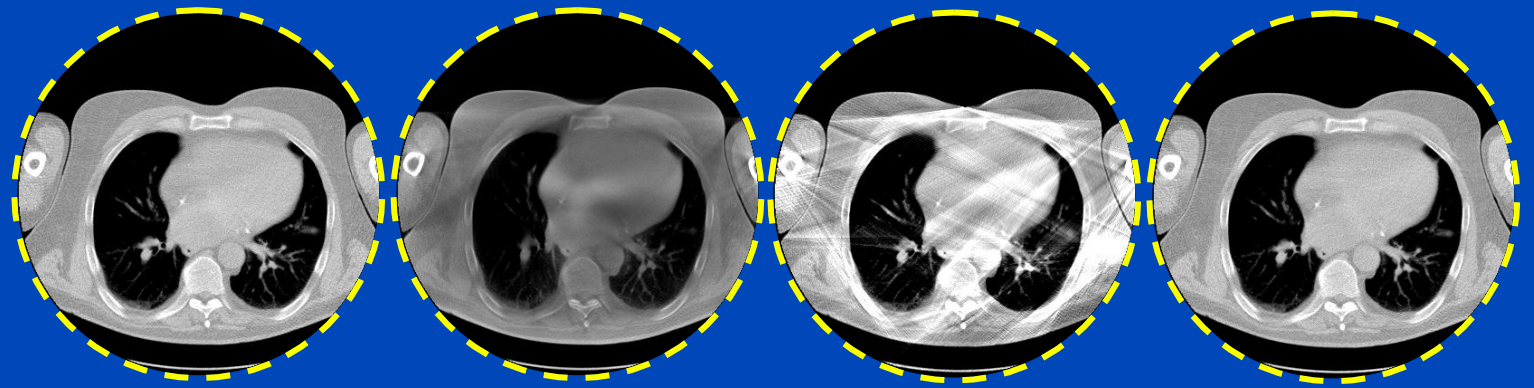

To learn why MC fails at truncated data and what significant efforts are necessary to cope with that situation see [Kachelrieß et al. Effect of detruncation on the accuracy of MC-based scatter estimation in truncated CBCT. Med. Phys. 45(8):3574-3590, August 2018].

J. Maier, M. Kachelrieß et al. Deep scatter estimation (DSE). SPIE 2017 and Journal of Nondestructive Evaluation 37:57, July 2018.
J. Maier, M. Kachelrieß et al. Robustness of DSE. Med. Phys. 46(1):238-249, January 2019.

dkfz.

Does DSE Generalize to Different Anatomical Regions?

- **Simulation parameters:**
  - 7 head and 14 thorax/abdomen clinical CT data sets
  - Apply affine transforms to obtain 28 volumes for each region
  - Regions: head, thorax and abdomen
  - Tube voltage: 120 kV, 140 kV.
  - Prior volumes: 28 head phantoms
  - Simulate 45 projections over 360° for each volume and voltage
  - Number of z-positions: 1 for head, 4 for thorax and abdomen
  - Data augmentation for head: vertical & horizontal flipping
  - Total number of projections: $2 \times 28 \times 45 \times 2 \times 2 = 10080$

J. Maier, M. Kachelrieß et al. Deep scatter estimation (DSE). SPIE 2017 and Journal of Nondestructive Evaluation 37:57, July 2018.
J. Maier, M. Kachelrieß et al. Robustness of DSE. Med. Phys. 46(1):238-249, January 2019.

Does DSE Generalize to Different Anatomical Regions?

- **DSE:**

DSE	Head	Thorax	Abdomen
Head	1.2	21.1	32.7
Thorax	8.8	1.5	9.1
Abdomen	11.9	10.9	1.3
All data	1.8	1.4	1.4

Values shown are the mean absolute percentage errors (MAPEs) of the testing data.
Note that thorax and head suffer from truncation due to the small size of the 40×30 cm flat detector.

- **KSE** (“trained” using the same data)**:**

KSE	Head	Thorax	Abdomen
Head	14.5	26.8	32.5
Thorax	16.2	18.5	19.4
Abdomen	16.8	22.1	17.8
All data	14.9	20.5	19.3

J. Maier, M. Kachelrieß et al. Deep scatter estimation (DSE). SPIE 2017 and Journal of Nondestructive Evaluation 37:57, July 2018.
J. Maier, M. Kachelrieß et al. Robustness of DSE. Med. Phys. 46(1):238-249, January 2019.

Results

	Testing Head	Thorax	Abdomen
Training			
KSE			
Head	14.5	26.8	32.5
Thorax	16.2	18.5	19.4
Abdomen	16.8	22.1	17.8
All data	14.9	20.5	19.3
HSE (Truncated prior, 22 cm FOM)			
-	6.2	293.2	237.6
HSE (Truncated prior, shifted detector, 40 cm FOM)			
-	-	22.9	26.5
DSE, $M_{\text{ep}} : e^{-p_{\text{sim}}} \longrightarrow S_{\text{MC}}$			
Head	3.9	17.6	23.5
Thorax	12.2	2.5	11.6
Abdomen	27.1	13.2	2.3
All data	4.7	2.5	2.4
DSE, $M_{\text{p}} : p_{\text{sim}} \longrightarrow S_{\text{MC}}$			
Head	1.3	14.9	15.2
Thorax	6.7	1.6	7.7
Abdomen	15.7	12.1	1.5
All data	1.7	1.6	1.6
DSE, $M_{\text{pep}} : p_{\text{sim}} \cdot e^{-p_{\text{sim}}} \longrightarrow S_{\text{MC}}$			
Head	1.2	21.1	32.7
Thorax	8.8	1.5	9.1
Abdomen	11.9	10.9	1.3
All data	1.8	1.4	1.4

Mean absolute percentage error of the kernel-based scatter estimation (KSE), the hybrid scatter estimation (HSE) and the deep scatter estimation (DSE) with respect to the ground truth scatter distribution (MC simulation). Training data were generated simulating head, thorax and abdomen data at 120 kV, 140 kV. The training was performed for head, thorax and abdomen data separately as well as using all data together (left column). DSE was trained for three different mappings ($M_{\text{ep}} : e^{-p_{\text{sim}}} \rightarrow S_{\text{MC}}$, $M_{\text{p}} : p_{\text{sim}} \rightarrow S_{\text{MC}}$, $M_{\text{pep}} : p \cdot e^{-p_{\text{sim}}} \rightarrow S_{\text{MC}}$). Note that there are no training data for the HSE as it is optimized on a coarse MC simulation of the testing data.

Values shown are the mean absolute percentage errors (MAPEs) of the testing data.
Note that thorax and head suffer from truncation due to the small size of the 40×30 cm flat detector.

dkfz.

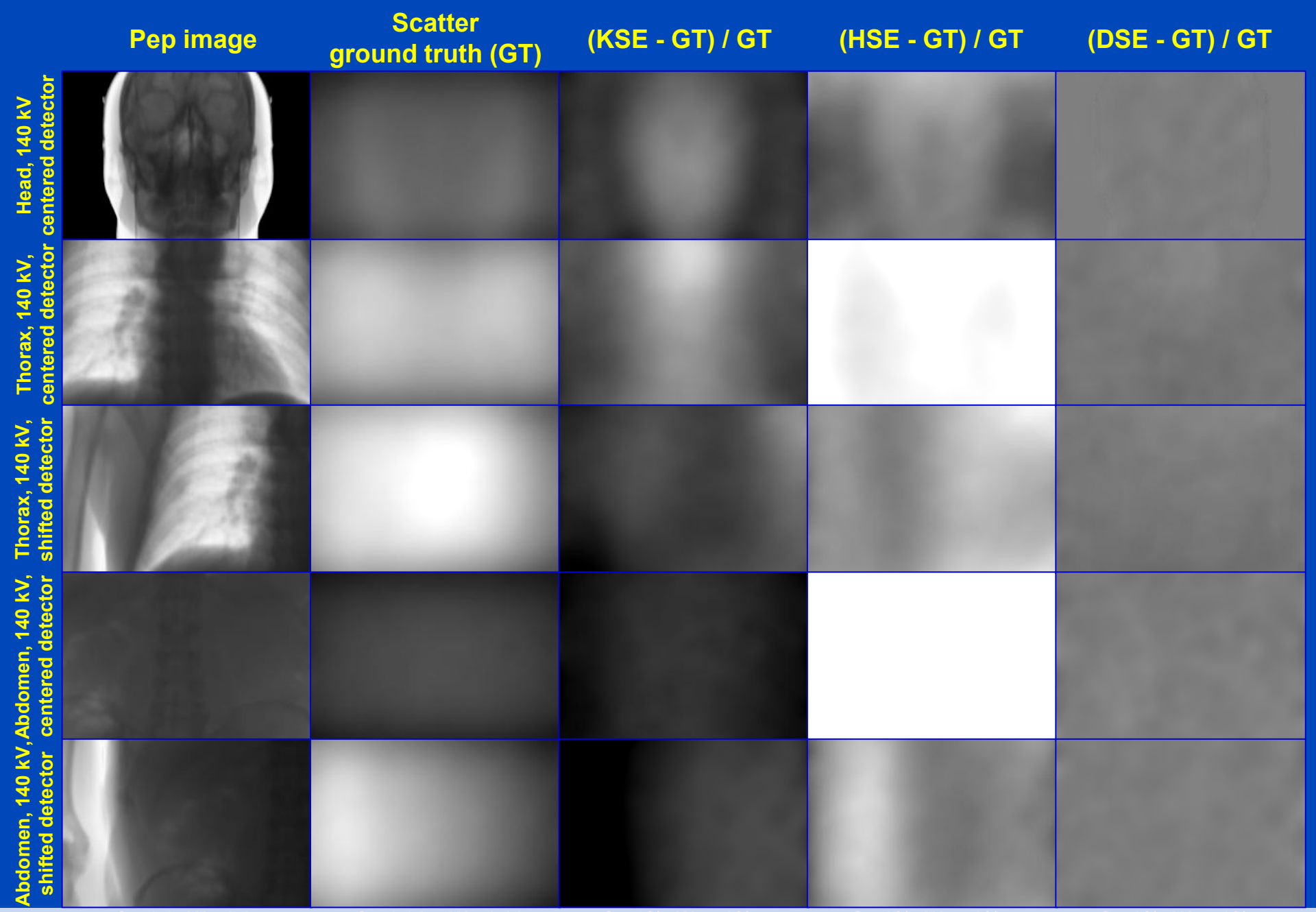
Pep image
Scatter ground truth (GT)
(KSE - GT) / GT
(HSE - GT) / GT
(DSE - GT) / GT
Head, 140 kV centered detector
Thorax, 140 kV, centered detector
Thorax, 140 kV, shifted detector
Abdomen, 140 kV, centered detector
Abdomen, 140 kV, shifted detector
C = 0.2, W = 0.35
C = 0.015, W = 0.02
C = 0%, W = 50%
C = 0%, W = 50%
C = 0%, W = 50%

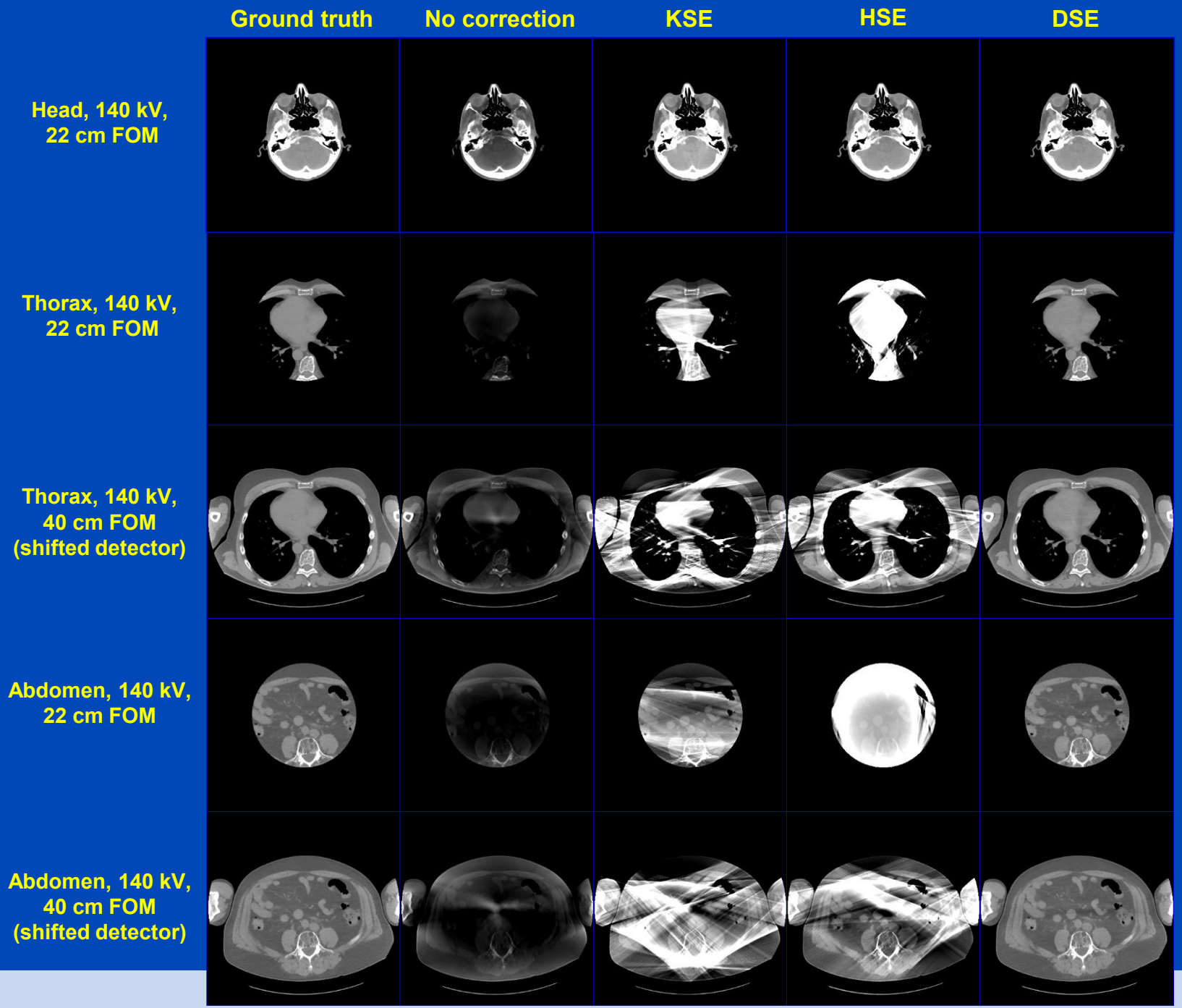
Ground truth
No correction
KSE
HSE
DSE
Head, 140 kV, 22 cm FOM
Thorax, 140 kV, 22 cm FOM
Thorax, 140 kV, 40 cm FOM (shifted detector)
Abdomen, 140 kV, 22 cm FOM
Abdomen, 140 kV, 40 cm FOM (shifted detector)

C = 0 HU
W = 700 HU

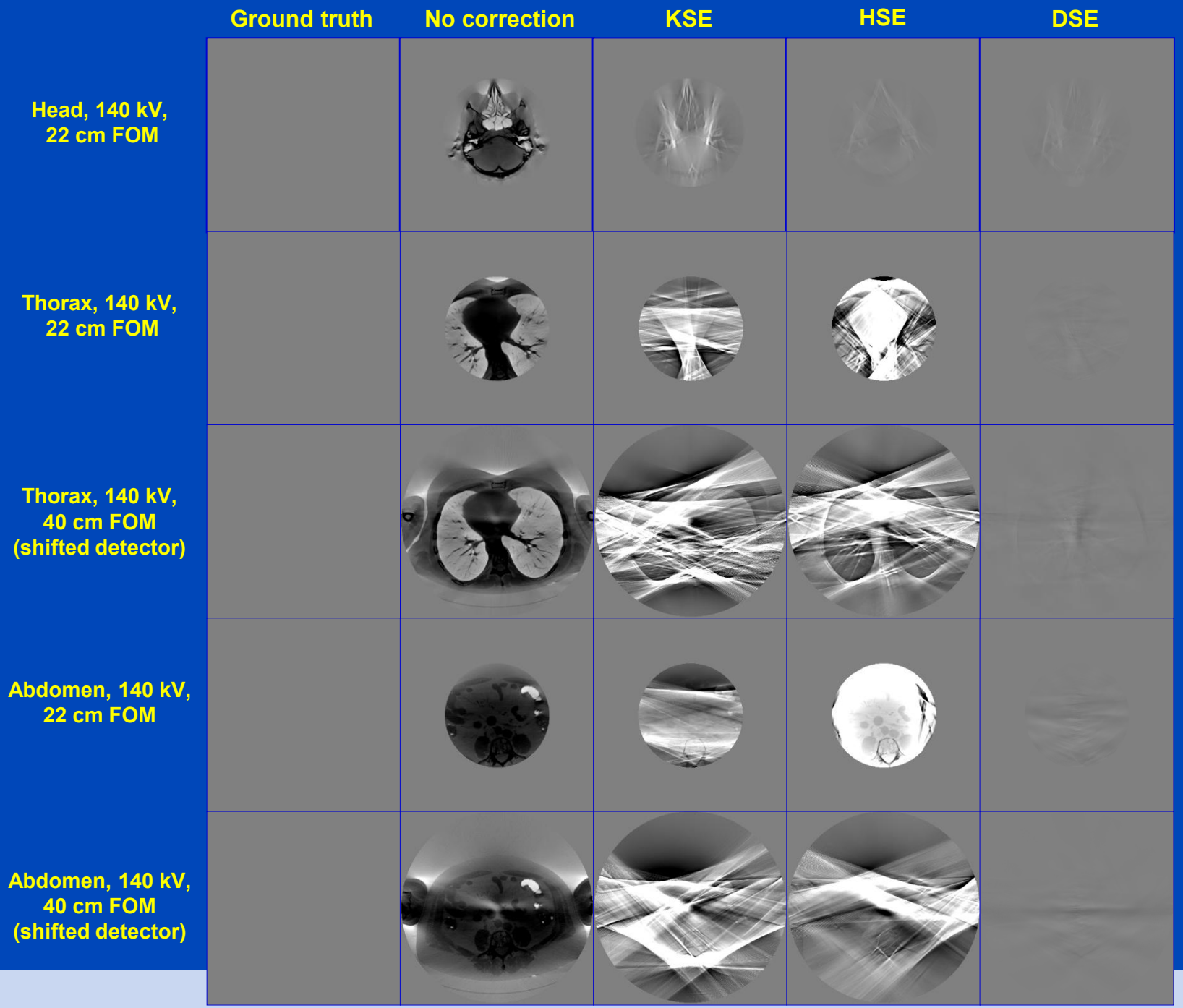
Ground truth
No correction
KSE
HSE
DSE
Head, 140 kV, 22 cm FOM
Thorax, 140 kV, 22 cm FOM
Thorax, 140 kV, 40 cm FOM (shifted detector)
Abdomen, 140 kV, 22 cm FOM
Abdomen, 140 kV, 40 cm FOM (shifted detector)

C = 0 HU
W = 700 HU

Scatter in Dual Source CT (DSCT)

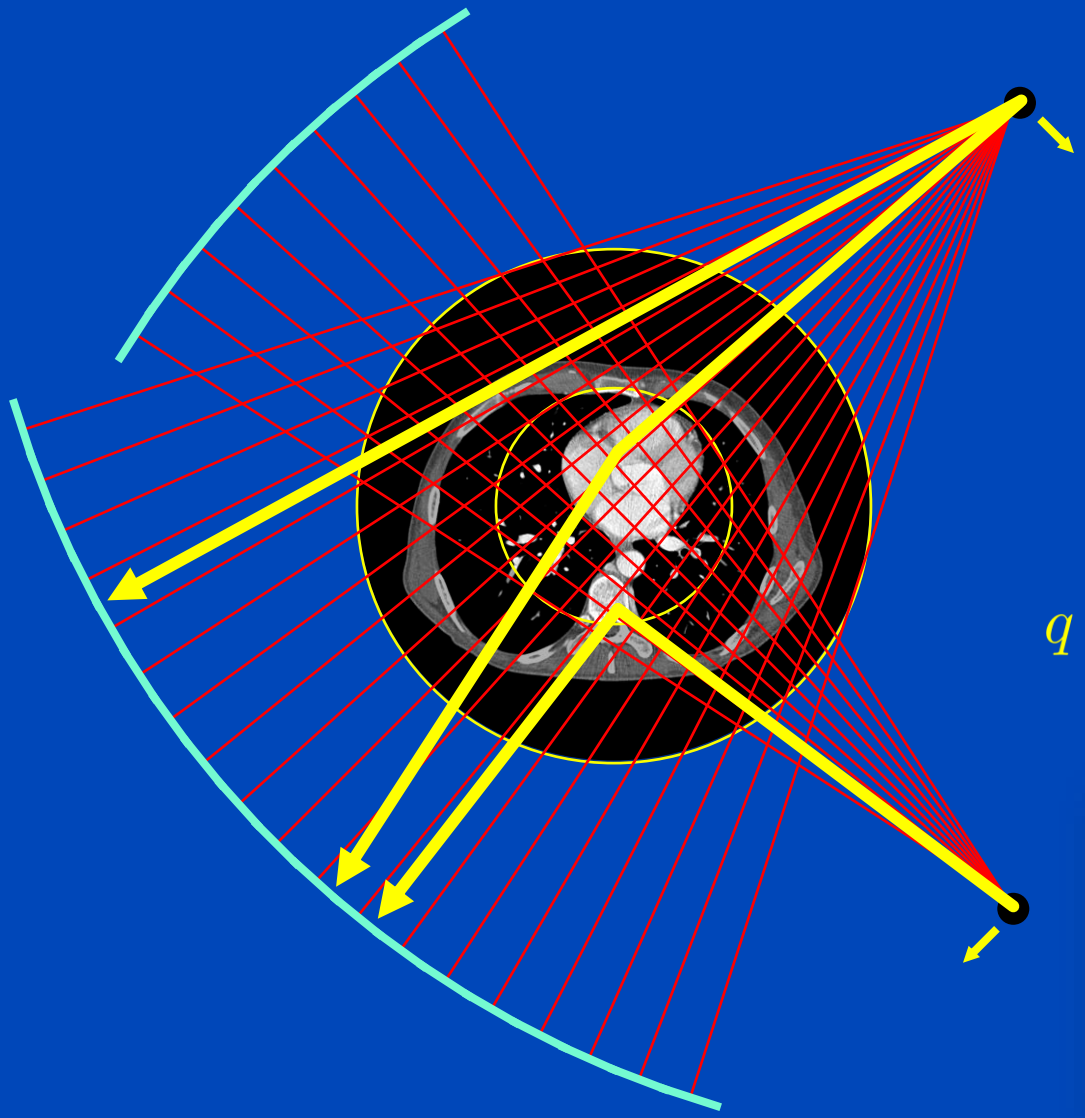

$$q = -\ln \frac{I_{\text{primary}} + S_{\text{forward}} + \rho\, S_{\text{cross}}}{I_0}$$

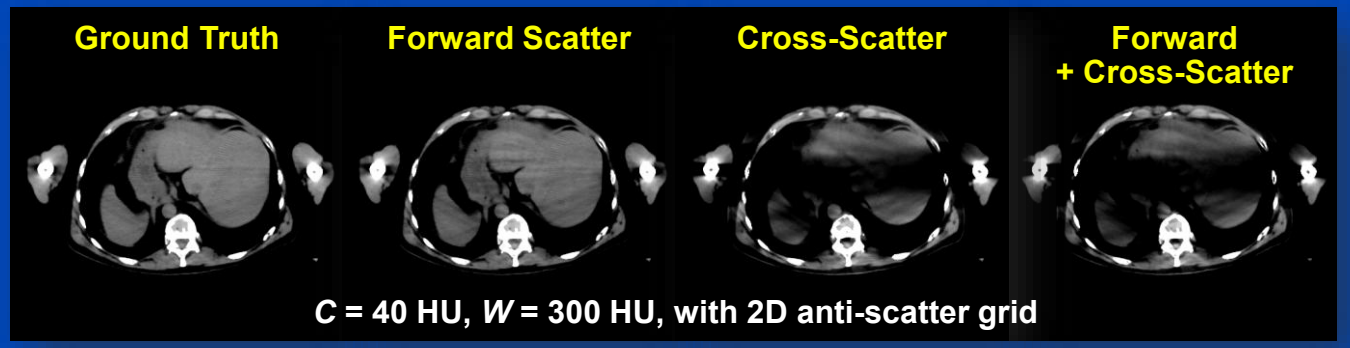

J. Erath, T. Vöth, J. Maier, E. Fournié, M. Petersilka, K. Stierstorfer, and M. Kachelrieß. Deep learning-based forward and cross-scatter correction in dual source CT. Med. Phys. 48:4824–4842, July 2021.

dkfz.

Measurement-Based Scatter Estimation

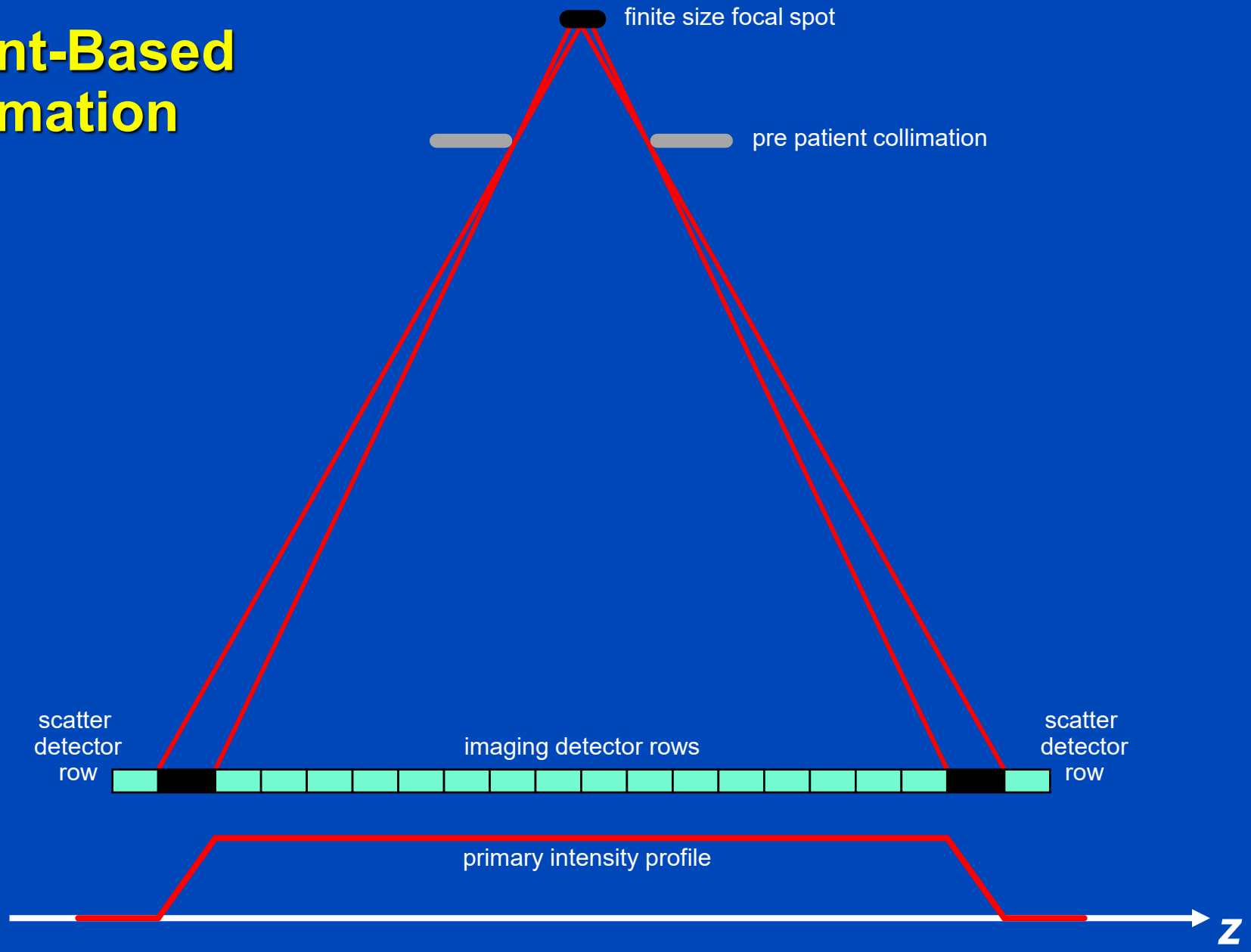

J. Erath, T. Vöth, J. Maier, E. Fournié, M. Petersilka, K. Stierstorfer, and M. Kachelrieß. Deep learning-based forward and cross-scatter correction in dual source CT. Med. Phys. 48:4824–4842, July 2021.

dkfz.

Cross-DSE

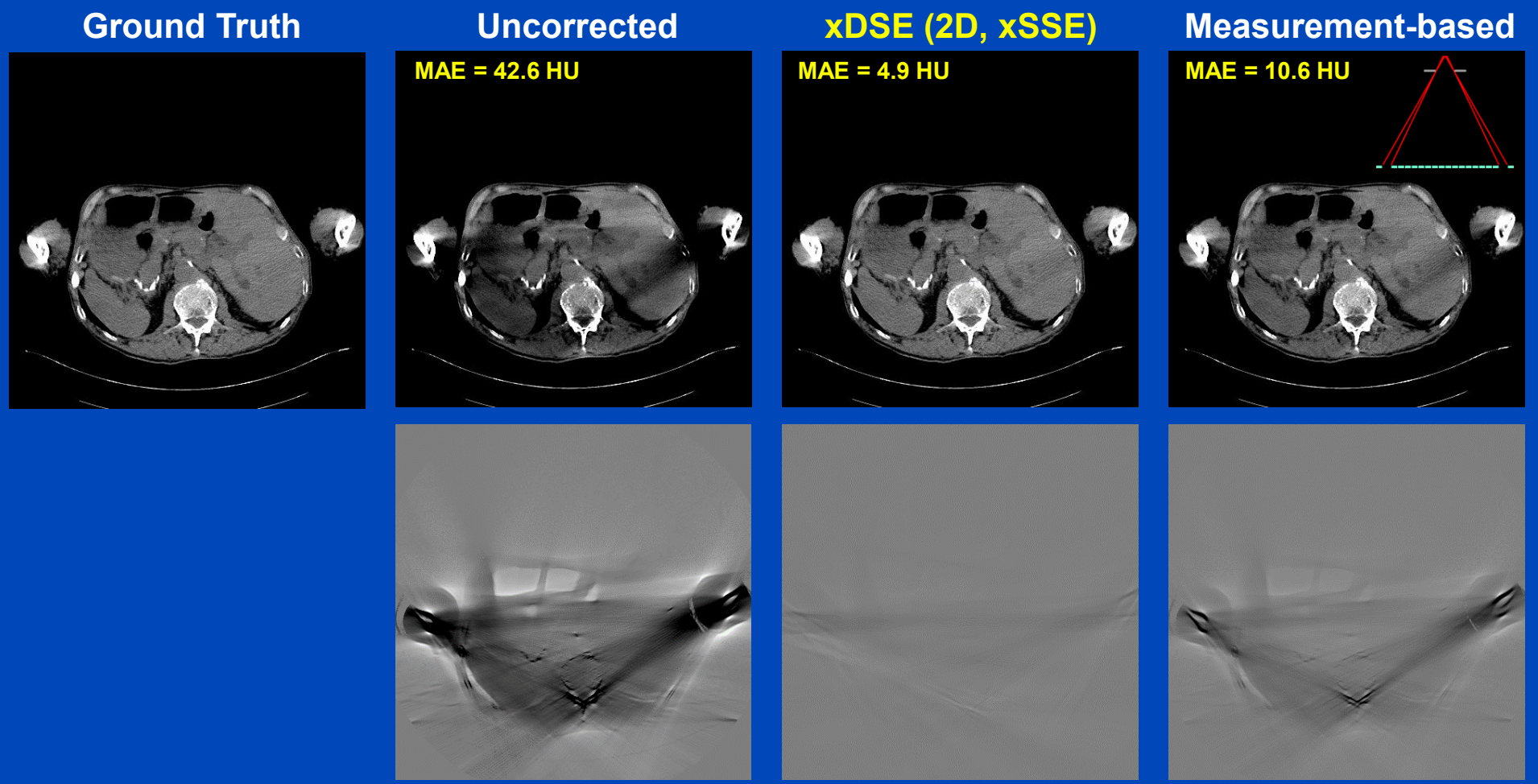

xDSE (2D, xSSE) maps
primary + forward scatter + cross-scatter + cross-scatter approximation → cross-scatter

Images *C* = 40 HU, *W* = 300 HU, difference images *C* = 0 HU, *W* = 300 HU

J. Erath, T. Vöth, J. Maier, E. Fournié, M. Petersilka, K. Stierstorfer, and M. Kachelrieß. Deep learning-based forward and cross-scatter correction in dual source CT. Med. Phys. 48:4824–4842, July 2021.

dkfz.

Conclusions on DSE

- DSE needs about 3 ms per CT and 10 ms per CBCT projection (as of 2020).
- DSE is a fast and accurate alternative to MC simulations.
- DSE outperforms kernel-based approaches in terms of accuracy and speed.
- Facts:
  - DSE can estimate scatter from a single (!) x-ray image.
  - DSE can accurately estimate scatter from a primary+scatter image.
  - DSE generalizes to all anatomical regions.
  - DSE works for geometries and beam qualities differing from training.
  - DSE may outperform MC even though DSE is trained with MC.
- DSE is not restricted to reproducing MC scatter estimates.
- DSE can rather be trained with any other scatter estimate, including those based on measurements.

J. Maier, M. Kachelrieß et al. Deep scatter estimation (DSE). SPIE 2017 and Journal of Nondestructive Evaluation 37:57, July 2018.
J. Maier, M. Kachelrieß et al. Robustness of DSE. Med. Phys. 46(1):238-249, January 2019.

Thank You!

- This presentation will soon be available at www.dkfz.de/ct.
- Job opportunities through DKFZ's international PhD or Postdoctoral Fellowship programs (marc.kachelriess@dkfz.de).
- Parts of the reconstruction software were provided by RayConStruct® GmbH, Nürnberg, Germany.